1989

Numerical study of heat transfer across a closed cavity and its application to a double glazed window.

Anil. Murgai
University of Windsor

NOTICE

The quality of this microform is heavily dependent upon the quality of the original thesis submitted for microfilming. Every effort has been made to ensure the highest quality of reproduction possible.

If pages are missing, contact the university which granted the degree.

Some pages may have indistinct print especially if the original pages were typed with a poor typewriter ribbon or if the university sent us an inferior photocopy.

Reproduction in full or in part of this microform is governed by the Canadian Copyright Act, R.S.C. 1970, c. C-30, and subsequent amendments.

AVIS

La qualité de cette microforme dépend grandement de la qualité de la thèse soumise au microfilmage. Nous avons tout fait pour assurer une qualité supérieure de reproduction.

S'il manque des pages, veuillez communiquer avec l'université qui a conféré le grade.

La qualité d'impression de certaines pages peut laisser à désirer, surtout si les pages originales ont été dactylographiées à l'aide d'un ruban usé ou si l'université nous a fait parvenir une photocopie de qualité inférieure.

La reproduction, même partielle, de cette microforme est soumise à la Loi canadienne sur le droit d'auteur, SRC 1970, c. C-30, et ses amendements subséquents.

NUMERICAL STUDY OF HEAT TRANSFER ACROSS A CLOSED CAVITY AND ITS APPLICATION TO A DOUBLE GLAZED WINDOW

by

© Anil Murgai

A Dissertation
submitted to the
Faculty of Graduate Studies and Research
through the Department of
Mechanical Engineering in Partial Fulfillment
of the requirements for the Degree
of Doctor of Philosophy at
the University of Windsor

Windsor, Ontario, Canada

1988

ISBN 0-315-50522-2

Canada

ACB7007

ABSTRACT

Steady, laminar, natural convection in a vertical, rectangular, air filled enclosure, has been studied numerically. The enclosure is formed by two flat, parallel vertical plates, enclosed on the top and bottom by flat horizontal parallel plates. A 2 - dimensional model is considered in the present study. Emphasis has been given to treating the cavity as a double glazed window, which requires the height to width (distance between vertical plates) ratio to be as high 80. The present study has considered the environmental factors affecting the heat transfer across the window. They are the temperature difference between the interior and the exterior, the wind speeds and the solar radiation absorbed in the glass panes of the window. The Boussinesq approximation and constant physical properties of the fluid (in this case air) inside the cavity have been assumed. The set of primitive variables is used to solve the full Navier-Stokes equations and the energy equation. A finite domain technique, is used to develop a code using a staggered grid. Results of the heat flux variation over a wide range of aspect ratios and Grashof numbers are presented. Detailed

temperature profiles and streamlines have also been shown. Results of the present study have been compared with the experimental and numerical data of other investigators. This has served to validate the mathematical formulation and the numerical code that has been developed.

ACKNOWLEDGEMENTS

I want to express my gratitude to Dr. W.T. Kierkus for his guidance and assistance throughout my research. I would also like to thank the other members of the committee, Dr. T.W. McDonald, Prof. W.G. Colborne and Dr. R.M. Barron for their advice and interest during the course of this study.

I would also like to express my thanks to Dr. N.W. Wilson, Head of the Department, for his support and assistance.

The assistance rendered by several fellow graduate students especially G. Delaire is very much appreciated. Thanks are also due to the staff at the computer centre.

TABLE OF CONTENTS

LIST OF FIGURES

LIST OF TABLES

NOMENCLATURE

a	coefficient of variables in difference equations
A	vertical aspect ratio = L/D
b	source term in difference equations
Cp	specific heat of air in cavity at constant pressure
D	width of cavity (fig. 1.1)
g	gravitational acceleration
Gr	Grashof number based on D = $\frac{g \beta D^3 \Delta T_m}{\nu^2}$
hi	heat transfer coefficient on outer surface of i-face
ho	heat transfer coefficient on outer surface of o-face
Hi	inner heat transfer number = $\frac{k}{L\ hi}$
Ho	outer heat transfer number = $\frac{k}{L\ ho}$
k	thermal conductivity of air in cavity
L	height of cavity
N	heat flux ratio = Ro/Ri
Nr	average room Nusselt number = $\frac{q_1 D}{k \Delta T}$
Nu	average Nusselt number based on width D = $\frac{1}{A}\int_0^1 \frac{\partial T^*}{\partial X} dY$
p	pressure of air in cavity
P	dimensionless pressure of air in cavity = $\frac{(p - p_\infty)L^2}{\rho \alpha^2}$
Pr	Prandtl number = ν/α
q_1, q_2	heat flux at i-face (fig 3.1)
q_3, q_4	heat flux at o-face (fig 3.1)

Ra	Raleigh number = Gr * Pr
R_f	radiation factor = 1 + N So + Si
Ri	radiation per unit area absorbed on i-face
Ro	radiation per unit area absorbed on o-face
Si	inner radiation number = Ri/(hi ΔT)
So	outer radiation number = Ri/(ho ΔT)
T	temperature of air in cavity
T^*	dimensionless temperature = $\frac{T - To_\infty}{\Delta T_r}$
Ti_∞	interior ambient temperature
To_∞	exterior ambient temperature
ΔT	temperature difference = $Ti_\infty - To_\infty$
ΔT_m	modified temperature difference = $\Delta T\ R_f$
u	velocity component in x-direction
U	dimensionless velocity component in x-direction = $\frac{u}{\nu/L}$
v	velocity component in y-direction
V	dimensionless velocity component in y-direction = $\frac{v}{\nu/L}$
W	depth of cavity normal to paper
x	spacial coordinate along the width of cavity
X	dimensionless spacial coordinate along width of cavity = x/L
y	spacial coordinate along the height of cavity
Y	dimensionless spacial coordinate along height of cavity = y/L

Greek symbols

α	thermal diffusivity of air in cavity
β	coefficient of thermal expansion of air contained in cavity
μ	dynamic viscosity of air contained in cavity
ν	kinematic viscosity of air contained in cavity = μ/ρ
ρ	density of air in cavity
ϕ	angle of inclination of cavity with respect to horizontal

Subscript

∞	ambient condition

Chapter I

INTRODUCTION

1.1 Objective

Buoyancy driven natural convection is an important mode of heat transfer in many engineering systems. The problem of laminar free convection in a rectangular cavity has received considerable attention in the past. Figure 1.1 illustrates the system under study. The vertical walls are referred to as 'faces' and are maintained at different temperatures. The top and bottom walls are designated as 'ends' and are considered adiabatic. The problem of heat transmission between cavity 'faces' is especially important to designers who wish to estimate heat losses or gains across windows, from solar collectors and in building and equipment components where fluid layers are encountered. Some understanding has also been gained in undertanding the convection processes occurring in nature through the study of thermally driven motion in enclosures. Such problems also provide good test problems for numerical solution procedures.

The focus of the present investigation is to study the cavity with emphasis on its application as a system simulat-

ing the performance of a double glazed window. Heat is transferred by free convection from the room to the interior glass pane of the window, while the external glass pane loses heat to the atmosphere, usually, by forced convection. The heat transfer in the cavity itself, formed by the double glazed window, is a combination of conduction, convection and low temperature radiation exchange between the glass panes. The significant environmental factors affecting the heat transfer are the temperature difference between the interior and the exterior, the velocity of the winds, and the solar radiation absorbed in the glass panes.

The objective of the present study is to formulate a mathematical model and develop a numerical code to compute the heat flux through a double glazed window, taking into account the above factors. Heat transfer coefficients are specified on the outer surfaces of the faces of the window to account for the wind speeds. The solar radiation absorbed in the faces is considered to be heat generation in the glass panes. The temperature of the faces is not specified, but is now a dependent variable, and its value is obtained as a part of the solution. The interior and exterior ambient temperatures are specified.

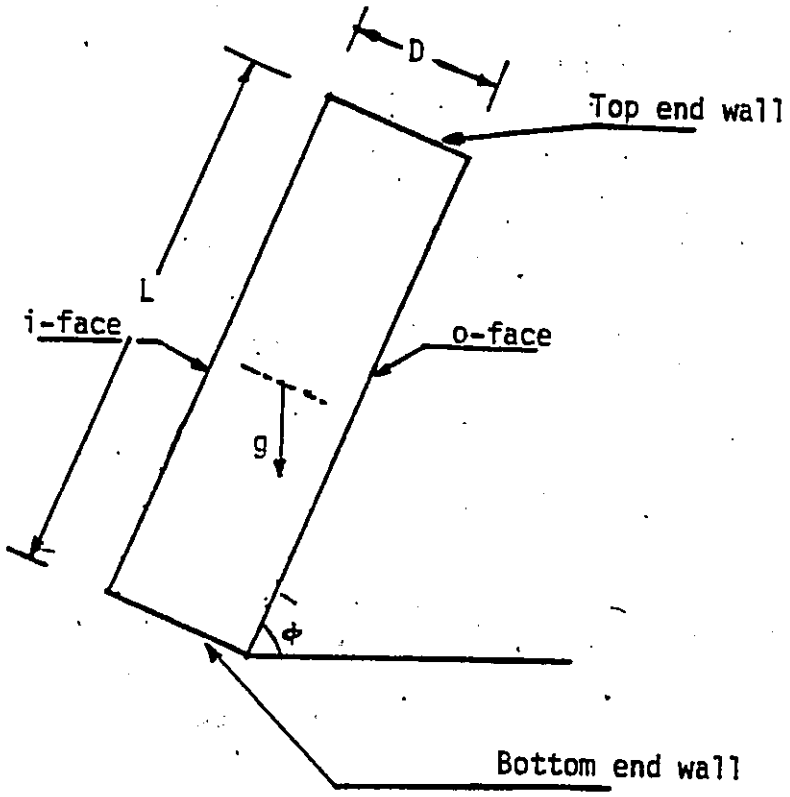

Figure 1.1: Schematic of inclined rectangular cavity.

1.2 Outline of the Present Study

The physics of the flow and heat transfer processes occurring in an air filled cavity has been extensively analysed in the past. However, no study has been found which has treated rigourously the cavity as a double glazed window, by considering the environmental factors.

The literature reviewed refers to the cavity problem, which has the temperature specified on its faces. One face is maintained at a high temperature, while the other face is kept at a low temperature. The end walls are assumed adiabatic. This problem has been studied for over 50 years, using experimental, analytical and numerical techniques. Jakob (1946), proposed a Nusselt number correlation (heat transferred from the hot face to the fluid), based on the experiments of Mull and Reiher (1930). Batchelor (1954) presented an analytical study and demonstrated that the flow is determined by the Prandtl number, Raleigh number and the aspect ratio (=L/D). Eckert and Carlson (1961), carried out an experimental study and presented detailed temperature profiles across the cavity. Yin(1978), also conducted an experimental study and reported results over a wide range of aspect ratios and Grashof numbers. Early numerical studies, used simplifying assumptions. As such their results did not agree with experimental values. They also encountered convergence problems. Successful studies were made later by

MacGregor and Emery (1969), Jones (1979) and others, but were restricted to aspect ratios up to 20. Raithby and Wong (1981) made a detailed numerical study and reported results up to aspect ratios of 80.

Chapter Three examines three environmental conditions that affect heat transfer from a double glazed window, temperature difference, wind speed and solar radiation. Using dimensional analysis, dimensionless groups are formed that influence heat transfer and wall temperature. In addition to the familiar groups like Grashof number and Prandtl number, six additional groups are formed. They are the inner heat transfer number Hi, outer heat transfer number Ho, inner radiation number Si, outer radiation number So, heat flux ratio N and the aspect ratio A. Thus a total of eight dimensionless groups influence the heat transfer. Given the large number of groups it is not feasible to do a complete parametric study, and only trends are studied.

In Chapter Four a finite volume method is described, which is used to solve the full Navier-Stokes equations and the energy equation. Primitive variables are used in a staggered grid. It is based upon the SIMPLER (Semi Implicit Pressure Linked Equation Revised) algorithm first developed by Patankar (1980). An improved method of solving the pressure equation suggested by Doormaal and Raithby (1982) has

been incorporated. Underrelaxation parameters in the difference equations are introduced in a modified manner, described as the E-factor formulation. The use of this formulation, together with the SIMPLER technique makes the method used in the present study different from others.

Chapter Five reports the results of the numerical study. The first task is to validate the numerical code developed. This is accomplished by comparing the results obtained from this code, with the experimental data of Mynett and Duxbury (1974) and Yin (1978), and, also the numerical data of Raithby and Wong (1981). The values agree closely.

Attention is now focused on the problem of interest in the present study. The dependence of Nusselt number on the aspect ratio has been plotted for a wide range of aspect ratios and Grashof numbers. The results are presented for three cases depending on the values of the parameters indicated above. Detailed temperature profiles are presented and the physics of the flow is discussed. Isotherms and streamlines are also illustrated.

Finally, a room Nusselt number Nr, is defined as a measure of the heat transferred from the room to the i-face, and an equation is derived relating it to the dependent dimensionless parameters. The heat flux q_i from the room to the i-face is plotted for the cases considered in this study. A

procedure has been outlined, to use the results of the present study, for computing the heat flux.

Chapter Six summarizes the findings in the present work and outlines suggestions for future work.

Appendix A contains the details of a grid senstivity analysis. A listing of the code named WINDSAV used to solve the problem under study is enclosed in Appendix B.

Chapter II

LITERATURE REVIEW

Natural convection in cavities has been investigated extensively over the past 50 years, using analytical, experimental and numerical techniques. Most studies used a steady state, 2-dimensional model. One vertical face of the cavity was maintained at a high temperature, while the other face was at a lower temperature. Buoyancy effects were set up due to this temperature difference. The end walls of the cavity were usually assumed adiabatic. Fluids of various Prandtl numbers have been used. A wide range of aspect ratios (=L/D) and temperature differences between the faces has been investigated.

The aim of these studies was to understand the physics of the flow and heat transfer occurring in the cavity. Nusselt number correlations (average heat transferred from the hot face to the fluid) for a range of Grashof numbers and aspect ratios (=L/D), were presented. The correlations were of the form shown below:

$$Nu = C\,(Gr)^{a}\,(A)^{b} \qquad (2.1)$$

where Nu is the Nusselt number, Gr is the Grashof number and A is the aspect ratio. C, a and b are empirical constants.

Jakob (1946) was among the first to give a correlation in the form of equation 2.1, based upon the experimental findings of Mull and Reiher (1930). Eckert and Carlson (1961) carried out an experimental study and presented detailed temperature profiles. A Nusselt number correlation was also given. Elder (1965) used a high Prandtl number fluid. He used thermocouples to obtain the temperature field and measured the velocity field also. He confirmed the findings of Eckert. Mynett and Duxbury (1974) studied a range of aspect ratios up to 20. Yin (1978) carried out a study up to an aspect ratio of 80. Both investigators presented detailed temperature profiles which agreed closely.

An analytical study made by Batchelor (1954) concluded that various flow regimes exist depending on the value of the Raleigh number and on the geometry. The early numerical studies were based on boundary layer assumptions, and dealt generally with aspect ratios less than 5. The results of these studies did not agree with the experimental data. Often there were convergence difficulties too. MacGregor and Emery (1969), Newell and Schmidt (1970), Jones (1979)

carried out numerical studies, using the stream function-vorticity formulation. Their results agreed with experimental data. However, they restricted their studies to aspect ratios less than 20. Raithby and Wong (1981) carried out the most extensive study, up to aspect ratio of 80. They used the stream function-vorticity formulation in a staggered grid.

However, no study has been found which has treated the cavity as a double glazed window by rigourously considering the effect of the environmental factors on the window surfaces. As such, the literature reviewed pertains to the study of the physics of the flow and heat transfer in the cavity by natural convection and conduction.

The literature reviewed below is classified into experimental and numerical studies.

2.1 Experimental Studies

Jakob (1946) analyzed the experimental results of Mull and Reiher (1930) and proposed the following correlations:

$$Nu = 0.18\ (Gr)^{0.25}(A)^{-0.111} \qquad 2*10^4 < Gr < 2*10^5 \qquad (2.2)$$

$$Nu = 0.065\ (Gr)^{0.333}(A)^{-0.111} \qquad 2*10^5 < Gr < 1*10^7 \qquad (2.3)$$

Equations 2.2 and 2.3 are supposed to be valid for aspect ratio A in the range of 3.12 to 42.2. Equation 2.3 is intended to describe turbulent flow conditions.

De Graaf and Van der Held (1953) made a systematic investigation of the heat transfer and the convective phenomenon in enclosed plane air layers in horizontal, vertical and oblique positions. Formulae for the heat transfer are given. Some interesting types of convection flow patterns are described and the influence they have upon the heat transfer is deduced from the measurements. They proposed the following relations:

$$Nu = 1 \qquad Gr < 7*10^3 \tag{2.4}$$

$$Nu = 0.0384\,(Gr)^{0.37} \qquad 10^4 < Gr < 8*10^4 \tag{2.5}$$

$$Nu = 0.0317\,(Gr)^{0.37} \qquad Gr > 2*10^5 \tag{2.6}$$

Eckert and Carlson (1961) investigated the temperature field with the help of a Zehnder-Mach Interferometer. They proposed that the flows may be classified into conduction, transition and boundary layer regimes; the horizontal temperature gradient at the cavity centre provides a useful cri-

terion. The cavity centre is a point midway between the faces and the ends of the cavity.

The apparatus consisted of 2 vertical copper plates 15" high, 16" wide and .5" thick. One of the plates was heated by an electric heater. The second copper plate was cooled by water running through a jacket attached to the back surface of the plate. The upper and lower ends enclosing the air space were made of balsa wood. Two glass windows were inserted into the end plates so that the light beams of the interferometer could pass through the air layer. The temperature difference between the hot and cold plate was varied between 10 and 160 F at 25 F intervals. Steady state conditions were established before any measurements were taken.

Local heat transfer coefficients were derived from the temperature gradients in the air normal to the plate. For the boundary layer regime a correlation was proposed given as below:

$$Nu = 0.119\,(Gr)^{0.3}(A)^{-0.1} \qquad 8*10^4 < Gr < 2*10^5 \qquad (2.7)$$

The heat transfer coefficients calculated with the above equation are 20% higher than previous measurements.

Elder (1965) carried out an experimental study of the interaction of buoyancy and shear forces in free convective

flow of a liquid in a rectangular cavity across which there is a uniform temperature difference ΔT.

He established the flow in a rectangular cavity. The lower end was packed with an insulator, while the upper end was a free surface. The fluid used was silicone, which is highly viscous and has a high Prandtl number. Velocity measurements were made by direct observation through the glass of the aluminium particles suspended in the fluid, by timing the passage of a single particle between fixed marks in the eye piece of a travelling microscope. Temperatures were measured with copper-constantan thermocouples and a potentiometer. The temperature field closely satisfies the Laplace equation. The flow is vertical throughout the slot except for regions within a distance of order D from the ends. For $10^3 < Ra < 10^5$, large temperature gradients grow near the walls, and in an interior region a uniform vertical gradient is established. The flow is similar to that near an isolated, heated, vertical plate except that the vertical growth of the wall layers is inhibited in the central part of the slot by the presence of the other layer which prevents entrainment of the fluid. Near $Ra = 10^5$ the interior region of the flow generates a steady secondary flow. A regular cellular pattern becomes superimposed on the basic flow to produce a 'cats-eye' pattern of streamlines. Near Ra =

10^6 when the secondary cell amplitude is large, a further steady cellular motion is generated in the weak shear regions between each cell.

Mynett and Duxbury (1974) also used interferometric techniques and gave detailed temperature profiles and several flow visualizations within enclosed plane air cells with diabatic vertical faces. A variety of cell sizes was used giving a range of Ra numbers $10^3 < Ra < 10^5$ and a range of aspect ratios from 1.25 to 20. Within these ranges of the variables, there were three distinct regimes of characteristic temperature distributions, called the conduction, transition and boundary layer regimes. Their correlation is given by equation 2.8.

$$Nu = 0.216\ (Ra)^{0.283}(A)^{-0.21} \qquad (2.8)$$

Yin (1978) carried out an intensive experimental study for aspect ratios ranging from 4.9 to 78.7. Air was the fluid used. Thermocouple probes were used to obtain the temperature profiles. They were analyzed with respect to flow regimes. A Nu=f(Gr, A) correlation was presented, as shown, for the measured heat transfer data, which fit it with an average deviation of 7.8%.

$$Nu = 0.21\ (Gr)^{0.269}(A)^{-0.131} \qquad (2.9)$$

The Grashof number based on D, the distance between the faces, ranged from $1.5*10^3$ to $7.0*10^6$. The measured temperature profiles were found to be relatively independent of the temperature difference between the two vertical plates for each aspect ratio. Temperature inversions were observed in several test conditions. They are believed to be caused by a high rate of convection in the vertical direction relative to the low velocity in the horizontal direction.

Elsherbiny (1982) studied the effect of thermal boundary conditions on natural convection in vertical and inclined air layers. Measurements of the heat transfer by natural convection across vertical and inclined air layers are reported. The air layer is bounded by two parallel isothermal flat plates and around the edges by a low thermal conductivity wall. Aspect ratio of 5 is used. They cover a range in Raleigh number from 10^3 to 10^8 , and a range in the orientation from horizontal to vertical. The effect of the emissivity of the boundary wall on the heat transfer across

the air layer was evaluated from measurements obtained respectively with a low and a high value of the wall emissivity.

He has concluded that heat transfer by natural convection across a fluid layer between two isothermal plates at different temperatures depends on the boundary condition of the side and end walls that confine the extent of the layer. The side walls are usually assumed to have a linear temperature profile between the faces, or are considered adiabatic. When the fluid is air, or most any other gas, it is argued that the adiabatic condition cannot be achieved in practice, and that experimenters, analysts and designers must consider a larger list of parameters than is normally used to specify the heat transfer. Not only is the heat transfer induced in the walls due to convection in the layer, but radiation also affects both the convective heat transfer and the wall heat transfer.

2.2 Analytical and Numerical Studies

Batchelor (1954) studied the problem and from the governing equations determined that the flow is determined uniquely by the Prandtl number, the Raleigh number and the aspect ratio.

He investigated the problem in 3 cases

1. Small Raleigh numbers Ra < 1000 with A = 1
2. General Raleigh numbers with large A.

3. Large Raleigh numbers with general A's.

An analytical solution for the first case was found by utilizing a method of expanding the stream function and temperature in a power series in terms of the Raleigh number. For the second case he assumed that the temperature and stream function take up their asymptotic form, and he recommended an equation of the form as:

$$Nu = 1 + \left[(2\gamma - 1)/720\right]Ra/A \qquad (2.10)$$

could be used, where γ is a constant.

Poots (1958) attempted a solution of the problem by expanding the stream function and the temperature in a double series of orthogonal functions, the coefficients of whose terms were powers of the Raleigh number. Calculation difficulties and convergence problems restricted the results to a Raleigh number of less than a 1000. In this domain the effect of convection is minimal.

Emery and Chu (1965) used an integral approach. Boundary layer assumptions were made. The velocity and temperature profiles were considered to correspond to those for natural convection from a vertical plate in an infinite medium.

Wilkes and Churchill (1966) published one of the first attempts at solving the full 2-dimensional time dependent

differential equations describing the flow. They used an implicit alternating-direction finite difference method and were able to obtain steady state solutions for small values of A of 1. 2 and 3. The problem was solved as an initial value problem initially at rest in an isothermal cavity. which is suddenly subjected to the desired thermal boundary condition. It yields information on the transient conditions which exist prior to the the establishment of the steady state. but is subject to stability difficulties. Nusselt number values obtained were 70% higher than those given by Jakob (1946). As the solution varied widely with the experimental results. it was not acceptable.

MacGregor and Emery (1969) carried out numerical computations for laminar free convection for isothermal faces and for constant heat flux wall boundary conditions. The effect of the Prandtl. Grashof and Aspect ratios (range 1-20) was determined. Experimental measurements of net heat transfer through vertical plane layers and of velocity and temperature profiles are given for Prandtl numbers of 1-20.000. A comparison of the laminar data with the numerical results shows excellent correlation. An explicit finite difference technique is used in conjunction with a Gauss Siedel iterative method. for the solution of time dependent equations. A stream function. vorticity formulation was used. Convective

terms were approximated by backward differences for positive velocities and forward differences for negative velocities.

Newell and Schmidt (1970) studied the two dimensional laminar natural convection in air contained in a long horizontal rectangular enclosure with isothermal walls at different temperatures. The time dependent governing differential equations were solved using a method based upon that of Crank-Nicholson. Steady state solutions were obtained for height to width ratios of 1, 1.25, 10 and 20, and for Grashof numbers covering the range of $4*10^3$ to $1.4*10^5$ The results were correlated with a three dimensional power law which yielded:

$$Nu = 0.386\ (Gr)^{0.315} \qquad (2.11)$$

The results compare favorably with experimental results.

Jones (1979) studied laminar free convection in an air filled rectangular cavity. He used a finite difference, second order method with the stream function and vorticity as the dependent variables. A time dependent approach is adopted, advancing the solution from some initial estimate until a steady state is a reached. A regular rectangular mesh was used. Aspect ratios up to 20 were considered. He compared his results with the experimental data of Mynett and Dux-

bury. The agreement was good. A correlation given by him is given below:

$$Nu = 0.216\ (Ra)^{0.283}(A)^{-0.210} \qquad (2.12)$$

Raithby and Wong (1981) have reported finite difference predictions of natural convection in vertical air layers for a wide range of Raleigh numbers and aspect ratios. Calculations were carried out for both perfectly conducting and adiabatic boundaries at the top and bottom ends of the layer. Comparisons between the predictions and measurements shows that the calculated heat transfer rates are valid only for a limited range of parameters, and that the points of departure correlate closely with predicted points of instability. They used the scheme of Wong and Raithby (1979) to obtain their prediction. This scheme uses vorticity and stream function as the dependent variables and a staggered mesh that guarantees the conservation of vorticity and energy over the entire solution domain. Equal grid spacing was used in both the directions. The finite difference equations for vorticity and stream function were solved simultaneously, using a sparse matrix solver, and the energy equation was solved separately with the same solver.

The correlations of the various investigators presented in this chapter are of the form of equation 2.1. For comparison purposes, they have been listed in Table 2.1. The values of the empirical constants C, a and b depend upon the range of Grashof numbers and aspect ratio covered. As the ranges of aspect ratios and Grashof numbers has varied from worker to worker, the values of the empirical constants also show a variation. However, the values of constants obtained by Mynett and Duxbury(1974) compare closely with those of Yin(1978).

Jones has compared the temperature profiles, obtained numerically, with the experimentally obtained profiles of Mynett and Duxbury(1974). There is close agreement. In the present study a comparison has been made with the experimental data of Mynett and Duxbury, and of Yin. A close agreement has been found.

The purpose of the present work is to study the air filled cavity, as applied to a double glazed window. As such the boundary conditions applicable at the i-face and o-face, would be different than those of the studies surveyed in this chapter. The temperature is no longer specified on the i and o faces. Instead, heat transfer coefficients shall be specified, along with the temperature of the interior and exterior ambients. The formulation of the problem is discussed in the next chapter.

Table 2.1: Empirical constants for Nu correlation

Worker	C	a	b	Range of A	Range of Gr
Jakob	.18	.25	-.011	3.12-42.2	$2*10^4 - 2*10^5$
Jakob	.065	.333	-.011	3.12-42.2	$2*10^5 - 2*10^7$
Eckert	.119	.3	-.100	10	$8*10^4 - 2*10^5$
Newell	.155	.315	-.265	2.5-20	$4*10^3 - 1.4*10^5$ (Horizontal cavity)
Mynett	.216	.263	-.210	1.25-20	$10^3 - 6.5*10^5$ (Raleigh no.)
Yin	.210	.269	-.131	4.9-78.7	$5*10^3 - 2.7*10^6$

Chapter III

FORMULATION OF THE PROBLEM

Steady laminar natural convection in a rectangular cavity is investigated numerically. The problem of natural convection in vertical layers bounded by heated and cooled isothermal walls has been investigated quite extensively. As it happens, we rarely find phenomenon in nature or engineering which fits such boundary conditions. The purpose of this study is to study natural convection in vertical air layers, with special reference to computing the heat flux across a double glazed window. A sketch of the cavity as applied to a double glazed window is shown in Figure 3.1. The left hand vertical wall of the cavity facing the room has been designated as the i-face, and the right hand vertical wall facing the atmosphere outside has been designated as the o-face. The distance between the i-face and o-face is the width of the window and is denoted by D. The depth of the window normal to the paper is given by W and the height of the window is given by L. The vertical aspect ratio A is defined as L/D. The ambient temperature of the room is denoted by Ti_∞ and the ambient temperature of the atmosphere

outside the room is denoted by To_{∞}. The temperatures of the i-face and o-face are not specified, but are obtained as a part of the solution.

3.1 Description of the problem

The computation of heat flux across a double glazed window depends on a number of environmental factors. The significant ones are listed below:

1. Temperature difference between the inside and outside.
2. Wind speed and direction.
3. Intensity of the solar radiation absorbed in the glass panes.

The effect of wind speed and direction is considered by prescribing heat transfer coefficients ho on the outer surface of the o-face. The air inside the room is considered to be still. As such heat transfer occurs by natural convection, on the outer surface of the i-face. hi denotes the heat transfer coefficient on this surface. Ri and Ro are respectively, the radiation absorbed in the i-face and o-face.

Heat is transferred by free convection from the inside to the i-face, and by forced convection from the o-face to the outside. The heat transfer in the cavity itself depends on a large number of variables, given by the properties of the air in the cavity, the geometry of the cavity, the emis-

sivities of the bounding walls and the temperatures of the bounding walls.

Also important are the thermal boundary conditions applied to the air near the top and bottom end walls. Theoretical studies of the problem have most often assumed that either a linear temperature profile (LTP) is established at these ends, or that the ends are perfectly adiabatic. But in real engineering systems or in an experimental apparatus, neither of these conditions will be satisfied exactly. If the fluid is air, a close match to the LTP is readily established. Establishing the adiabatic condition, on the other hand, is virtually impossible in practice because of the already low thermal conductivity of air. However, provided that the aspect ratio A is sufficiently large, the details of the thermal boundary conditions at the walls are unimportant in most cases. In the present study the adiabatic condition is imposed on the top and bottom end walls.

The conduction and convection in the air interacts with the conduction in the wall and radiation at the wall to establish the local temperature and heat exchange across the wall-air interface. This interaction causes the conduction in the solid and radiation exchange at the plates to be altered from that which would exist in the absence of convection. In general, a designer needing to know the magni-

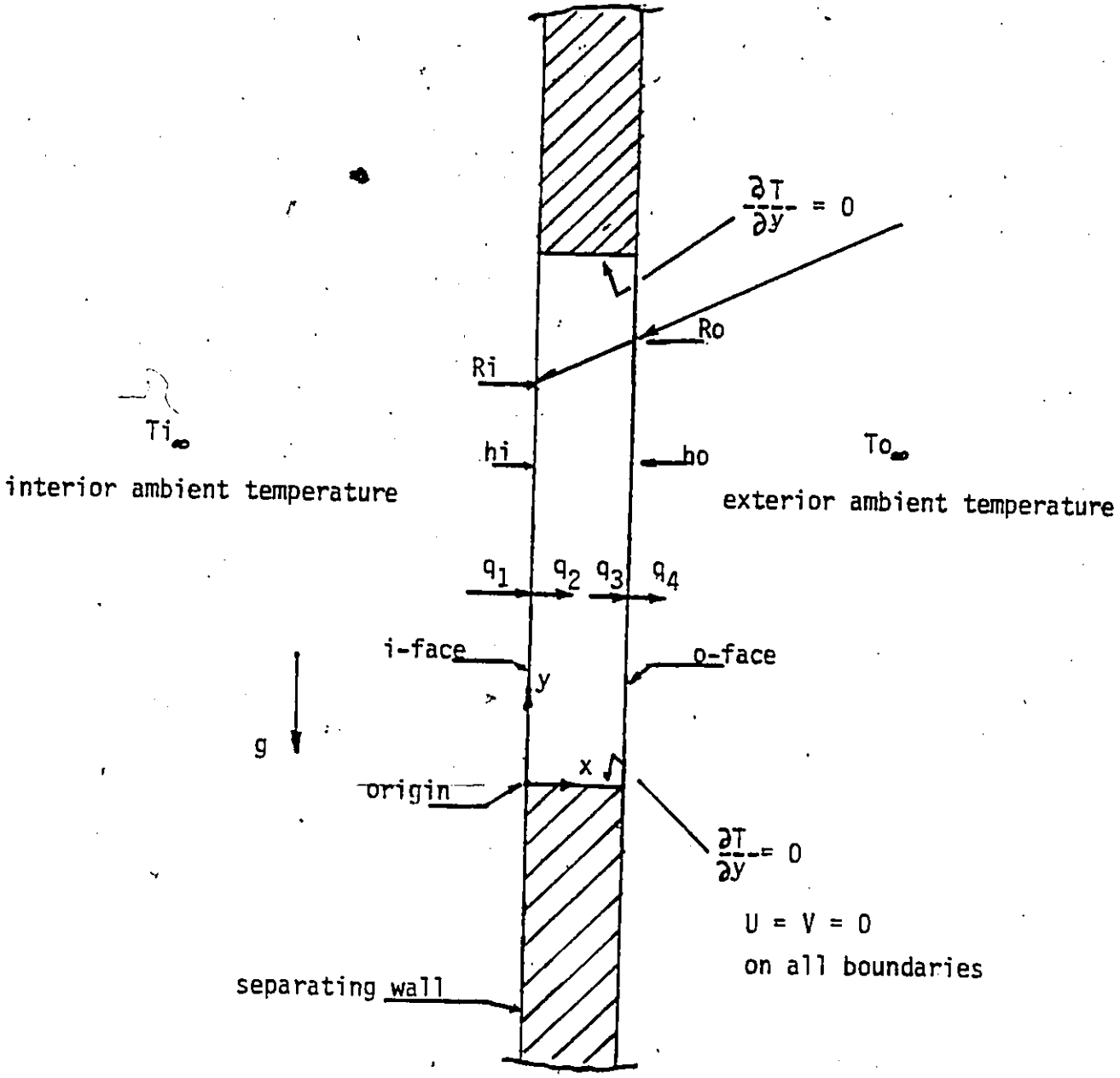

Figure 3.1: Double glazed window, geometry and boundary conditions.

tude of free convection heat transfer will also need to know the magnitude of these alterations in the conductive and radiative heat transfer, if he is to predict the total heat transfer accurately. So we have a fully coupled convection-conduction-radiation problem.

In the present study, certain simplifying assumptions have been made. W, the depth of the window normal to the paper, is much larger than D, and so the effect of the horizontal aspect ratio (W/D), can be ignored. A 2-dimensional problem results. The effect of radiation exchange between the walls is ignored in order to simplify the mathematical formulation of the problem. The walls are assumed to be thin and the effect of conduction is also neglected. The problem now involves only free convection in the window cavity, without any conduction or radiation interactions that might occur at, or between the solid boundaries. Thus, in the present study the Nusselt number is a function of the following variables:

$$Nu = f(\rho, Cp, \mu, k, L, D, Ri, Ro, hi, ho, \Delta T, g) \qquad (3.1)$$

where ρ, Cp, μ and k are the properties of air contained in the cavity and are respectivly, the density, specific

heat, coefficient of dynamic viscosity and thermal conductivity. L and D are the height and width of the cavity and g is the acceleration due to gravity.

The dependent parameter, the Nusselt number, is a function of 12 independent variables. A dimensional analysis results in the formation of eight dimensionless groups. The determination of the functional relationship between them is the desired end product.

In order to obtain meaningful dimensionless groups, we examine the equations of mass, momentum and energy conservation along with the appropriate boundary conditions.

3.2 Governing equations

The continuity, momentum and energy equations governing a steady state, two-dimensional, laminar flow of a Newtonian fluid, with no viscous dissipation, can be written as the following:

Mass conservation:

$$\frac{\partial}{\partial x}(\rho u) + \frac{\partial}{\partial y}(\rho v) = 0 \qquad (3.2)$$

Momentum conservation in x direction:

$$\frac{\partial}{\partial x}(\rho u^2) + \frac{\partial}{\partial y}(\rho uv) = -\frac{\partial p}{\partial x} + \frac{\partial}{\partial x}\left[\mu\frac{\partial u}{\partial x}\right] + \frac{\partial}{\partial y}\left[\mu\frac{\partial u}{\partial y}\right] \qquad (3.3)$$

Momentum conservation in y direction:

$$\frac{\partial}{\partial x}(\rho uv) + \frac{\partial}{\partial y}(\overline{\rho v^2}) = - \frac{\partial p}{\partial y} - \rho g + \frac{\partial}{\partial x}\left[\mu \frac{\partial v}{\partial x}\right] + \frac{\partial}{\partial y}\left[\mu \frac{\partial v}{\partial y}\right] \qquad (3.4)$$

Energy conservation:

$$u\frac{\partial}{\partial x}(\rho Cp\ T) + v\frac{\partial}{\partial y}(\rho Cp\ T) = \frac{\partial}{\partial x}\left[k\frac{\partial T}{\partial y}\right] + \frac{\partial}{\partial y}\left[k\frac{\partial T}{\partial y}\right] \qquad (3.5)$$

In these equations, x and y are the horizontal and vertical Cartesian coordinates. Horizontal and vertical velocities are u and v respectively.

Subtracting from the momentum equations the static equilibrium equation, with gravity g acting in the vertical direction:

$$\frac{\partial p_\infty}{\partial y} = - \rho_\infty g \quad , \quad \frac{\partial p_\infty}{\partial x} = 0 \qquad (3.6)$$

where p and ρ are the ambient pressure and density. Equation 3.4 then becomes:

$$\frac{\partial}{\partial x}(\rho uv) + \frac{\partial}{\partial y}(\rho v^2) = -\frac{\partial \left[p-p_\infty\right]}{\partial y} - (\rho - \rho_\infty)\, g + \frac{\partial}{\partial x}\left[\mu \frac{\partial v}{\partial x}\right] + \frac{\partial}{\partial y}\left[\mu \frac{\partial v}{\partial y}\right] \qquad (3.7)$$

which shows the buoyancy term more distinctly.

The assumption that the fluid properties are constant and that the Boussinesq approximation, shown below, (fluid density variations can be neglected except in the buoyancy term)

$$(\rho_\infty - \rho) \approx \rho\beta(T - T_\infty)$$

can be made by assuming small temperature differences.

In addition to the governing equations, the following energy balance equations must also be satisfied at the i-face and o-face. This takes into consideration the effect of heat generation in the faces due to the absorption of solar radiation. Carrying out the respective energy balances we have:

$$hi\left[Ti_\infty - T\right] + k\frac{\partial T}{\partial x}\bigg|_{x=0} + Ri = 0 \qquad (3.8)$$

$$-ho\left[T - To_\infty\right] - k\frac{\partial T}{\partial x}\bigg|_{x=D} + Ro = 0 \qquad (3.9)$$

3.3 Dimensionless form of the governing equations

In order to simplify the governing equations and the boundary conditions given by equations 3.2 -3.5, 3.8 and 3.9, nondimensionalized variables can be formed according to the following:

$$X = \frac{x}{L} \ , \ Y = \frac{y}{L} \ , \ P = \frac{\left[p-p_{\infty}\right]L^2}{\rho\nu^2} \tag{3.10}$$

$$U = \frac{u}{(\nu/L)} \ , \ V = \frac{v}{(\nu/L)} \tag{3.11}$$

$$T^{*} = \frac{T - To_{\infty}}{\Delta T_m} \tag{3.12}$$

$$\Delta T_m = \Delta T \cdot R_f \quad \text{and} \quad R_f = 1 + N\cdot So + Si \tag{3.13}$$

$$\Delta T = Ti_{\infty} - To_{\infty} \tag{3.14}$$

On account of the heat generation/solar radiation absorption in the i-face and o-face the dimensionless form of temperature requires special attention. The denominator in equation 3.12 instead of being a simple temperature differ-

ence ΔT is modified as shown in equation 3.13 and is denoted by a modified temperature difference ΔT . The radiation factor R_f appears as a result of the heating effect on the faces. For zero heat generation Rf reduces to 1. Accordingly the temperature difference term appearing in the Grashof number is also modified.

Using the non-dimensionalized variables formed by equation 3.10- 3.12 the dimensionless governing equations and the energy balance equations are given as below:

$$\frac{\partial U}{\partial X} + \frac{\partial V}{\partial Y} = 0 \tag{3.15}$$

$$U\frac{\partial V}{\partial X} + V\frac{\partial U}{\partial Y} = - \frac{\partial P}{\partial X} + \left[\frac{\partial^2 U}{\partial X^2} + \frac{\partial^2 U}{\partial Y^2}\right] \tag{3.16}$$

$$U\frac{\partial V}{\partial X} + V\frac{\partial V}{\partial Y} = - \frac{\partial P}{\partial Y} + Gr\ A^3\ T^* + \left[\frac{\partial^2 V}{\partial X^2} + \frac{\partial^2 V}{\partial Y^2}\right] \tag{3.17}$$

$$U\frac{\partial T^*}{\partial X} + V\frac{\partial T^*}{\partial Y} = \frac{1}{Pr}\left[\frac{\partial^2 T^*}{\partial X^2} + \frac{\partial^2 T^*}{\partial Y^2}\right] \tag{3.18}$$

$$\frac{1}{R_f} - T^*\Big|_{x=0} + Hi \cdot \frac{\partial T^*}{\partial X}\Big|_{x=0} + \frac{Si}{R_f} = 0 \qquad (3.19)$$

$$T^*\Big|_{x=1/A} + Ho \cdot \frac{\partial T^*}{\partial X}\Big|_{x=1/A} - \frac{So}{R_f} = 0 \qquad (3.20)$$

The dimensionless groups formed from the analysis of the governing equations are the Grashof number, Gr, Prandtl number Pr and the aspect ratio, A. The parameters formed from the energy balance equations are Hi, Ho, the inner and outer Nusselt numbers, Si and So, the inner and outer radiation numbers and N, the heat flux ratio. R_f is the radiation factor. The parameters are shown below:

$$Pr = \frac{Cp\ \mu}{k} \qquad (3.21)$$

$$Gr = \frac{g\ \beta\ D^3 \Delta T_m}{\nu^2}, \quad Ra = Gr \cdot Pr \qquad (3.22)$$

where $$Hi = \frac{k}{h_i L} \quad , \quad \hat{}Hi = \frac{k}{h_o L}$$

$$S_i = \frac{R_i}{h_i \Delta T} \quad , \quad S_o = \frac{R_i}{h_o \Delta T} \quad , \quad N = \frac{R_o}{R_i} \qquad (3.23)$$

The top and bottom end walls are assumed to be adiabatic. These conditions, in their dimensionless forms are given by:

$$\left.\frac{\partial T^*}{\partial Y}\right|_{Y=0} = 0 \quad , \quad \left.\frac{\partial T^*}{\partial Y}\right|_{Y=1} = 0 \qquad (3.24)$$

The velocity is assumed to be zero on all the solid boundaries.

$$U = V = 0 \quad \text{on solid boundaries} \qquad (3.25)$$

The relevant physical parameters that affect the heat transfer and wall temperature are A, Gr, Pr, Hi, Ho, Si, So, and N. They are listed in Table 3.1. The Nusselt number, then is a function of the above parameters and is defined as the heat transfer from the i-face to the fluid in the cavi-

ty. It is a dimensionless temperature gradient averaged over the i-face. and it provides a measure of the convection heat transfer occurring at the i-face.

$$Nu = \frac{1}{A}\int_0^1 \left.\frac{\partial T^*}{\partial X}\right|_{X=0} dY \qquad (3.26)$$

The governing equations 3.15 - 3.18 and the boundary conditions given by equations 3.19. 3.20. 3.24 and 3.25 define the problem.

Table 3.1: List of Dimensionless Groups

Prandtl number	$Pr = Cp\,\mu/k$
Grashof number	$Gr = g\beta D^3 \Delta T / \nu^2$
where $\Delta T_m = \Delta T * R_f$ and	$R_f = 1 + N\,So + Si$
Aspect ratio	$A = L/D$
Inner heat transfer number	$Hi = k/(hi\ L)$
Outer heat transfer number	$Ho = k/(ho\ L)$
Inner radiation number	$Si = Ri/\ hi\,\Delta T$
Outer radiation number	$So = Ri/\ ho\,\Delta T$
Heat flux ratio	$N = Ro/Ri$

3.4 Method of analysis

The Nusselt number is dependent upon eight dimensionless groups. As such, a complete parametric study is impractical. The following three cases have been selected for study.

In the first case, the parameter values Hi, Ho, Si and So are reduced to zero. Physically this implies that the effect of solar radiation absorbed in the glass panes and the winds impinging on them is disregarded. The i-face and o-face temperatures are specified and correspond to the interior ambient temperature and exterior ambient temperature respectively. This problem conforms to the studies in the past, and has been reviewed in chapter 2. This has been designated as Case A.

Some results of this part of the study have been used to validate the mathematical formulation and the numerical code developed by comparing the results with the numerical and experimental data of other investigators.

In the second case the values of Si and So are still kept at zero. Hi and Ho are now given non-zero numerical values. The effect of the wind speeds on the heat transfer is now considered. The temperature of the i-face and o-face is no longer specified, but becomes a dependent variable. This is designated as Case B.

In the third case, the values of Hi and Ho remain the same as in Case B. Numerical values are prescribed to Si and So. The parameter N, is relevant only in this case, and its value depends on the qualities of the glass panes. The effect of the solar radiation absorbed in the glass panes along with the effect of the wind are simultaneously considered in this case. This is designated as Case C.

The end walls are considered adiabatic. The fluid enclosed in the cavity is assumed to be air, and it is in a vertical configuration.

In all cases the dependence of Nusselt number on the aspect ratio is plotted at constant Grashof numbers. The aspect ratio is varied from 1 to 80. A comparison of the three cases is made.

To summarize, the equations to be solved in the present problem are:

1. Two momentum equations to obtain the velocity components u and v.
2. Poisson equations to obtain the pressure field, and correct the velocity field.
3. One energy equation to obtain the temperature field.

Most studies of the low speed (viscous effects neglected) buoyancy driven flow in cavities made use of the stream function and vorticity as variables in their computation.

The reason for their not using the physical variables - velocities and pressure - is that by eliminating pressure coupling from the momentum equation, the system contains one less equation and is easier to handle. However, with an eye to extending this program to other applications, like solar collectors, the primitive variable formulation is adopted in the present study, as it is not possible to specify an open boundary in the former formulation. The formulation used is described in the next chapter.

Chapter IV

FINITE VOLUME SOLUTION TECHNIQUE

The momentum equations formulated in the previous chapter are highly non-linear and at present cannot be solved analytically except for a few simple cases. Numerical solution of the above equations is the only viable analytical approach. With numerical techniques it is possible to solve these equations for flow conditions of practical interest. The complexity of the equations requires careful consideration in selecting a solution scheme that will be simple to incorporate and yet provide efficient and accurate results. In the present study the finite domain method is used to solve the governing equations. It generates discrete sets of algebraic equations in the solution domain, which has been divided into rectangular grids. The equations are first linearised and decoupled. This permits the momentum equations to be solved sequentially. This type of solution procedure is called the segregated approach. The objective of this chapter is to describe such a procedure used to solve the governing equations.

4.1 Finite Volume Formulation

The first step in the numerical process is the discretization of the governing equations. The finite volume technique has been used to obtain this.

The most attractive feature of this formulation is that the resulting solution would imply that the integral conservation quantities, such as mass, momentum and energy are exactly satisfied over any group of control volumes, and, of course over the whole calculation domain.

The next step is the solution of the resulting algebraic equations. For an assumed pressure distribution, the two linearized momentum equations establish the velocity components. If these velocities satisfy the mass conservation, the pressure distribution was correct, if mass conservation is violated then the pressure distribution requires refinement. The development of an algorithm to improve the estimate of pressure, so that the momentum equations mass conserving velocities, is complicated by the fact that the pressure does not appear explicitly within the mass consera-tion equations. This is called the velocity-pressure coupling problem. The nonlinearity of the equations and other sources of coupling present further difficulties.

The velocity-pressure coupling problem can be overcome if the discretized equations could be solved simultaneously.

However, a simultaneous solution is prohibitive mainly due to high solution costs. The velocity-pressure coupling problem can be averted if the so called vorticity-stream function formulation is employed, which involves the elimination of the pressure through a suitable manipulation of the momentum equations. This works well in two dimensional problems, although the determination and application of the boundary conditions becomes difficult. However, there is no direct counterpart of this formulation in three dimensions, while the velocity-pressure (or primitive variable) formulation can be easily extended to 3-dimensional flows.

An alternative approach is to use a segregated solution procedure, which involves solving the linearized equations for each variable sequentially, and imbedding the sequence in an iterative procedure which results in an improved satisfaction of the mass and momentum conservation at the end of each iteration.

Various segregated solution procedures have been proposed. The choice of method is not easy, but the consequences of the choice in terms of the total solution cost could be substantial. It has been the experience of others, Raithby and Schneider (1979) and Patankar(1980), that the velocity pressure coupling problem is often mainly responsible for the slow convergence of the available solution procedures.

The procedure used in this study is due to Patankar(1980). In this the correct pressure field is written as the sum of an intermediate pressure field and a correction on this pressure. The pressure correction determined by a Poisson equation is first used to correct the intermediate velocity field to ensure mass conservation, and then to update pressure.

4.2 Description of Numerical Code

In this code, primitive or physical variables U,V,P and T are used in a staggered grid system. The computational domain is divided into rectangular control volumes with one grid point located at the center of the control volume which forms the basic cell. Pressure P and temperature T are calculated at these grid points. Velocities U and V are calculated for points that lie on the faces of these basic cells. Typical basic cell, U-cell and V-cell are arranged as shown in Fig.4.1. Balance equations in integral forms of energy, momentum and mass flux are written for each cell. For example the vertical momentum equation written for a V-cell located about node s, shown in Fig.4.2, forms a difference equation in the form of:

$$a_s V_s = \sum a_{nb} V_{nb} + b + \left[P_s - P_p\right] A_s \qquad (4.1)$$

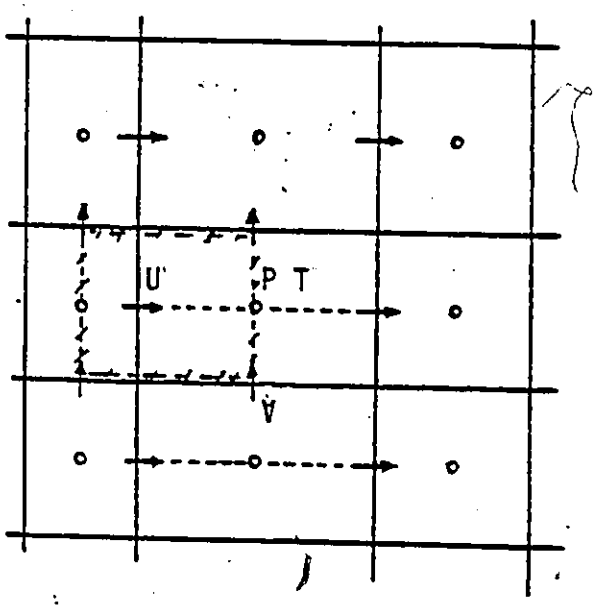

Basic cell ————
U-cell - - - - -
V-cell .....

Figure 4.1: Staggered grid diagram, showing the location of U, V, P and T

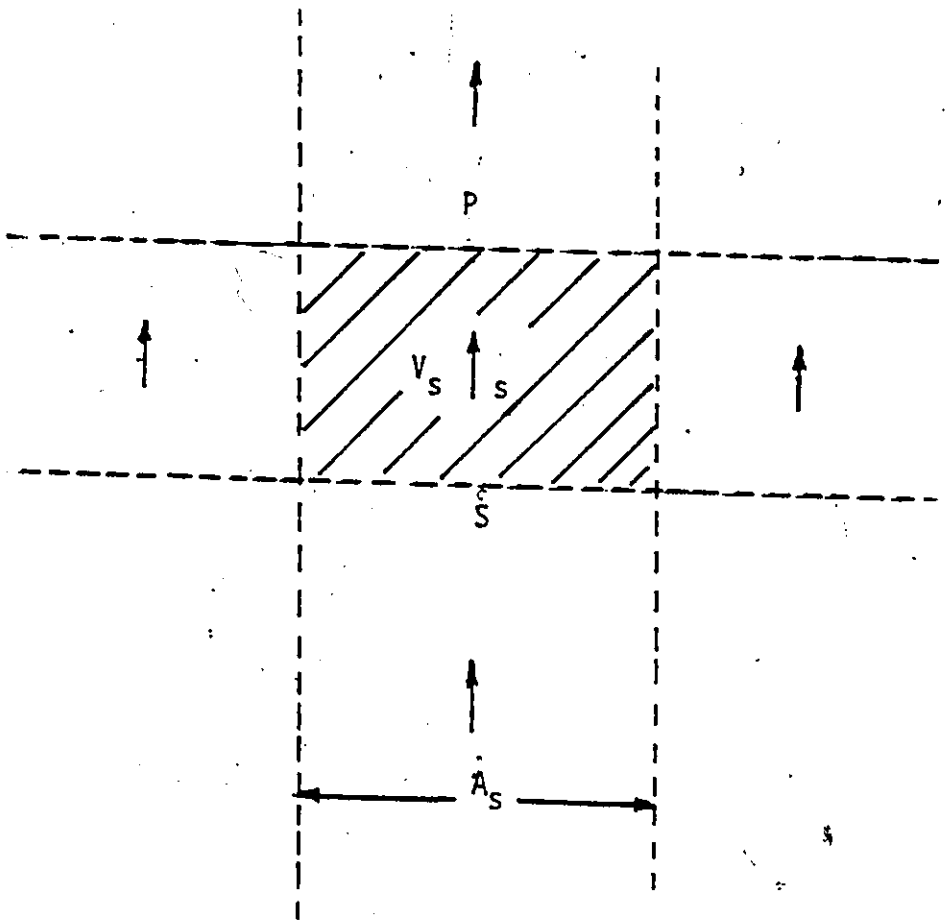

Figure 4.2: V-Cell node about s

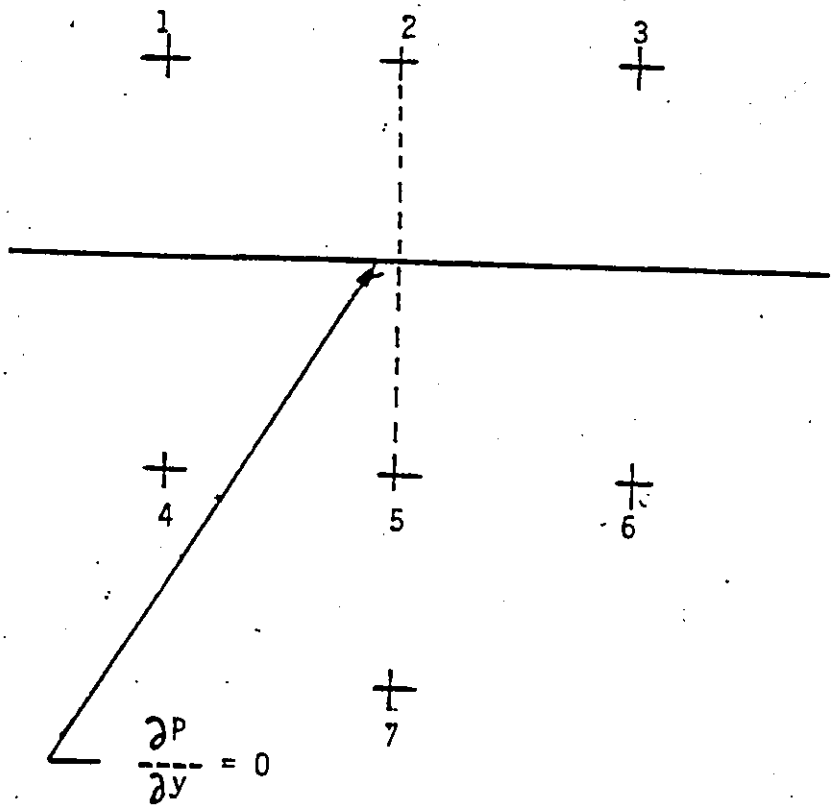

Figure 4.3: Application of gradient type boundary condition.

where the subscript "nb" denotes a neighbor, and the summation is to be taken over all four neighbors. The pressures P_p and P_s denote those at point P and S respectively, while A is the area or width on which the pressures are acting. The source term b includes the buoyancy term. The 'a' coefficients are functions of the dependent variables U, V, P and T. Their numerical values depend on the kind of differencing scheme chosen. In this program, the power law scheme is used which models exponential differences but involves less expensive computations. Solutions can be obtained using different schemes for comparisons, but the results presented all used power law scheme. The differencing scheme is explained in detail in Patankar (1980).

Similar discretization equations for U and T can be obtained. The continuity equation is employed in the solution for the pressure correction. These discretization equations are solved by the Alternating Direction Implicit (ADI) method. The ADI scheme developed by Douglas and Gunn (1964) is used to solve the pressure and pressure correction equation. Assuming two of the neighboring values are known from their latest values, a tridiagonal matrix can be formed from the discretization equations for grid points along a chosen line. This tridiagonal matrix is solved by the Thomas Algorithm. The solution procedure of updating values by

traversing each line in sequence is continued by alternating directions. The idea is to bring the information from the boundaries to the interior.

In this algorithm, the continuity equation is turned into an equation for the pressure correction. If the superscript * stands for guessed or old values, and the superscript ' stands for the correction, there follow:

$$P = P^* + P'$$

$$U = U^* + U'$$

$$V = V^* + V'$$

Subtracting equation 4.1

$$a_s V_s = \sum a_{nb} V_{nb} + b + \left[P_s - P_p\right] A_s \qquad (4.1)$$

from a starred equation 4.1

$$a_s V_s^* = \sum a_{nb} V_{nb}^* + b + \left[P_s^* - P_p^*\right] A_s \qquad (4.2)$$

gives

$$a_s V_s' = \sum a_{nb} V_{nb}' + \left[P_s' - P_p'\right] A_s \qquad (4.3)$$

The correction procedure calls for dropping the $\sum a_{nb} V_{nb}$ terms and choosing the velocity correction as:

$$a_s V_s' = \left[P_s' - P_p'\right] A_s \qquad (4.4)$$

so it results in

$$V_s = V_s^* + \left[\frac{A_s}{a_s}\right]\left[P'_S - P'_P\right] \qquad (4.5)$$

and a similar expression for U. By substituting these back to the continuity equation, in its integral form with all the mass fluxe's (U's and V's), an equation for P', the pressure correction is obtained.

$$(\rho UA)_w - (\rho UA)_e + (\rho VA)_s - (\rho VA)_n = 0 \qquad (4.6)$$

$$a_P P'_P = a_E P'_E + a_W P'_W + a_N P'_N + a_S P'_S + b \qquad (4.7)$$

This is the essence of the algorithm called SIMPLE (Semi-Implicit Method for Pressure Linked Equations). The SIMPLER (SIMPLE Revised) consists of solving a pressure equation obtained from a guessed velocity field and use the pressure-correction equation to correct the velocities only.

The algorithm used in the present work uses an improvement over SIMPLER, in the manner in which the Poisson equation for pressure and pressure correction is solved. This procedure is explained in the next section.

4.2.1 Solution of the Poisson Equation for Pressure

The Poisson equation 4.7 for pressure is of elliptic type. Since P' is governed by a Neumann boundary value problem its solution requires the use of a more efficient solver than SLOR (Successive line over relaxation). The solution of the P' equation can represent as much as 80% (Van Doormaal & Raithby 1984) of the total cost of solving the fluid flow problem. It is therefore a high priority to solve for P' in an efficient manner. The use of direct solution methods tends to be unattractive because of the large storage requirements and computer effort. Extremely fast Poisson solvers are available but the coefficients of P' change on each cycle so that the sparse matrix solvers that are available require a new decomposition each time the coefficients are updated. Van Doormall and Raithby (1984) have suggested a method. Equation 4.7 for P' can be restated as follows for solution along a line of constant j:

$$a_{ij}P_{ij} = b_{ij}P'_{i+1j}+c_{ij}P'_{i-1j}+\left[d_{ij}P'_{ij+1}+e_{ij}P'_{ij-1}\right]+f_{ij} \qquad (4.8)$$

where

$$a_{ij} = a_P, \quad b_{ij} = a_E, \quad c_{ij} = a_W$$
$$d_{ij} = a_N, \quad e_{ij} = a_S, \quad f_{ij} = b$$

and where i and j denote nodal locations in the x and y directions. With the dependent variables that lie off the line (those in brackets in equation 4.8) temporarirly fixed, a direct solution for all the P^* values on the line can be obtained with one Tri diagonal matrix algorithm (TDMA) application. Such a line solution is the basis of an iteration scheme that solves along each j line and then each i line, and repeats the pattern until convergence is achieved. The rate of convergence of such a scheme depends crucially on the treatment of the off line dependent variables.

Suppose that a partially converged P^* field, denoted by $[P^*]$, has been obtained from one or more TDMA base iterations. In the current iteration equation 4.8 is to be solved along each j line, sweeping in the direction of increasing j. On the j line the best available estimate of P^* is that obtained from the just completed solution along the j-1 line. This is the offline value used in equation 4.8. The available estimate of $P^*_{i,j+1}$ is from the previous iteration, ie. $[P^*_{i,j+1}]$, and substitution of this value into equation 4.8 can cause slow convergence. To accelerate

$$\left[P'_{ij+1}\right]_{BE} = \left[P'_{ij+1}\right]^{o} + (\Theta-1)\left[P'_{ij+1} - \left[P'_{ij+1}\right]^{o}\right] \qquad (4.9a)$$

$$\approx \left[P'_{ij+1}\right]^{o} + (\Theta-1)\left[P'_{ij} - \left[P'_{ij}\right]^{o}\right] \qquad (4.9b)$$

In these expressions θ is a relaxation parameter such that for $\theta = 1$, $[P' ij+1]BE$ is taken as $[P' ij+1]$ The approximation in equation 4.9b is therefore introduced into equation 4.9a to obtain

$$\left\{a_{ij} - d_{ij}(\Theta - 1)\right\} P'_{ij} = b_{ij} P'_{i+1j} + c_{ij} P'_{i-1j}$$

$$+ d_{ij}\left\{\left[P'_{ij+1}\right]^{o} - (\Theta - 1)\left[P'_{ij}\right]^{o}\right\} + e_{ij} P'_{ij-1} + f_{ij} \qquad (4.10)$$

A similar estimate is made for solutions along i lines. Values of θ used are determined by the aspect ratio and have varied from 1.1 to 1.85.

4.2.2 Treatment of boundary conditions

Since a staggered grid is being used, not all the points at which U, V, P and T are being computed lie on the bounding walls. A vertical wall passes through the horizontal-velocity mesh points, and the velocities at these points vanish at all times. A vertical wall does not pass through vertical-velocity mesh points. The calculation requires a value V', a typical velocity beyond the wall. In the following discussion a prime refers to the exterior cell quantity. For a no-slip wall the boundary condition is $V' = -V$. Analogous boundary conditions are applied at a horizontal wall. In general, the tangential velocity reverses for a no slip condition.

Wall boundary conditions are also needed for the solution of the pressure equation. The boundary condition for P must be consistent with the identical vanishing of the normal component of the velocity. The gradient of the pressure must therefore be equal to zero. Figure 4.3 illustrates the application of the boundary condition. The pressure equation that requires to be satisfied is as below:

$$a_{57} P_7 + a_{54} P_4 + a_{55} P_5 + a_{58} P_6 + a_{52} P_2 = b_5 \qquad (4.11)$$

The boundary condition demands that $P_2 - P_5 / y = 0$, or $P_2 = P_5$ Hence a_{55} is replaced by $a_{55} + a_{52}$, and a_{52} is set to zero.

The following is a brief description of the numerical code and its subroutines:

1. Initialize velocity and pressure field to zero.
2. Calculate the coefficients for the momentum equations, and hence evaluate pseudo velocities for the pressure equation.
3. Calculate the coefficients for the pressure equation and solve it to obtain the pressure field.
4. Solve the momentum equations to obtain new velocity field, based on the just computed pressure field.
5. Calculate the mass source term b and hence solve the P' equation.
6. Correct the velocity field using the corrected pressure field, without correcting the pressure field.
7. Solve the discretization equation for temperature.
8. Return to step-2 and repeat until convergence criteria are satisfied.

These criteria include checks on the overall mass and energy balance for the cavity, and the relative changes between consecutive iterations. The convergence criteria for the pressure equation governs the time taken for the entire

computation. If iteration of the P' equation is terminated before sufficient convergence is achieved, the continuity constraint is poorly satisfied by the corrected velocities. These velocities are later used to calculate new coefficients, so that the error is propogated with the possible result of divergence or slow convergence. On the other hand, it is uneconomical and wasteful to drive the P' equation to a tight convergence each time it is solved. If P'o is the initial P' distribution, the initial value of the Euclidean norm of the residuals ||rp|| is given by:

$$\|r_p\|^0 = \left[\sum\left[a_E P'^0_E + a_W P'^0_W + a_N P'^0_N + a_S P'^0_S + b_P - a_P P'^0_P\right]^2\right]^{1/2} \quad (4.12a)$$

where the summation is over all interior volumes. After k iterations the corresponding norm ||rp|| is given by:

$$\|r_p\|^k = \left[\sum\left[a_E P'_E + a_W P'_W + a_N P'_N + a_S P'_S + b_P - a_P P'_P\right]^2\right]^{1/2} \quad (4.12b)$$

The performance of the entire solution procedure depends on the criteria used for terminating iteration on the P' equation. The residuals of the P' equation given by equation

4.12 are computed. Iteration is continued until the following criteria is satisfied.

$$\|r_p\|^k \leq \gamma_p \|r_p\|^o \tag{4.13}$$

The values of the residual reduction factor γ_p used vary from .10 to .4 depending on the Grashof number.

Underrelaxation parameters are used in different subroutines to control the advancement of the solution field. The E factor formulation is used as shown in the eguation below.

$$a_p\left[1+\frac{1}{E}\right]V_p = \sum a_{nb} V_{nb} + b + \frac{a_p}{E} V_p^o \tag{4.14}$$

Typical values of E for U and V vary from 4 to 6, while values less than 4 have been used for T. Time on the IBM 3046 computer for each iteration is approximately 2.4 seconds and the number of iterations for convergence varies from 300 to 700.

Chapter V

RESULTS AND DISCUSSION

Numerical solutions for buoyancy induced natural convection in enclosures are presented in the following sections. Computations were performed using a variable staggered grid system. Grid size varied from 18X42 for a low aspect ratio to 8X80 for an aspect ratio of 80. The steady state, laminar flow conditions were assumed. Solutions were obtained for aspect ratios varying from 1 to 80, and Grashof numbers ranging from 10^3 to 10^5 for boundary conditions corresponding to Cases A, B and C. The Nusselt number as defined by equation 3.27 is a measure of the heat transfer from the i-face to the fluid in the cavity. The results are presented in 4 sections. The first section explains the parameter values used in Cases A, B and C. The second section studies the dependence of the Nusselt number on the aspect ratio. The third section presents the temperature profiles and discusses the physics of the flow and heat transfer. Finally, in the last section a room Nusselt number is defined and a relation is derived showing its dependence on the other parameters.

The stream function values are obtained by computing the vorticity field, and then solving the Poisson equation for the stream function. The stream function equals zero on all solid boundaries. They are used for illustration purposes only and do not enter any kind of computation or approximation in the numerical solution.

5.1 Parameter Values

The parameter values are based upon the values of the twelve independent variables. The height of the cavity is considered to be 1 metre. The values of hi and ho are taken to be 4 W/m^2 C and 22.7 W/m^2 C respectively. These values correspond to still air surrounding the i-face, and a strong wind impinging on the o-face. The values are based on empirical data, obtained from ASHRAE Handbook1985 Fundamentals. The thermal conductivity of air is taken to be .0263 W/m K . Accordingly, the values of Hi and Ho are determined to be .007 and .001 respectively.

The solar radiation incident on the earth's surface varies widely, depending upon the time of the year, the latitude and the condition of the sky. Values of Solar intensity for a cloudless day, are listed in ASHRAE Handbook 1985 Fundmentals. The major part of the incident radiation on the o-face, is transmitted to the i-face and then to the room. A

small portion is reflected and the remainder is absorbed in the faces forming the double glazed window. The magnitude absorbed depends on the quality of the glass and is quantified by the absorption coefficient of that material.

In the present study we are concerned with the heating effect of the solar radiation, in the i-face and o-face. For a latitude of 40 Deg North, on July 21 at 4 P.M., the solar radiation intensity on a horizontal surface is 762 W/M**2. Considering an absorption coefficient of 0.1 for the o-face, the radiation absorbed Ro, in the o-face is taken to be 80 W/M**2. Assuming that the i-face is made of glass of such a material, that Ri is given by 60 W/M**2. The ratio N=Ro/Ri is, therefore computed to be 1.333.

The temperature difference between the inner ambient and the outer ambient is taken to be 20 Deg. C. Accordingly, the values of So and Si are determined to be .13 and .75 respectively.

1. Case A, Isothermal Vertical Walls: The parameter values are Hi=0, Ho=0, Si=0, and So=0. This corresponds to the case of isothermal faces.
2. Case B, Convective vertical walls with no heat generation: The parametric values are Hi=.007, Ho=.001, Si=0, and So=0.

3. Case C. Convective vertical walls with heat generation: The parametric values are Hi=.007, Ho=.001, Si=.75, So=.13 and N=1.333.

In all the cases the Prandtl number has been assumed to be .71 for air. Temperature profiles and fluxes have been plotted for aspect ratios ranging from 1 to 80 and Grashof numbers ranging from 10^3 to 10^5 Streamlines and isotherms have also been presented to illustrate the features of the flow.

5.2 Average Nusselt Number

The overall Nusselt number is the ratio of the total heat transferred across the cavity to that transferred by conduction alone. This gives little information on the internal flow structure, but is a quantity of importance in practical applications. It is calculated as the integral of the non-dimensional temperature gradient at the faces. It is quite difficult to evaluate it accurately, since it involves a one sided difference approximation to calculate the derivative.

For the thermal boundary condition adopted in this study, there is no heat loss from the top and bottom ends. The average Nusselt number computed in the present study, is the heat transferred from the i-face to the fluid. Its definition is given by equation 3.27.

In order to validate the mathematical formulation and the numerical code developed, the values of the parameters Hi, Ho, Si, and So have been reduced to zero. This corresponds to the same boundary conditions as those of Raithby and Wong (1981). Figure 5.1 shows a plot of the dependence of the average Nusselt number on the aspect ratio at a constant Grashof number value of $1.4*10^4$ for aspect ratios 1, 2, 5, 10, 20, 40 and 80. The results of the present study are compared with those of Raithby and Wong. The agreement is excellent. Their scheme used the stream function-vorticity formulation while in the present study the primitive variables are used.

The dependence of the average Nusselt number on the aspect ratio have been plotted in Figures 5.2 -5.7. The Grashof numbers were held constant at 10^3, 10^4 and 10^5. The value of the Prandtl number was .71. The values of the other parameters Hi, Ho, Si, So and N correspond to Cases A, B and C. The aspect ratio values used are 1, 2, 5, 10, 20, 40 and 80.

Figure 5.2 shows the dependence of the average Nusselt number with aspect ratio for parameter values given by Case A. The Grashof numbers are kept constant at 10^3, 10^4 and 10^5. At low Grashof number there is very little variation in the Nusselt number. For larger values i.e. 10^4 and great-

er. of Grashof number a maximum occurs at an aspect ratio of 2. At Gr = 10^5 the maximum value of Nusselt number occurs at aspect ratio 1.

Figure 5.3 shows a similar variation for case B. The decrease in Nusselt number is more rapid as the aspect ratio increases. At higher aspect ratios the effect of Grashof number on Nusselt number declines.

Figures 5.5, 5.6 and 5.7 show a comparison between Cases A, B and C for constant values of Grashof numbers at 10^3, 10^4 and 10^5 . The Nusselt numbers are lower for Case B, as is expected, since the temperature difference between the i-face and o-face would be less than that of Case A.

5.3 Temperature Profiles

As in the previous section, the initial effort has been devoted to comparing the results of the present study, with the experimental data of other investigators. Accordingly, the parametric values Hi, Ho, Si and So have been reduced to zero. The boundary conditions of the present problem now conform to those of Mynett and Duxbury (1974) and Yin (1978). Temperature profiles have been computed for aspect ratios ranging from 4.9 to 78.7, and Grashof numbers ranging from 4.96 * 10^3 to 1.07*10^6 The values selected conform to those of the above workers. The wide selection was made in order to identify the various flow regimes.

Later in this section temperature profiles for parametric values corresponding to Cases B and C are presented. The cases selected for comparison are listed below:

1. Aspect Ratio=5, Gr=2.39E4. Mynett and Duxbury(1974).
2. Aspect Ratio=10, Gr=2.44E4. Mynett and Duxbury(1974).
3. Aspect Ratio=6.5, Gr=1.07E6. Yin(1978).
4. Aspect Ratio=9.8, Gr=3.3E5. Yin(1978).
5. Aspect Ratio=13.1, Gr=1.38E5. Yin(1978).
6. Aspect Ratio=19.6, Gr=4.22E4. Yin(1978).
7. Aspect Ratio=39.2, Gr=4.96E3. Yin(1978).
8. Aspect Ratio=78.7, Gr=5.43E3. Yin(1978).

Profiles of temperature, versus horizontal distance X, have been plotted for three vertical locations, at Y/L = .15 from the bottom, Y/L = .50 and Y/L = .85. except in the case of items 1 and 2 above where Y/L=.1, Y/L=.5 and Y/L=.9 have been used. All the temperature profiles are dimensionless.

The numerical results of the present study are compared with the experimental data of Yin (1978), and also of Mynett and Duxbury (1974) and presented in Figures 5.8 to 5.15.

The agreement with the experimental values is quite good. The differences that occur can be ascribed to the end wall boundary conditions. The adiabatic boundary condition has been numerically imposed. Experimentally this cannot be

achieved if air is the enclosed gas. As the thermal conductivity of air is very low, we would require an insulating material on the top and bottom end walls which has a conductivity of an order of magnitude less than that of air. Such a material does not exist. Also in the present study the Boussinesq approximation has been made which implies constant physical properties. However, there is some variation in the properties of the fluid with change in temperature.

Figures 5.14 and 5.15 display linear temperature distribution across the major portion of the air layer except at both the ends, indicating that the heat from the hot side to the cold side is transported by conduction through the major portion of the layer, and by convection at the lower end of the hot face and upper end of the cold face. On the basis of previous work of Eckert and Carlson (1961) the flow field corresponding with this type of temperature distribution is defined as the regime of conduction, as long as the horizontal temperature gradient dT/dX at the cavity centre remains at a value of about -1.

Figures 5.10 and 5.11 display a sharp drop of temperature in the region immediately adjacent to both the hot and cold faces with a horizontal temperature line in the central core. It reveals that the heat is mainly transported from

the hot face to the cold face by convection. Furthermore, temperature inversions were observed in the central regions as shown in Figures 5.8, 5.10 and 5.11. These inversions are a manifestation that the flow immediately adjacent to the vertical faces is so strong that it produces a high rate of convection of heat along the surface of the hot face relative to the transport of heat from the surface of the hot face across to the cold face. Conduction in the central region of the cavity is actually opposite to the overall direction of heat flow. Such inversions have not been observed by Eckert and Carlson. On the other hand, these temperature inversions confirm the flow studies of Elder (1965), where he found secondary vortices to occur in the core flow at higher Raleigh numbers. Such vortices could also account for temperature inversions, as have been found by Yin(1978) and verified numerically in the present study. When a flow field under such temperature distribution with a core of uniform temperature in a direction along horizontal line exists, it is referred to as the boundary layer regime. In other words, this flow regime is characterized by its temperature field with the value of dT/dX at cavity centre being larger or equal to zero.

In the boundary layer region, the flow can be considered as an interaction between two thermal boundary layers, one

on the hot face and the other on the cold face. At the lower end the buoyancy forces exceed the viscous forces and accelerate the fluid but owing to the vertical temperature gradient the buoyancy forces diminish till they are balanced by the viscous forces. The fluid is decelerated beyond this point. The boundary layer entrains fluid at all levels, with the strongest entrainment at the bottom, where the horizontal temperature gradients which are responsible for the flow are the greatest. As there are two layers competing for the fluid, one would expect the layer on the warmer face to entrain fluid from the lower half of the cavity, and the layer on the cooler wall to entrain fluid from the upper half. The entrainment into the lower part of the warmer layer brings fluid from the cooler layer opposite. The influx of cooler fluid maintains a strong horizontal temperature gradient across the layer, and this gradient maintains the upward flow in the layer and the entrainment into the layer. The flow across the core brings cooler fluid into the lower half and warmer fluid into the upper half, leading to a stable vertical temperature gradient in the core. This vertical temperature gradient is of profound importance as it is the main factor in determining the structure of the boundary layer on the vertical wall. Its existence allows the boundary layer to eject as well as to entrain fluid.

The flow in the core is weaker than in the boundary layer on the vertical walls and is not strong enough to maintain a horizontal temperature gradient. Thus the isotherms in the core are nearly horizontal. (Reference Figures 5.42 and 5.43)

It is interesting to point out that all the inversions were observed in the cavities with small aspect ratio. This may illustrate for one thing that the effect of convection will be reduced in cavities with high aspect ratio.

Figures 5.12 and 5.13 show that the temperature profiles have a sharp drop along the hot face and cold face, with a linear temperature drop in the central core. It indicates that in addition to the heat transported by convection, along the surface of both the faces, there is heat conduction through the central core of the layer. This flow field regime is called the transition regime, in which the temperature gradient dT/dX at the cavity centre is ranged between -1 and 0. The appearance of this kind of temperature distribution is thought to be due to some rotation of the core fluid occurring in the air layer. It would seem that the bounday layer interference occurs throughout the conduction regime, and in the boundary layer regime no boundary layer interference occurs and the core fluid is relatively staganant. Thus, in the transition regime the boundary layer will

not interfere, but will almost meet near the centre of the cavity. This will cause some rotation of the core fluid, which prevents the fluid in the core from being isothermal in the horizontal direction. On the other hand, the velocity here is much less than that in the boundary layer, which prevents the linear temperature profile. Summarizing the above one can identify three flow regimes according to the Grashof number.

1. Conduction Regime: The Grashof number is small and there is no variation of fluid temperature with height. Heat is transfered by conduction.
2. Transition Regime: The Grashof number is larger, and the horizontal temperature gradient ranges between -1 and 0.
3. Boundary layer Regime: The flow is confined to the faces and the dominant mode of heat transfer is by convection. The temperature gradient at the cavity centre is larger or equal to zero.
4. Above a certain critical value of Grashof number instability begins and the flow becomes turbulent.

The remaining results for Case B and Case C have been arranged according to the flow regimes. Figures 5.16 - 5.18 refer to the boundary layer regime for case B for aspect ratios 5, 10 and 20. Figures 5.19 - 5.21 refer to case C.

The Grashof number is 10^5 and the flow is strong mainly along the walls, where the temperature gradients are large. In mid cavity, the temperature gradient is close to zero, and, tending even to be positive, indicating temperature inversion. There is a slight variation in temperature at each of the vertical walls.

Figures 5.22 - 5.25 are temperature profiles of aspect ratios 5, 10, 40 and 80 corresponding to case B. Figures 5.26 - 5.28 are temperature profiles corresponding to case C. They fall into transition category. The temperature gradients are less steep here, and there is no region of zero temperature gradient.

Figures 5.29 - 5.34 refer to case B and Figures 5.35 - 5.40 refer to case C. They fall into the conduction zone. Heat transfer is by conduction alone. The temperature gradient is equal to -1. At lower aspect ratios slight convection occurs at the ends of the cavity. The vertical temperature gradient is zero. There is very little variation in temperature at the two vertical walls.

Plots of streamlines and isotherms are shown in Figures 5.41 - 5.52 for aspect ratios of 1, 2, 5, 10, 20, 40 and 80. The values of groups Hi and Ho are .007 and .001 which correspond to Case B.

An examination of Figures 5.42, 5.43, 5.49 show that three regions can be distinguished for high Grashof numbers: A wall region, an interior region, and an end region. In the wall region $0 < X < .2$, the isotherms are slightly inclined to the wall with the temperature gradient being nearly horizontal- the temperature gradients are largest here. The interior region $0.2 < X < 0.8$ has nearly horizontal regularly spaced isotherms, a region of nearly uniform, positive, vertical temperature gradient. Near the ends $Y < 0.1L$, or $> 0.9L$ the pattern is influenced by the end boundary conditions. For lower Grashof numbers Figures 5.47, 5.48, 5.50 and 5.52, the isotherms are vertical lines in most of the cavity. A little bending occurs towards the ends. Thus the convection effects are restricted to the ends.

5.4 Cavity as a Double Glazed Window

The chief emphasis in the present study has been the simulation of the vertical rectangular cavity as a double glazed window. As a result, the quantity of interest is the heat flux q_1, shown in Figure 3.1. To obtain this flux, an energy balance is carried out on the i-face given by equation 5.1 below:

$$q_1 - q_2 + Ri = 0 \qquad (5.1)$$

Using the dimensionless groups formed earlier, equation 5.1 can be put in the form given by equation 5.2.

$$Nr = R_f \, Nu - \frac{Si}{A \, Hi} \qquad (5.2)$$

where Nr is defined as the room Nusselt number and is defined by equation 5.3.

$$Nr = \frac{q_i \, D}{k \, \Delta T} \qquad (5.3)$$

Figure 5.53 is a plot of the room Nusselt number versus the aspect ratio, for Case C. Three curves have been plotted for Grashof numbers 10^3, 10^4 and 10^5. The values of Nr are obtained by substituting the values of Rf, Si, Hi and A in equation 5.2 above. The value of Nu is obtained from Figure 5.4.

For Cases A and B, Si and So are equal to zero which gives R_f equal to 1. Hence for these two cases the value of Nr and Nu are the same.

Using the results of the present study, a procedure is outlined below, to compute the heat flux q_i from the room to the i-face.

1. Fix the height L and gap D (space between the faces) of the window. The aspect ratio A = L/D is can be computed.
2. Establish the fluid contained in the cavity, and thus fix the properties of the fluid. Air is considered in this example with Pr=.71.
3. Select the values of the environmental variables, for which the computation is desired. The variables represent the wind speeds, given by hi and ho, the temperature difference between the two ambients given by ΔT, and the effect of heating in the faces given by Ro and Ri. The values of the dimensionless parameters Hi, Ho, Ri and Ro can now be computed.
4. Based on the values of the parameters computed above, the Radiation factor R_f and hence the modified temperaure difference ΔT can be computed. Finally, the Grashof number is obtained.
5. Using the values of A and Gr the value of the room Nusselt number Nr is obtained from Figure 5.7. This value is substituted in equation 5.3 to give the desired heat flux.

Following the above procedure, using the values of parameters given in the first section of this chapter, the heat flux q_i has been plotted for boundary conditions pertaining

to each of the Cases A, B and C. The results are presented in Figures 5.54 - 5.56. They are relevant to a window of height L=1.0 M only. Three values of D (gap between the faces) .0125, .0167 and .025 M have been used which correspond to aspect ratios of 80, 60 and 40.

Figure 5.54 shows the flux q_i plotted versus the aspect ratio. The results pertain to Case C. The values of the parameters are Hi=007, Ho=.001, Si=.75, So=.13, and N=1.333. The temperature difference between the ambients is 20 Deg. C. A single line is shown. It is a measure of the heat flux for a window of height L=1.0 M and D varying from .025 M to .0125M. The temperature difference between the ambients is 20 Deg. C.

Figure 5.55 shows the flux q_i, which is the heat loss from the room. It has been plotted for the same range of D. The height of the window L=1.0 meter. The values of parameters used correspond to Case B. No heating effects due to solar radiation are considered here. Accordingly the value of Hi and Ho are respectively .007 and .001, while So and Si are taken to be zero. The curves are plotted for three values of temperature differences between the ambients ie. 20, 10 and 5 Deg. C.

Finally, in Figure 5.57, a comparision is made between Cases A and B. Also included is Case S, which refers to a

simplified model, wherein the flux q_1 is computed using the concept of thermal resistance (Incropera, (1981)), given by equation 5.4 below. The heat transfer coefficients hi and ho are specified to be 4 and 22.7 W/M**2, which are the same values as used in obtaining the parameters Hi and Ho in Case B. k is the thermal conductivity of air in the cavity and D is the gap between the faces. The height L in this model is considered infinitely long.

$$q_1 = \frac{Ti_\infty - To_\infty}{Rt} \qquad (5.4)$$

where Rt is the total thermal resistance and is given by
1/hi + D/k + 1/ho

The fluxes have been computed for a temperature difference of 20 Deg. C between the ambients. The flux obtained for Case A is much higher than that for Case B, since in Case A the convective thermal resistances are disregarded. A comparision can be made between Cases B and S. Case B shows the results of the present study, obtained by rigorously solving the Navier-Stokes equations and energy equation inside the cavity, whereas Case S represents the results of a simplified model explained above. There is a variation ranging from 15 to 25%.

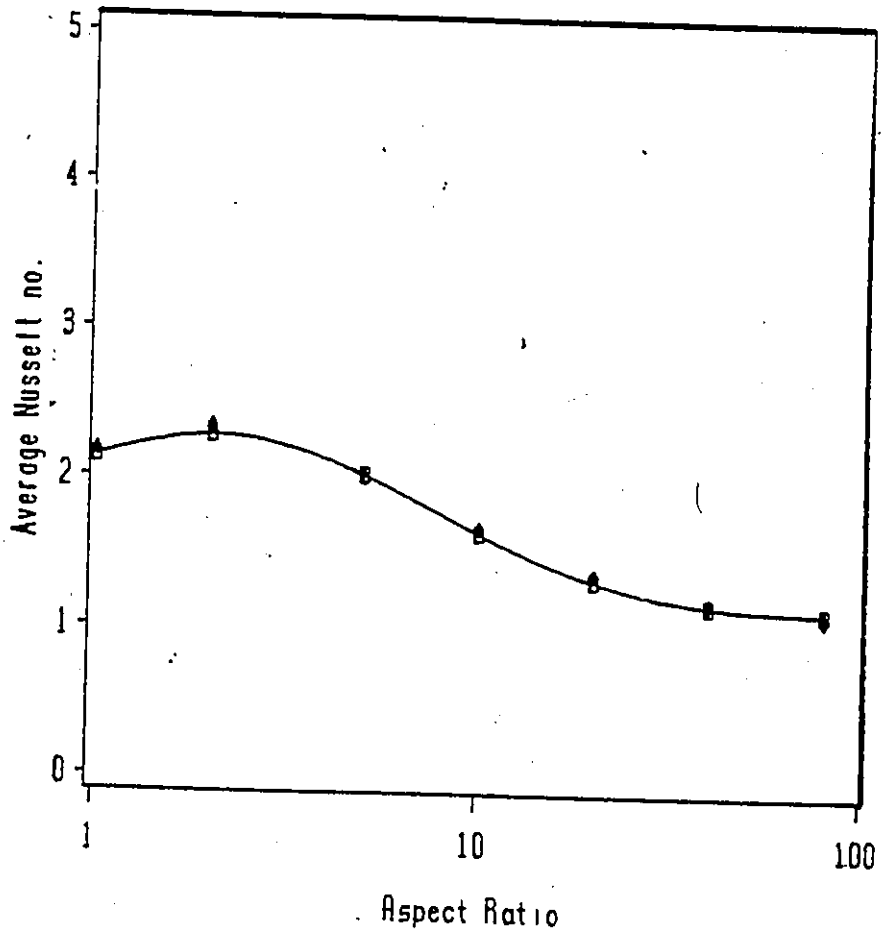

Figure 5.1: Dependence of Nu on A. Comparision with numerical data of Raithby and Wong(1981). Gr=1.4E4

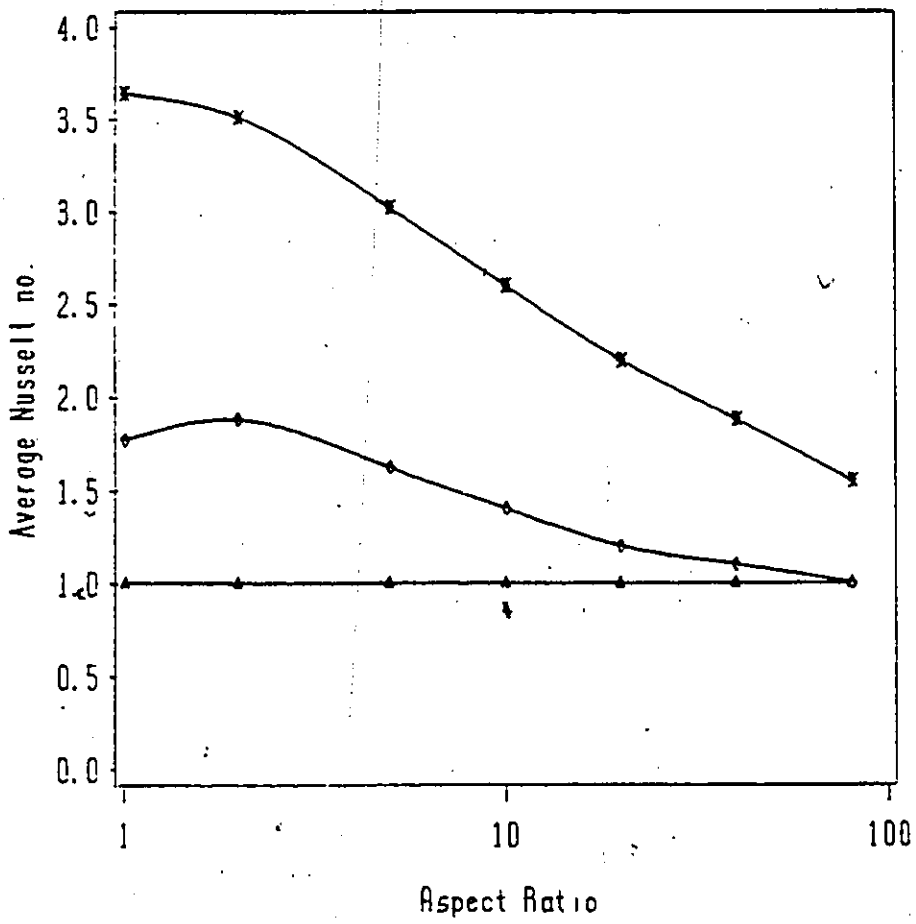

Figure 5.2: Dependence of Nu on A at constant Gr. Hi=0. Ho=0. Si=0. So=0. Case A

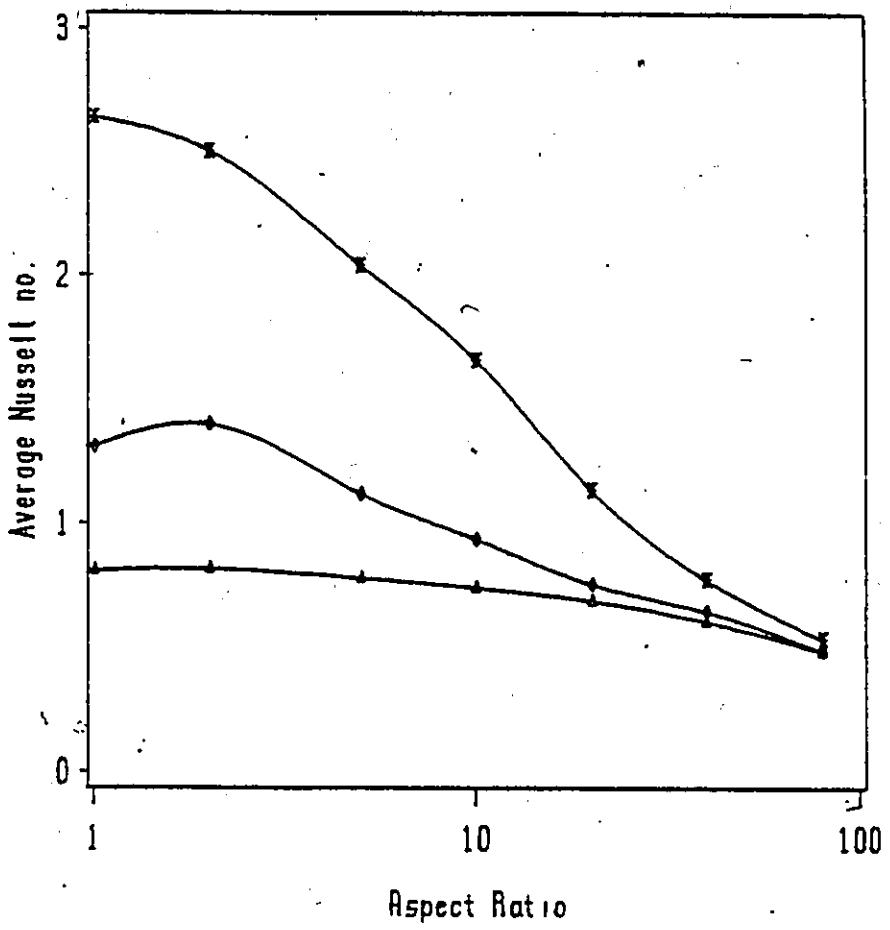

Figure 5.3: Dependence of Nu on A at constant Gr. Hi=.007, Ho=.001, Si=0, So=0. Case B

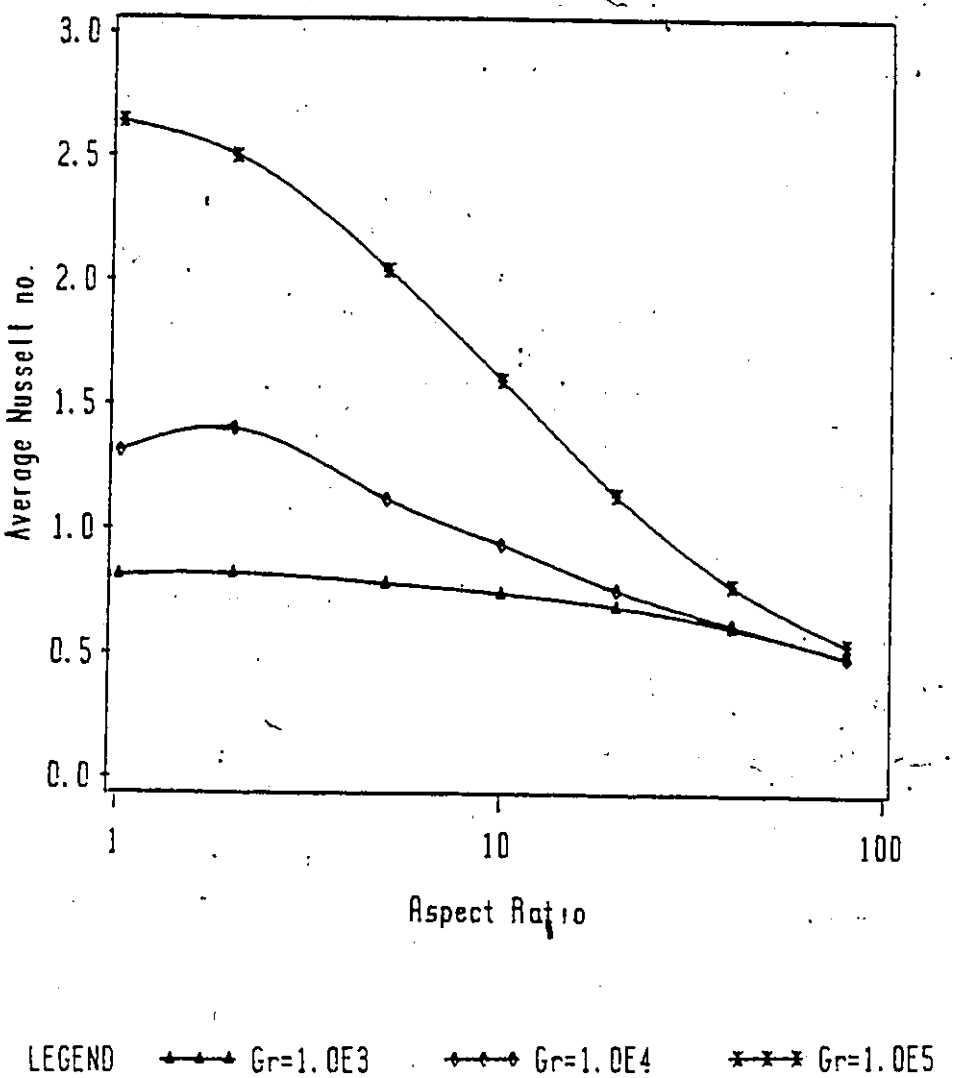

Figure 5.4: Dependence of Nu on A at constant Gr. Ri=.007, Ho=.001, Si=.75, So=.13, N=1.333. Case C

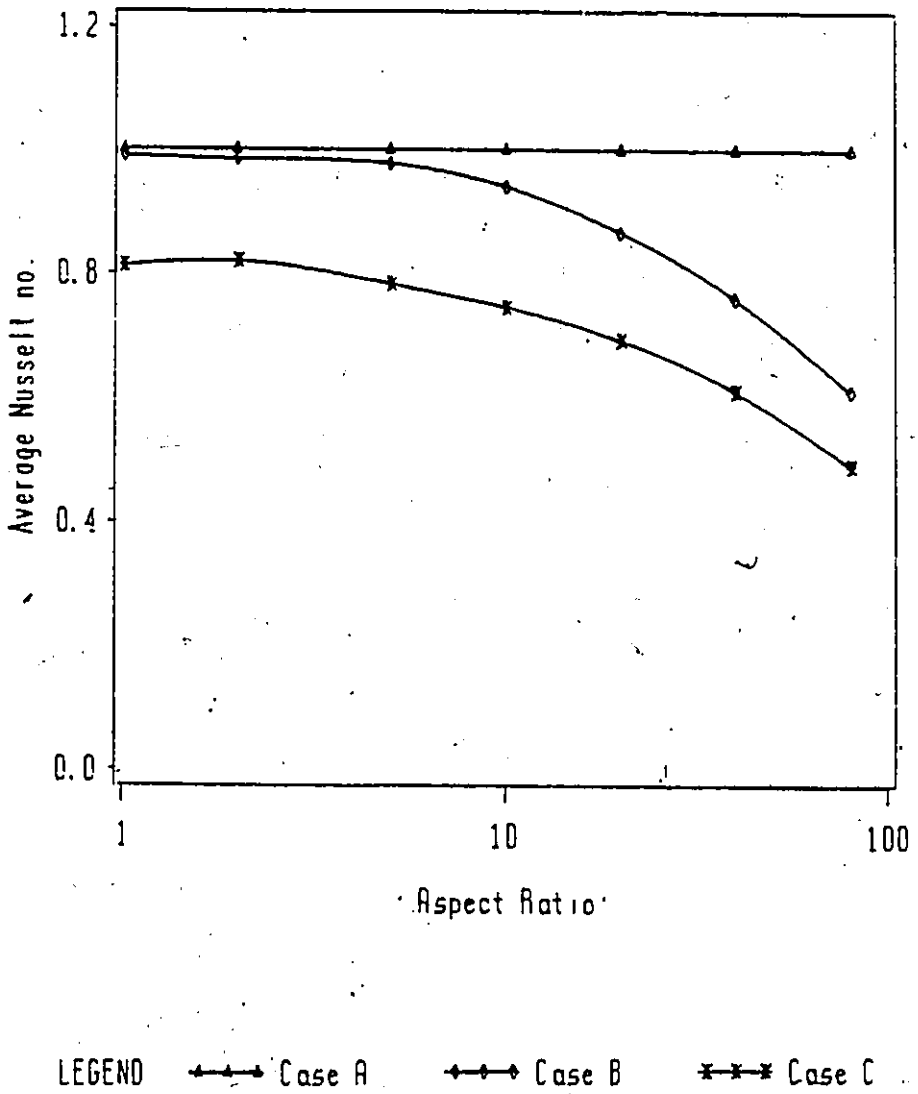

Figure 5.5: Dependence of Nu on A at Gr=1.E3. Comparison between Cases A, B and C.

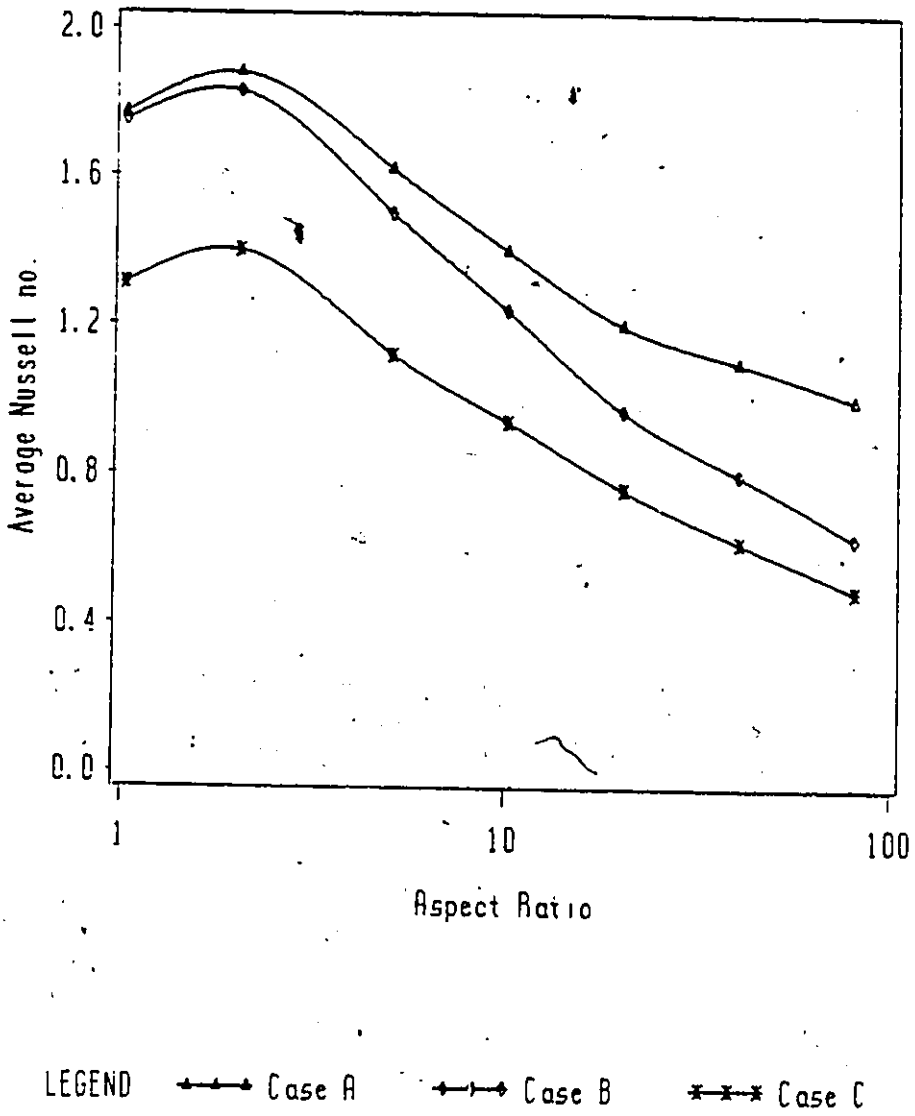

Figure 5.6: Dependence of Nu on A at Gr=1.E4. Comparison between Cases A, B and C.

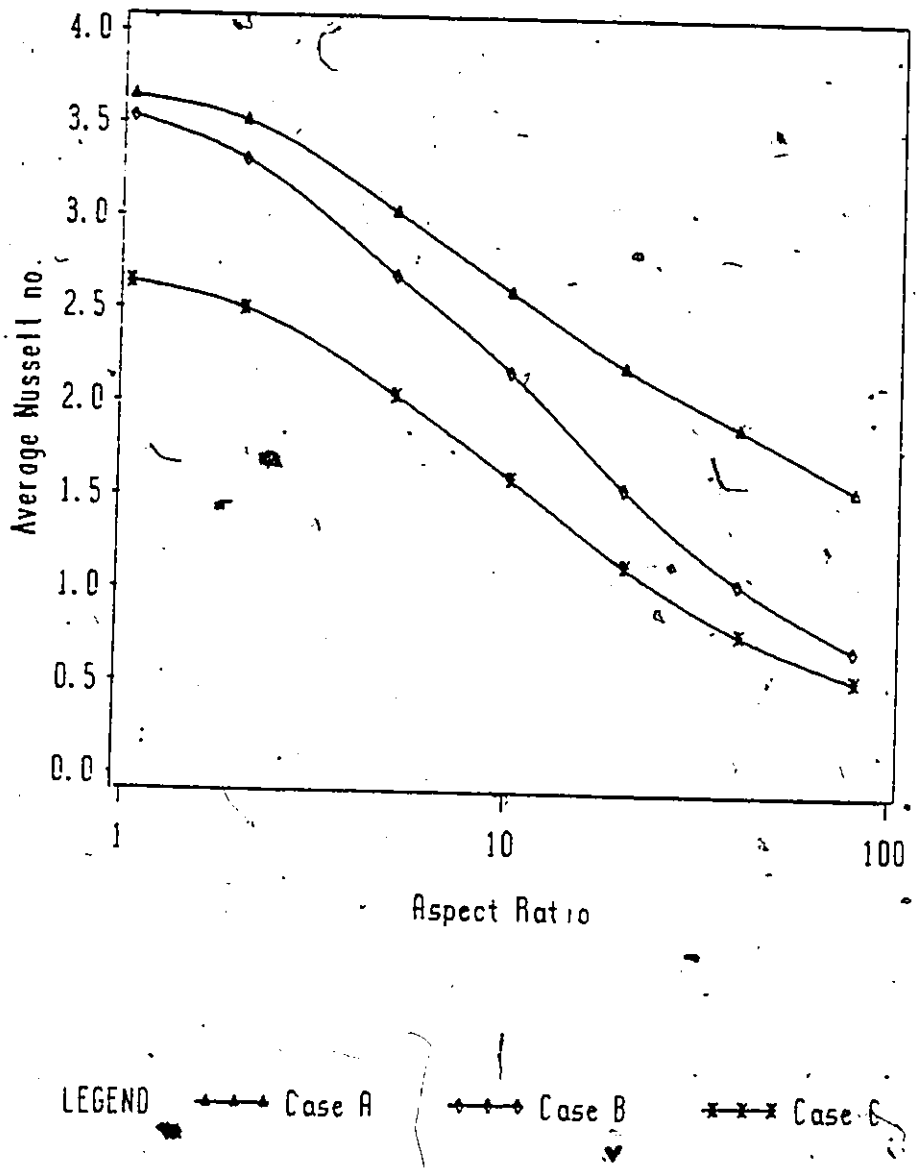

Figure 5.7: Dependence of Nu on A at Gr=1.E5. Comparison between Cases A, B and C.

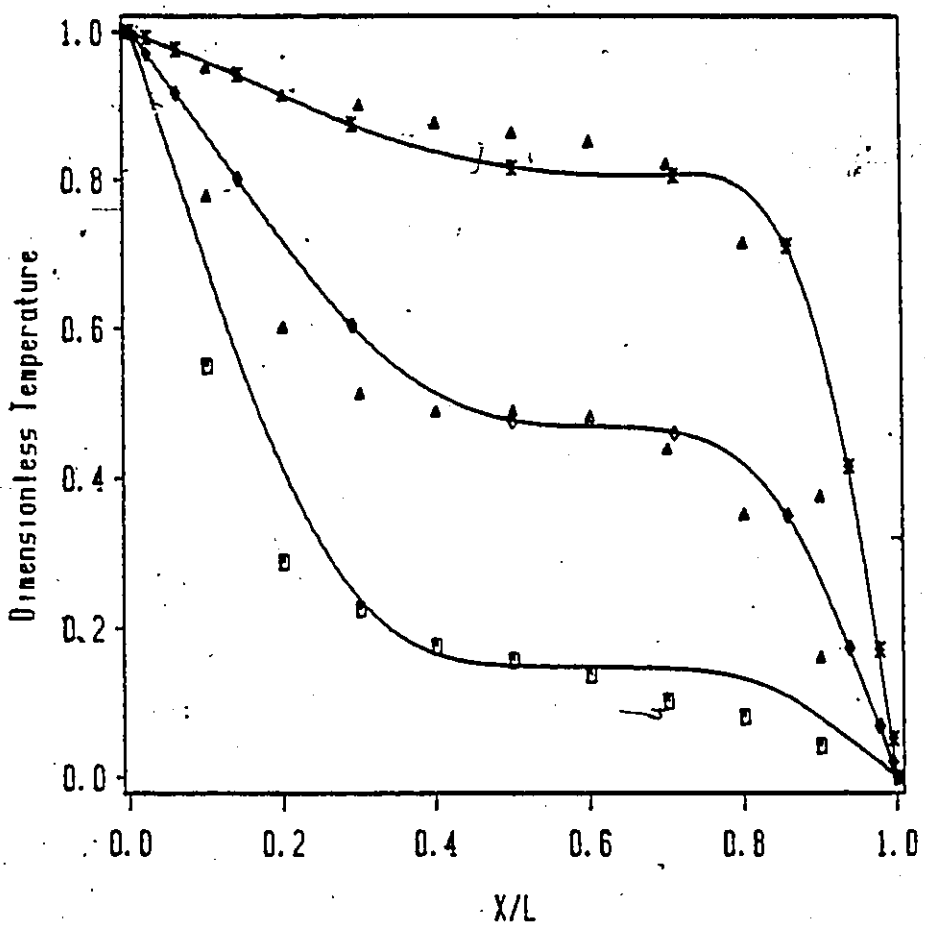

Figure 5.8: Temperature profiles for A=5, Gr=2.39E4. Comparison with experimental values of Duxbury(1974).

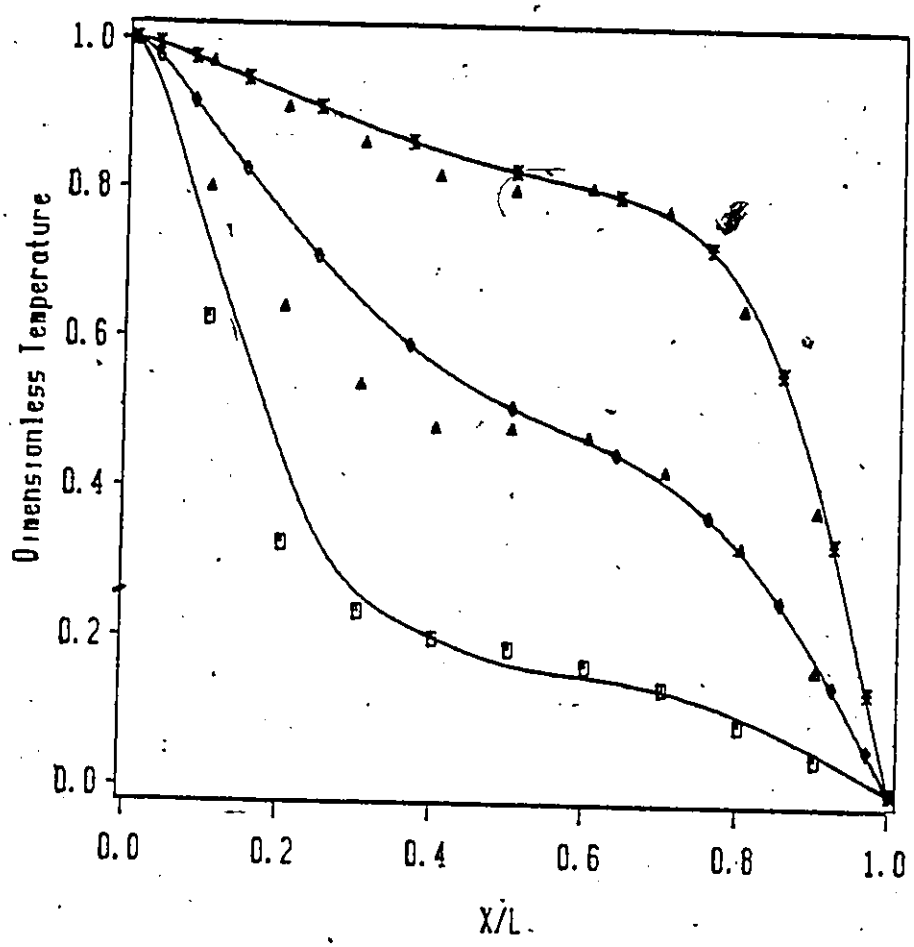

Figure 5.9: Temperature profiles for A=10. Gr=2.44E4. Comparison with experimental values of Duxbury(1974).

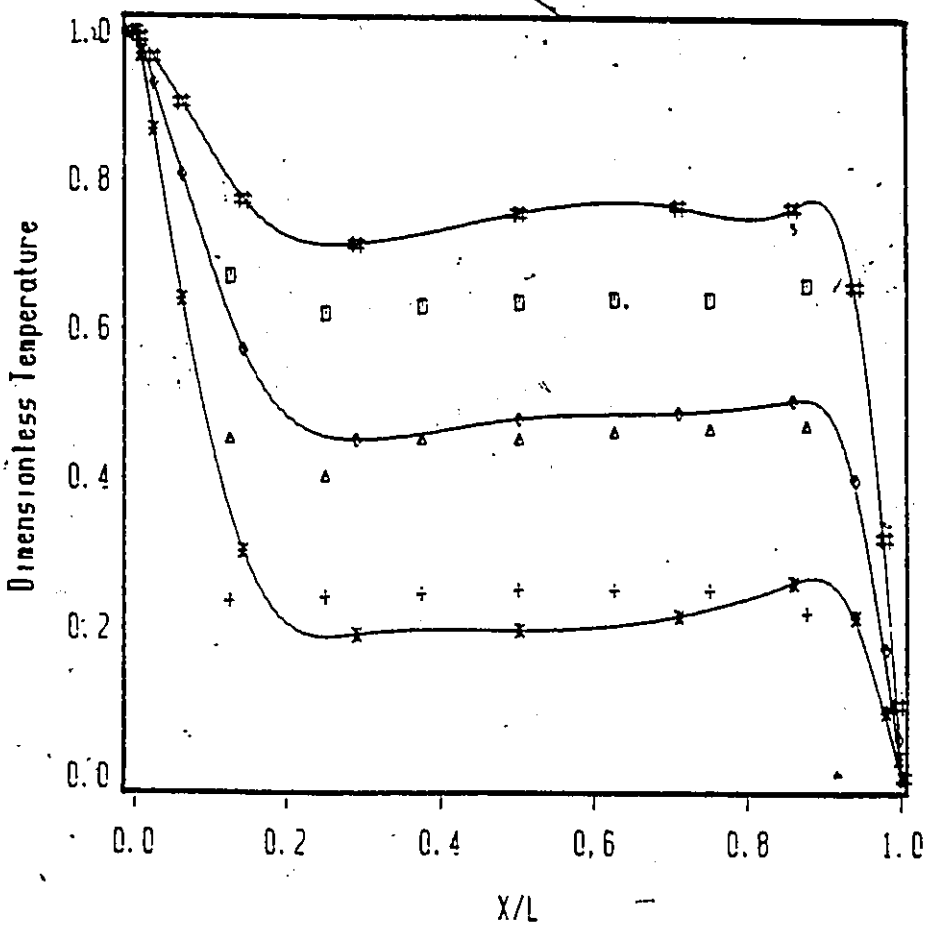

Figure 5.10: Temperature profiles for A=6.5, Gr=1.07E6. Comparison with experimental values of Yin(1978).

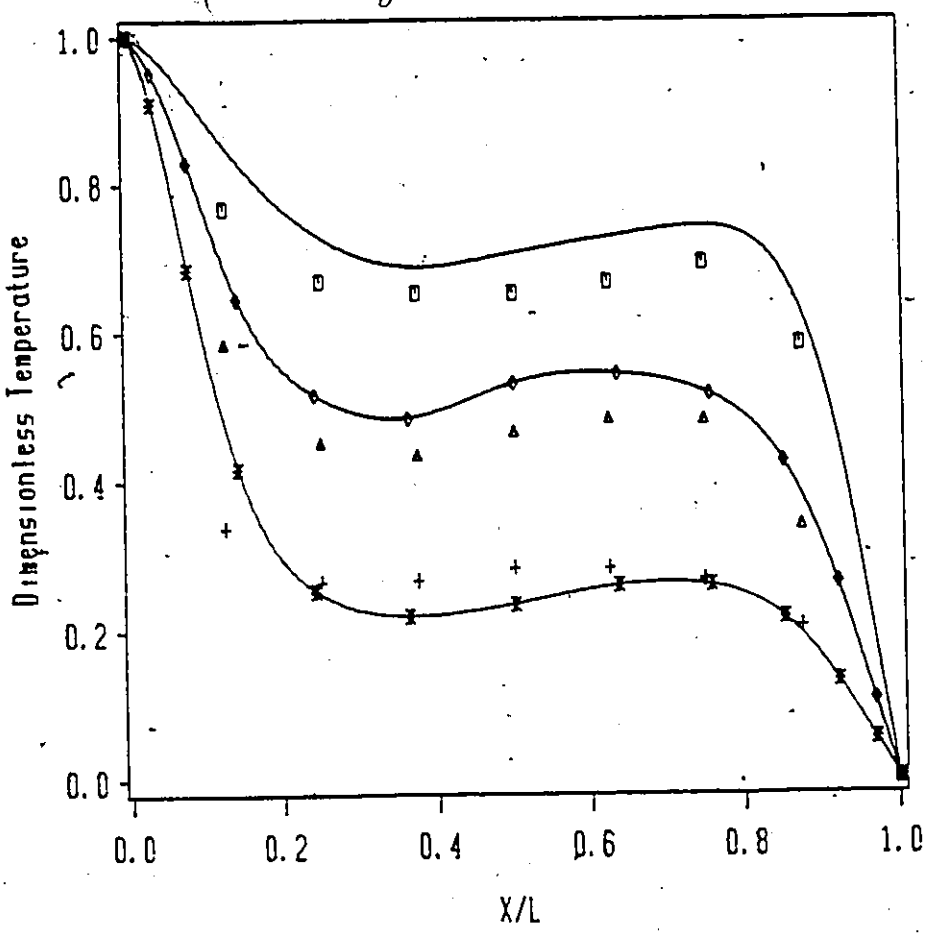

LEGEND —— Y/L=.85 ◆—◆—◆ Y/L=.5 ✕—✕—✕ Y/L=.15
□ □ □ Yin Y/L=.85 ▲ ▲ ▲ Yin Y/L=.5 + + + Yin Y/L=.15

Figure 5.11: Temperature profiles for A=9.8, Gr=3.3E5. Comparison with experimental values of Yin(1978).

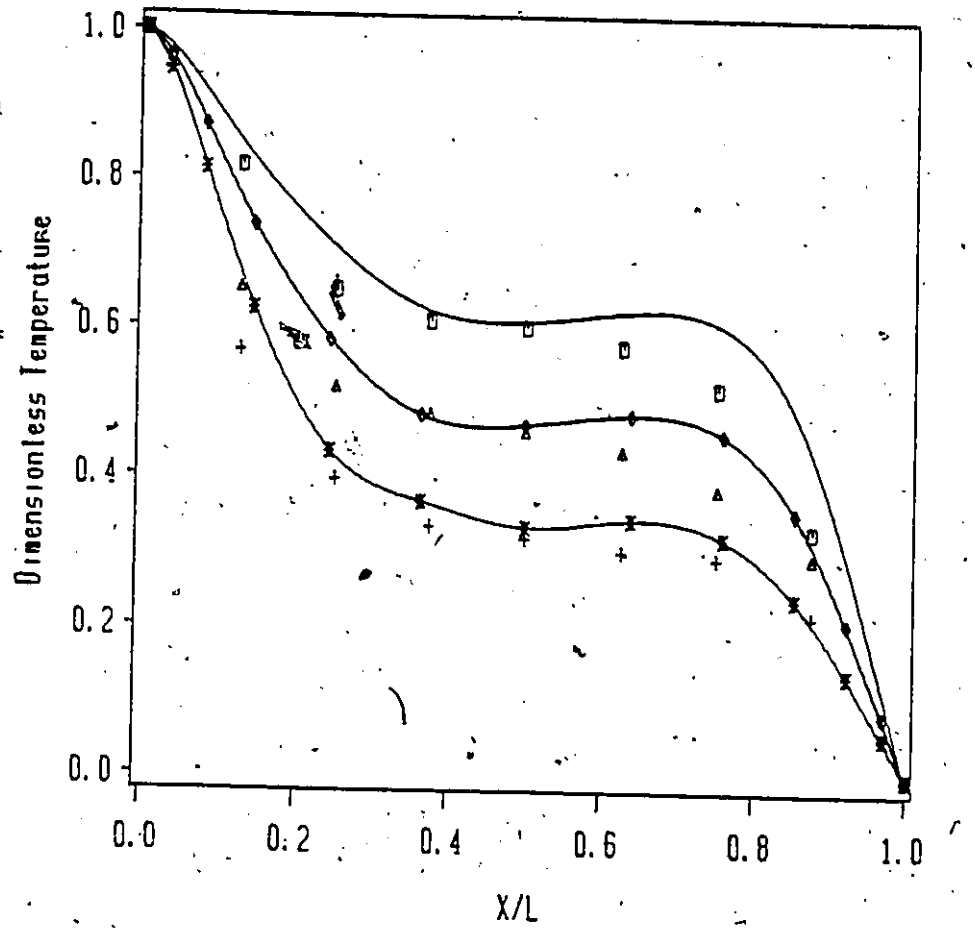

Figure 5.12: Temperature profiles for A=13.1, Gr=1.38E5. Comparison with experimental values of Yin(1978).

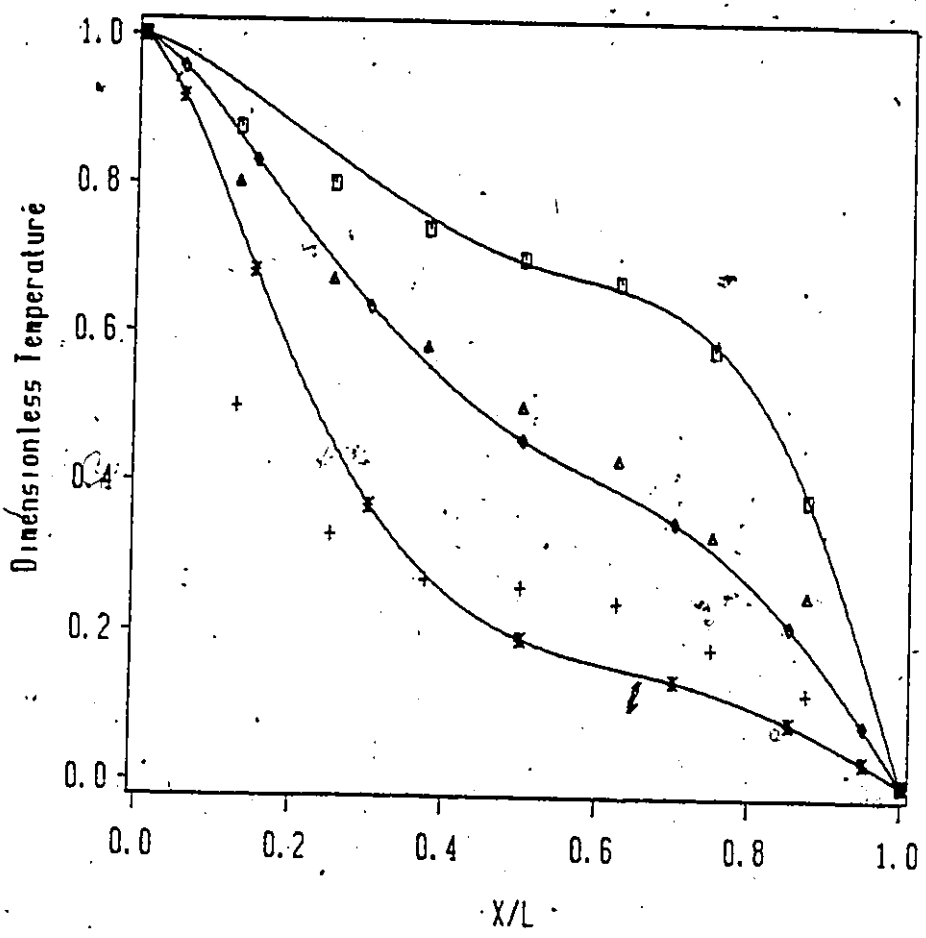

LEGEND —— Y/L=.85 ◆—◆—◆ Y/L=.5 ✕—✕—✕ Y/L=.15
□ □ □ Yin Y/L=.85 △ △ △ Yin Y/L=.5 + + + Yin Y/L=.15

Figure 5.13: Temperature profiles for A=19.6, Gr=4.22E4. Comparison with experimental values of Yin(1978).

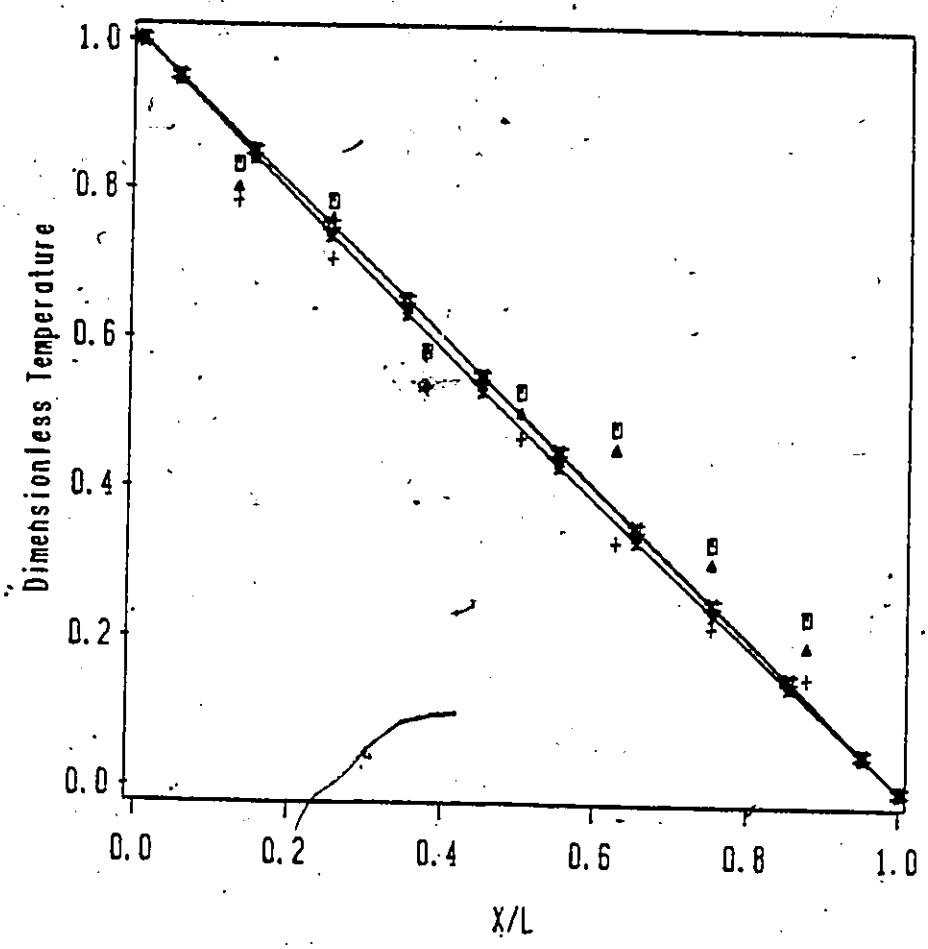

LEGEND
Y/L=.85
Yin Y/L=.85
Y/L=.5
Yin Y/L=.5
Y/L=.15
Yin Y/L=.15

Figure 5.14: Temperature profiles for A=39.2, Gr=4.96E3. Comparison with experimental values of Yin(1978).

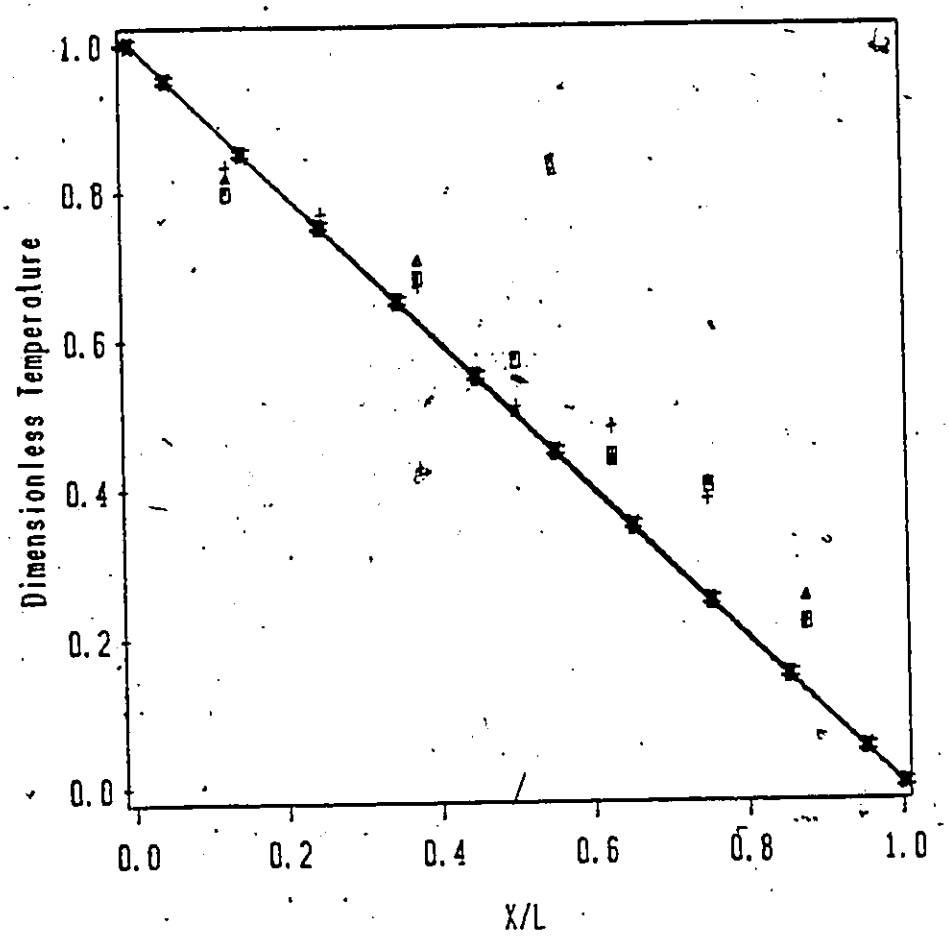

Figure 5.15: Temperature profiles for A=78.7, Gr=5.43E3. Comparison with experimental values of Yin(1978).

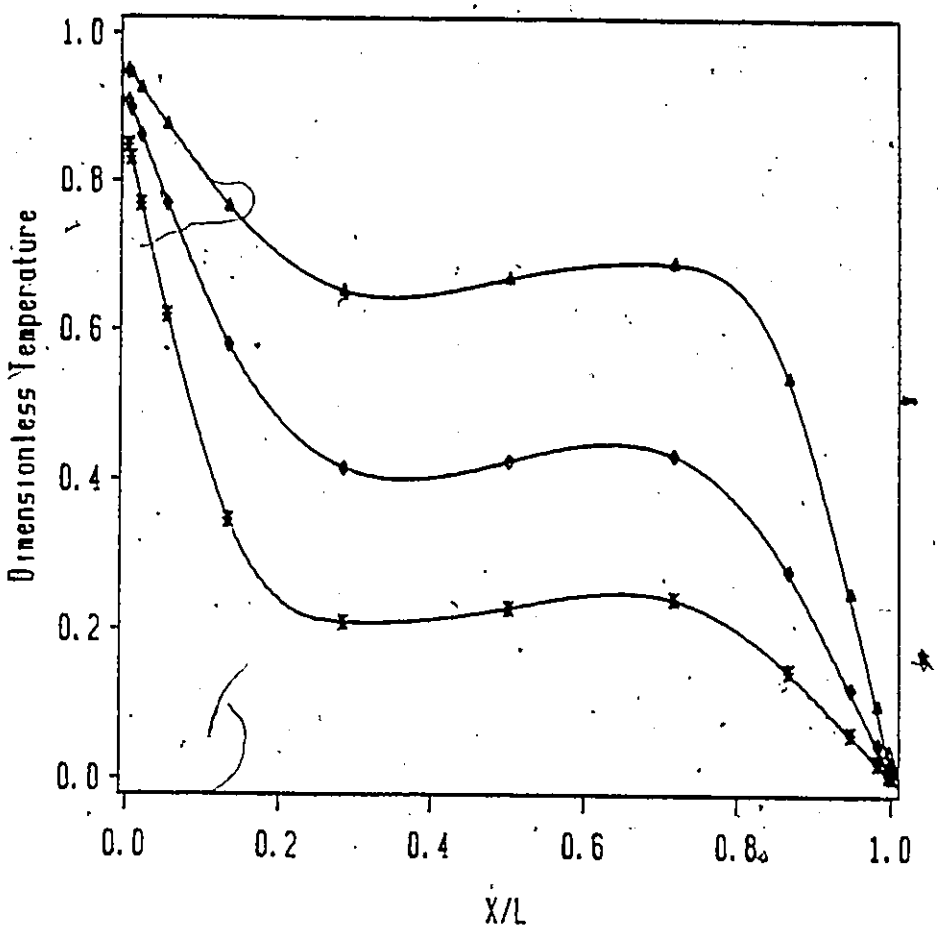

Figure 5.16: Temperature profiles for A=5, Gr=1.0E5, Hi=.007, Ho=.001. Si=0, So=0. Case B

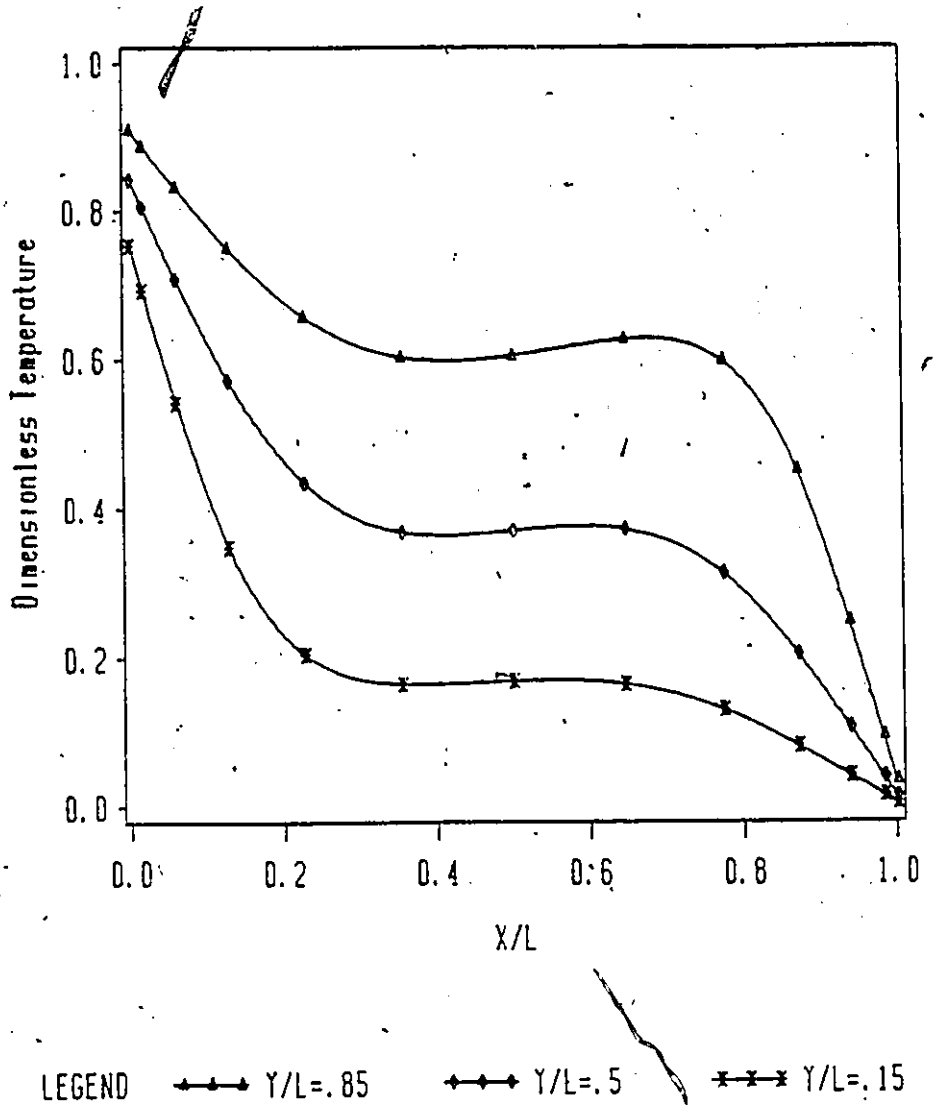

Figure 5.17: Temperature profiles for A=10, Gr=1.0E5, Hi=.007, Ho=.001. Si=0, So=0. Case B

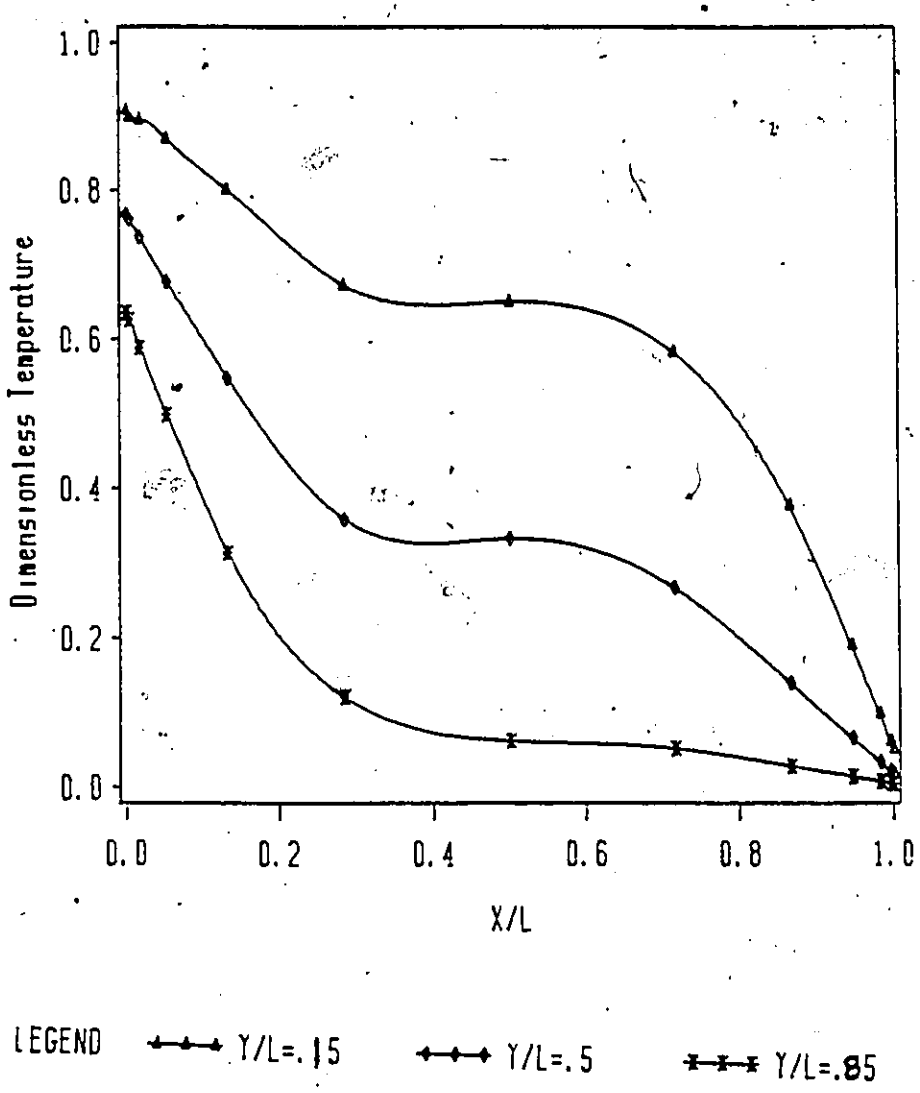

Figure 5.18: Temperature profiles for A=20, Gr=1.0E5, Hi=.007, Ho=.001. Si=0, So=0. Case B

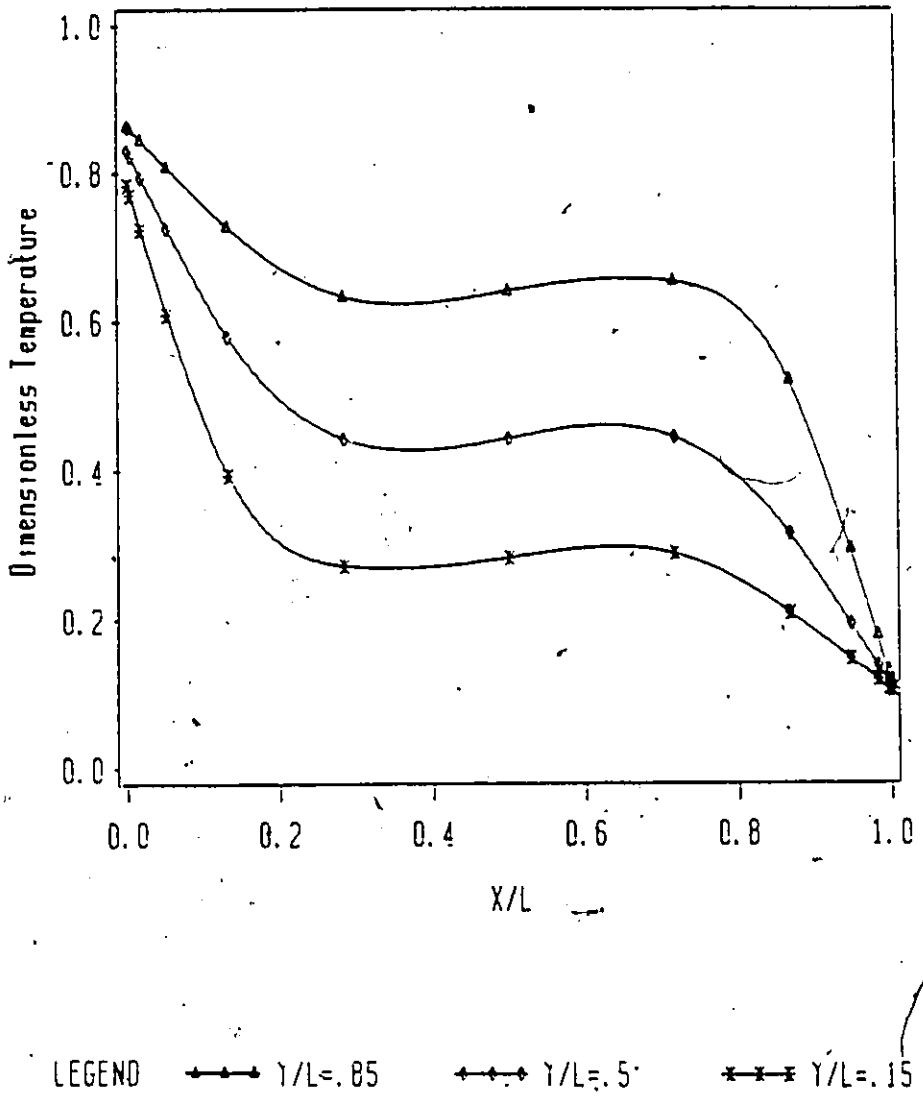

Figure 5.19: Temperature profiles for A=5, Gr=1.0E5, Si=.75, So=.13, N=1.333, Hi=.007, Ho=.001 Case C

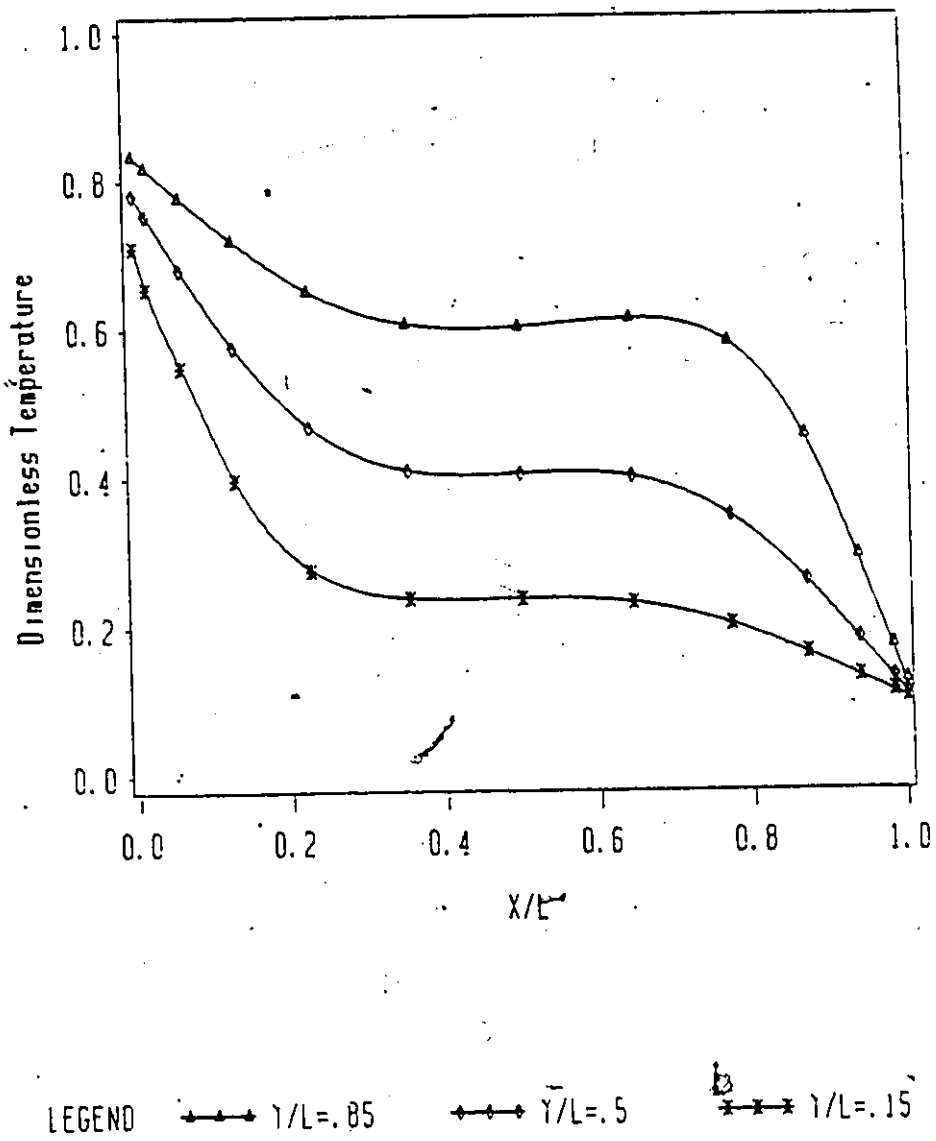

Figure 5.20: Temperature profiles for A=10, Gr=1.0E5, Si=.75, Si=.13. N=1.333, Hi=.007, Ho=.001 Case C

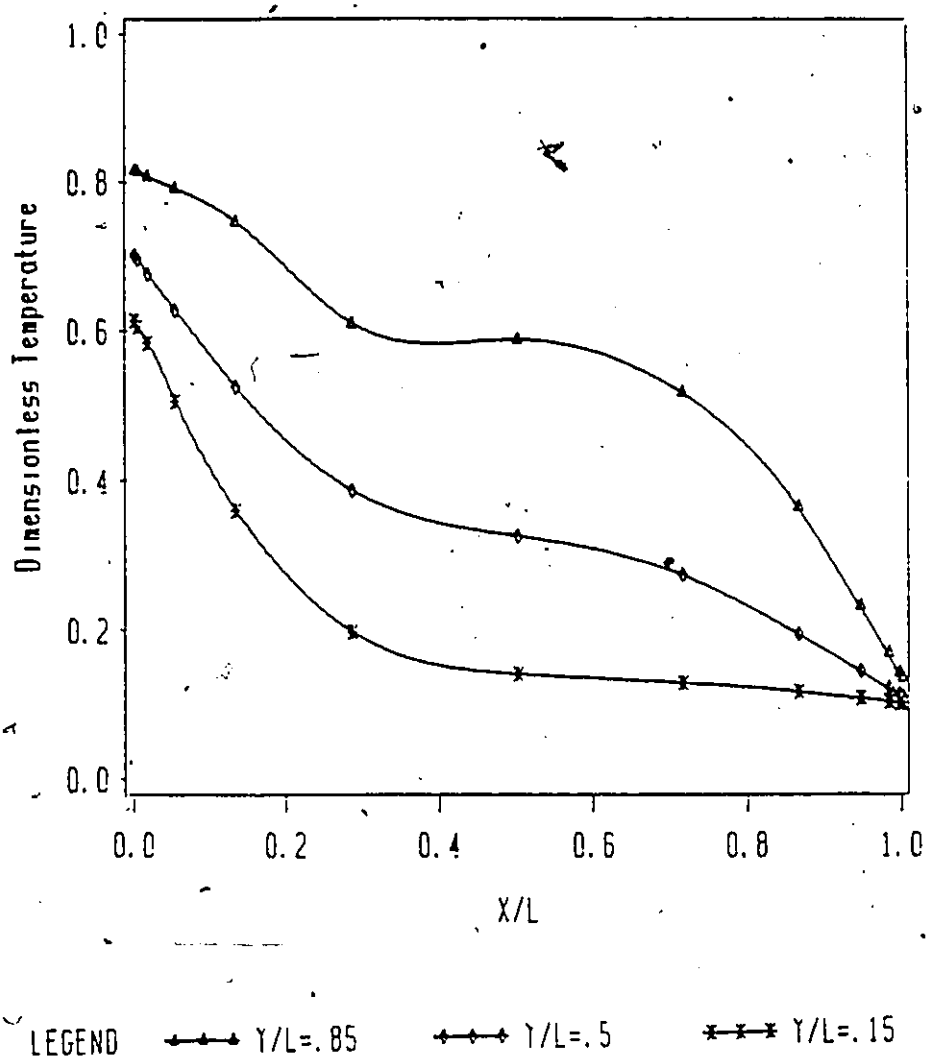

Figure 5.21: Temperature profiles for A=20, Gr=1.0E5, Si=.75, So=.13, N=1.333, Hi=.007, Ho=.001. Case C

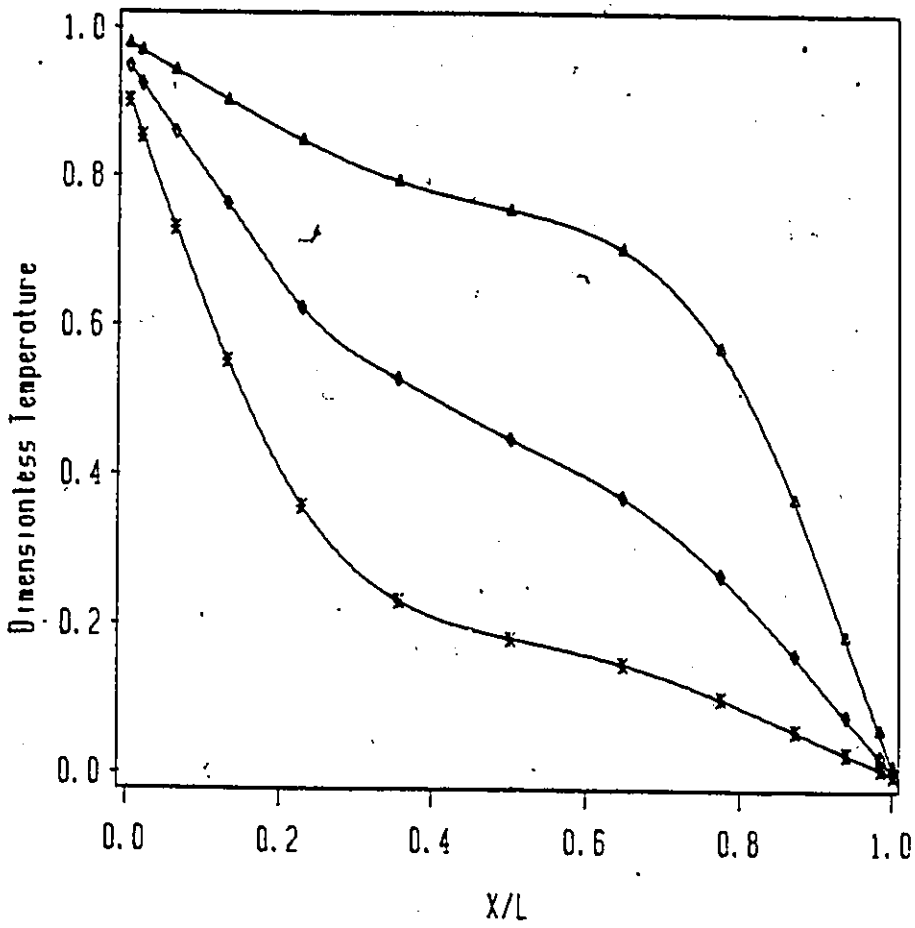

Figure 5.22: Temperature profiles for A=5, Gr=1.0E4, Hi=.007, Ho=.001. Si=0, So=0. Case B

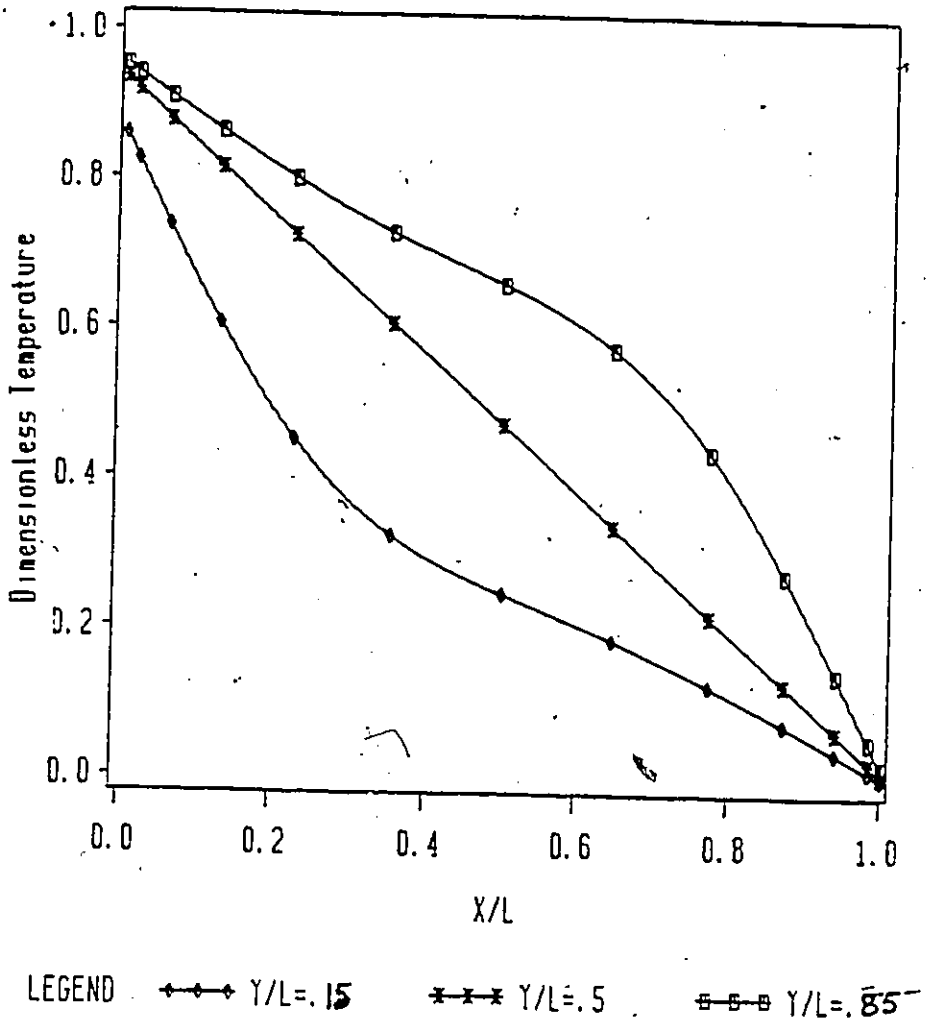

Figure 5.23: Temperature profiles for A=10, Gr=1.0E4, Hi=.007, Ho=.001. Si=0, So=0. Case B

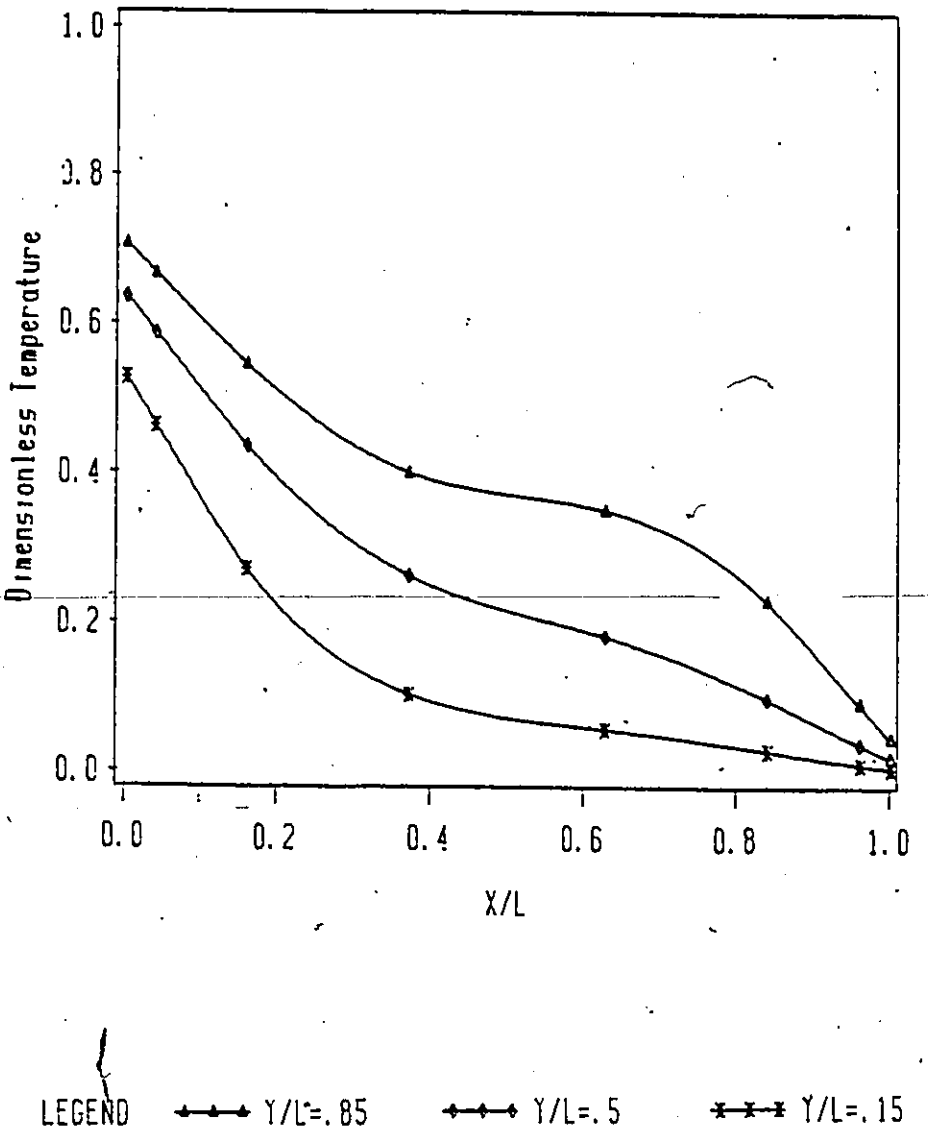

Figure 5.24: Temperature profiles for A=40, Gr=1.0E5, Hi=.007, Ho=.001, Si=0, So=0. Case B

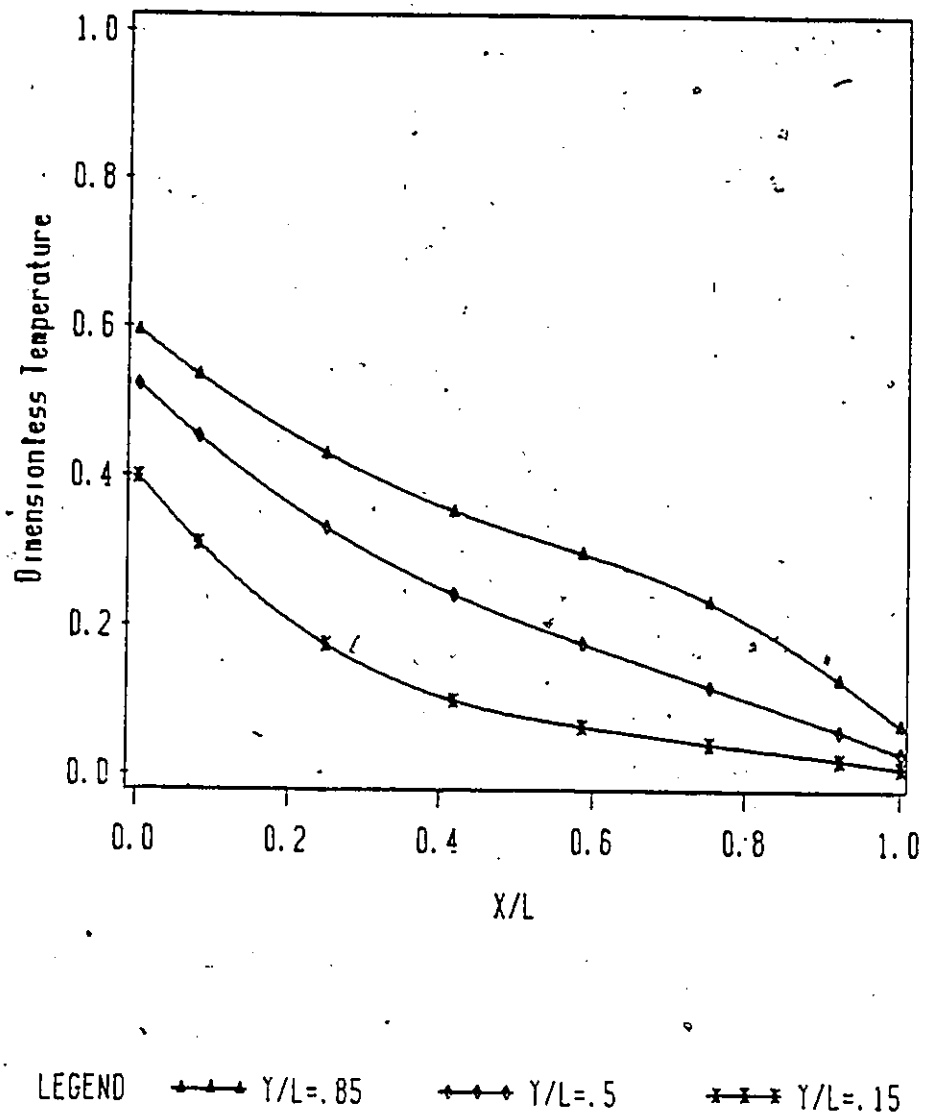

Figure 5.25: Temperature profiles for A=80, Gr=1.0E5, Hi=.007, Ho=.001, Si=0, So=0, Case B

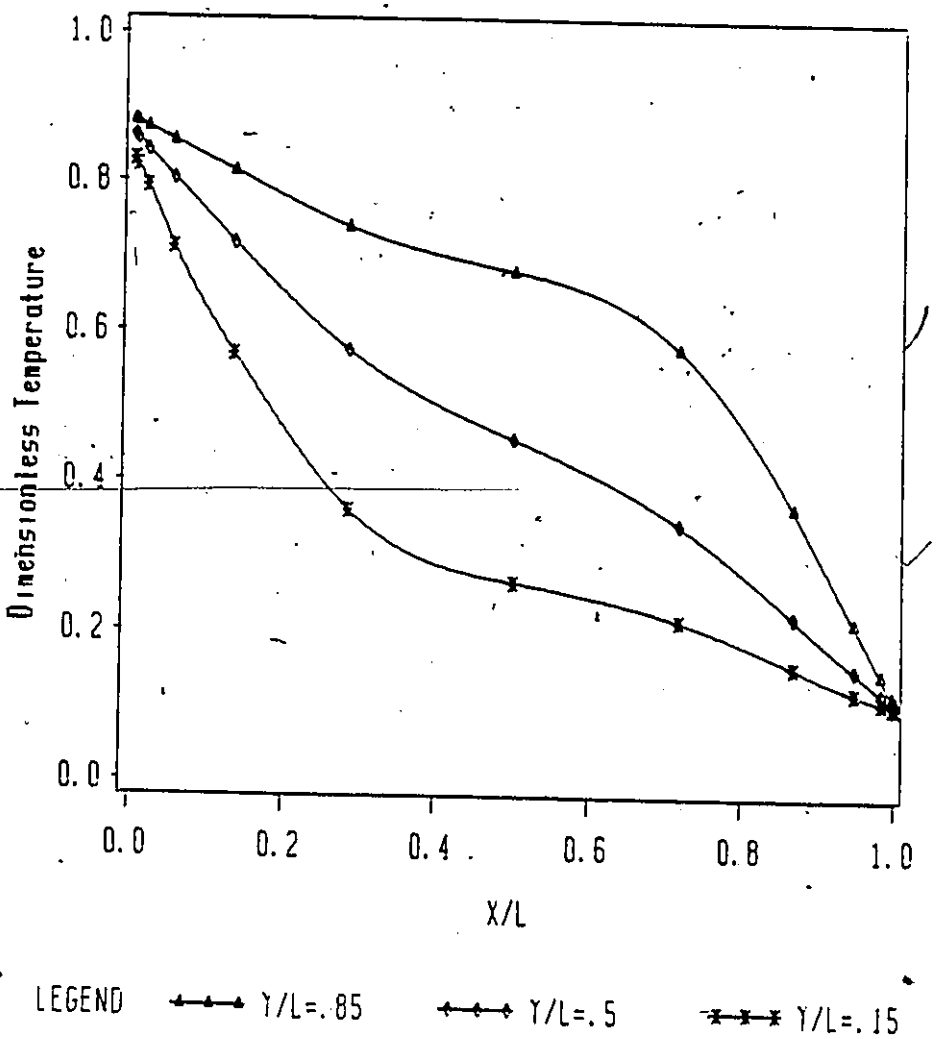

Figure 5.25: Temperature profiles for A=5, Gr=1.0E4, Si=.75, So=.13, N=1.333, Hi=.007, Ho=.001. Case C

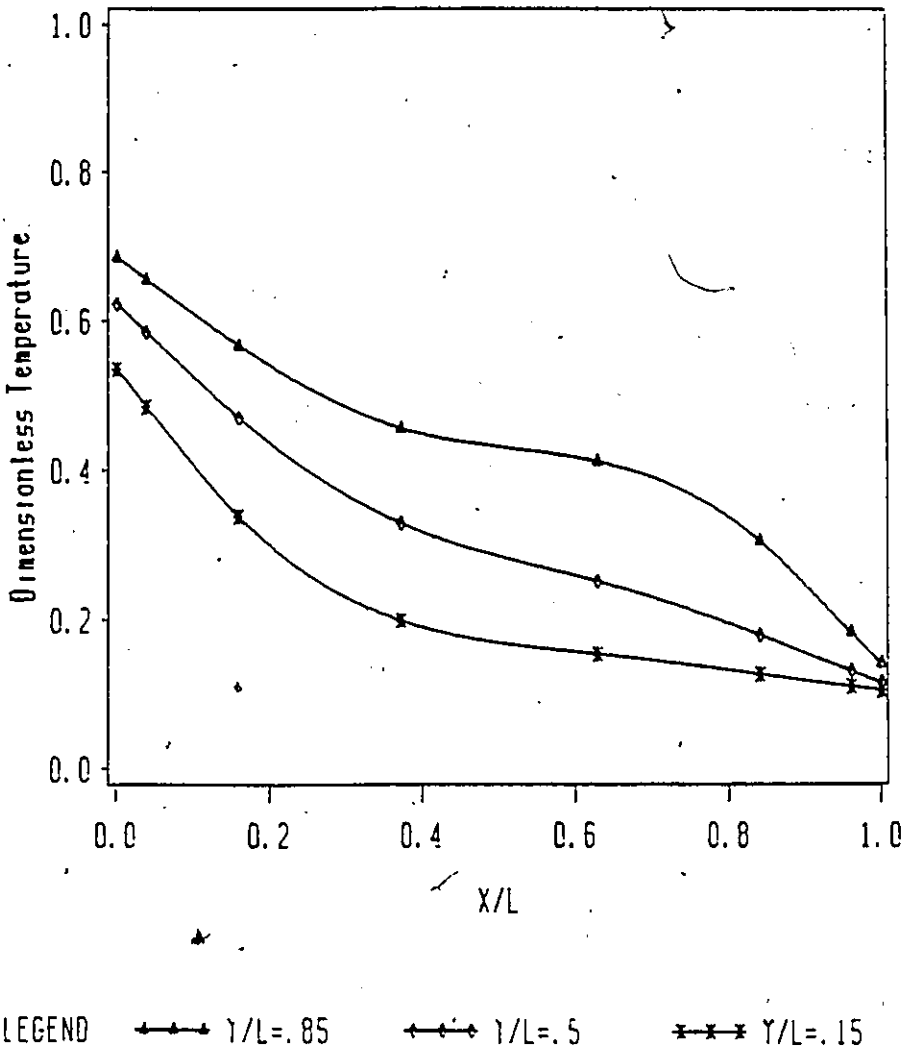

Figure 5.27: Temperature profiles for A=40, Gr=1.0E5, Si=.75, So=.13. N=1.333, Hi=.007, Ho=.001, Case C

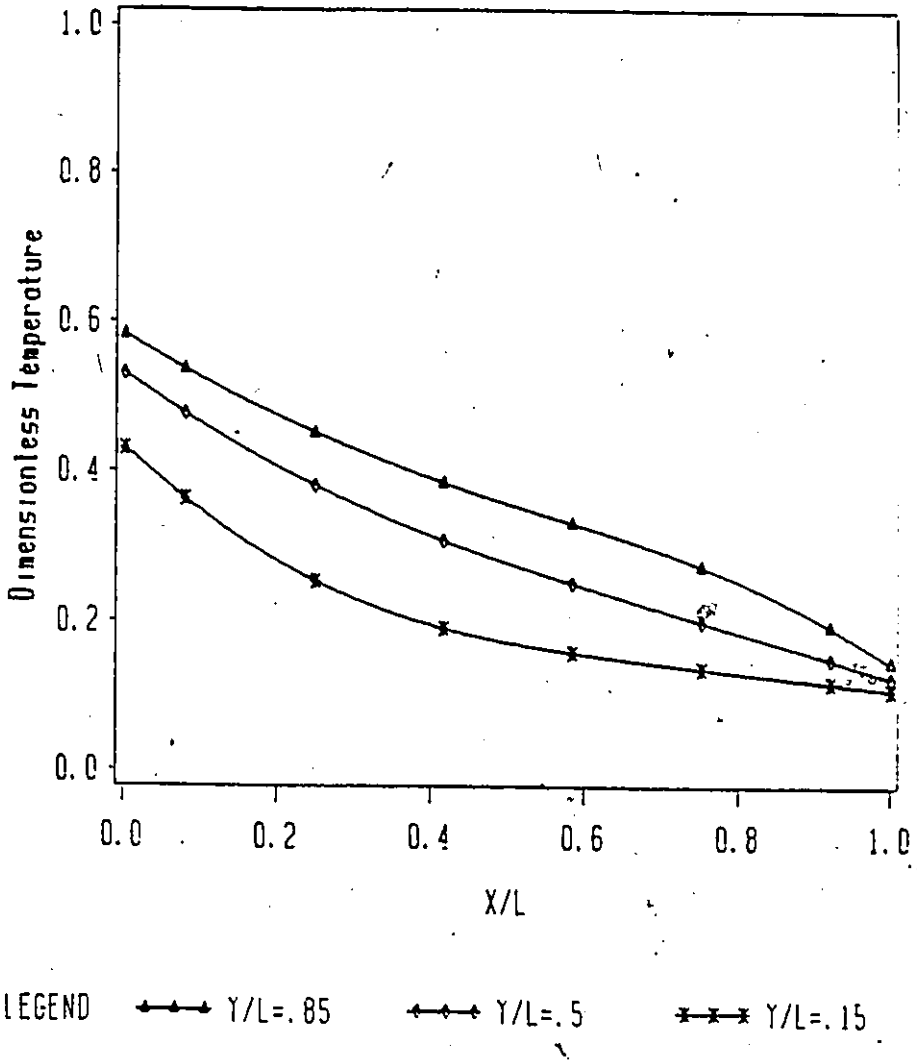

Figure 5.28: Temperature 'profiles' for A=80, Gr=1.0E5, Si=.75, So=.13. N=1.333, Hi=.007, Ho=.001. Case C

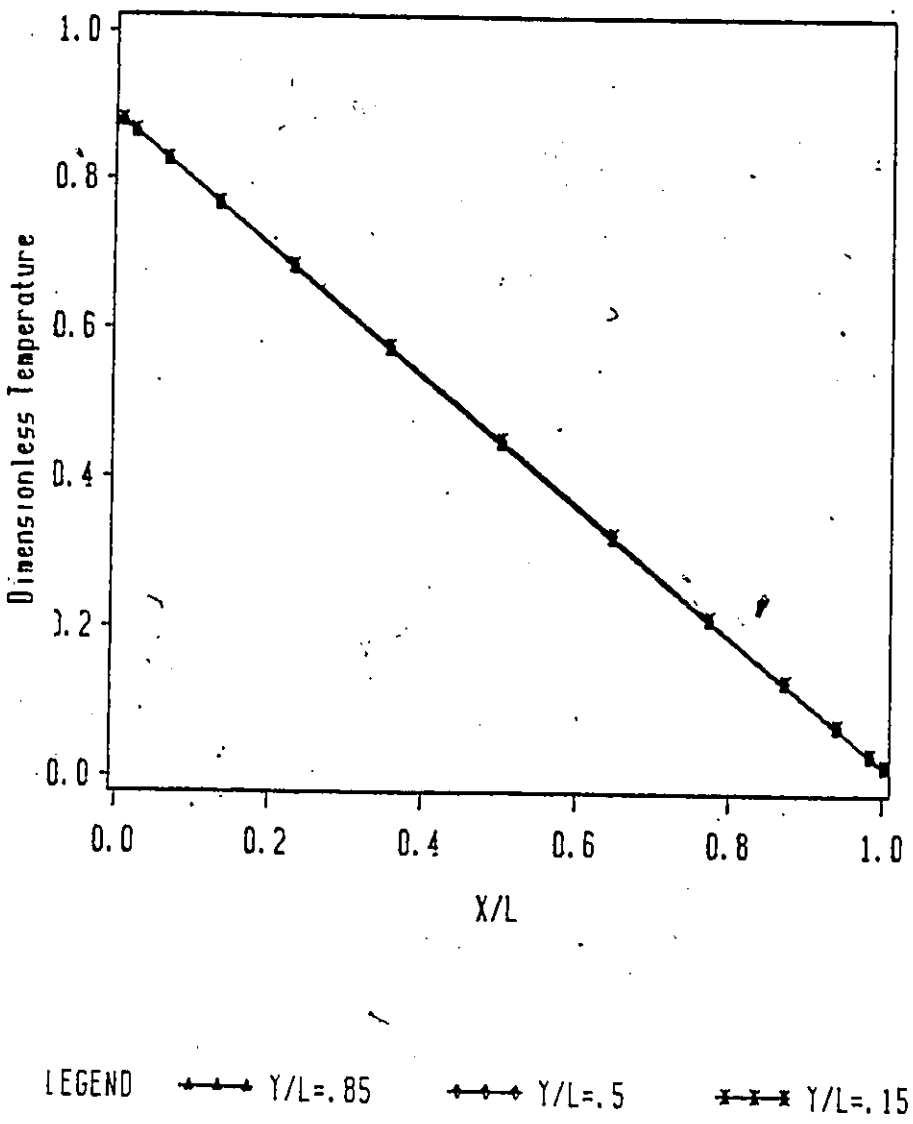

Figure 5.29: Temperature profiles for A=20, Gr=1.0E3, Hi=.007, Ho=.001. Si=0, Sc=0. Case B

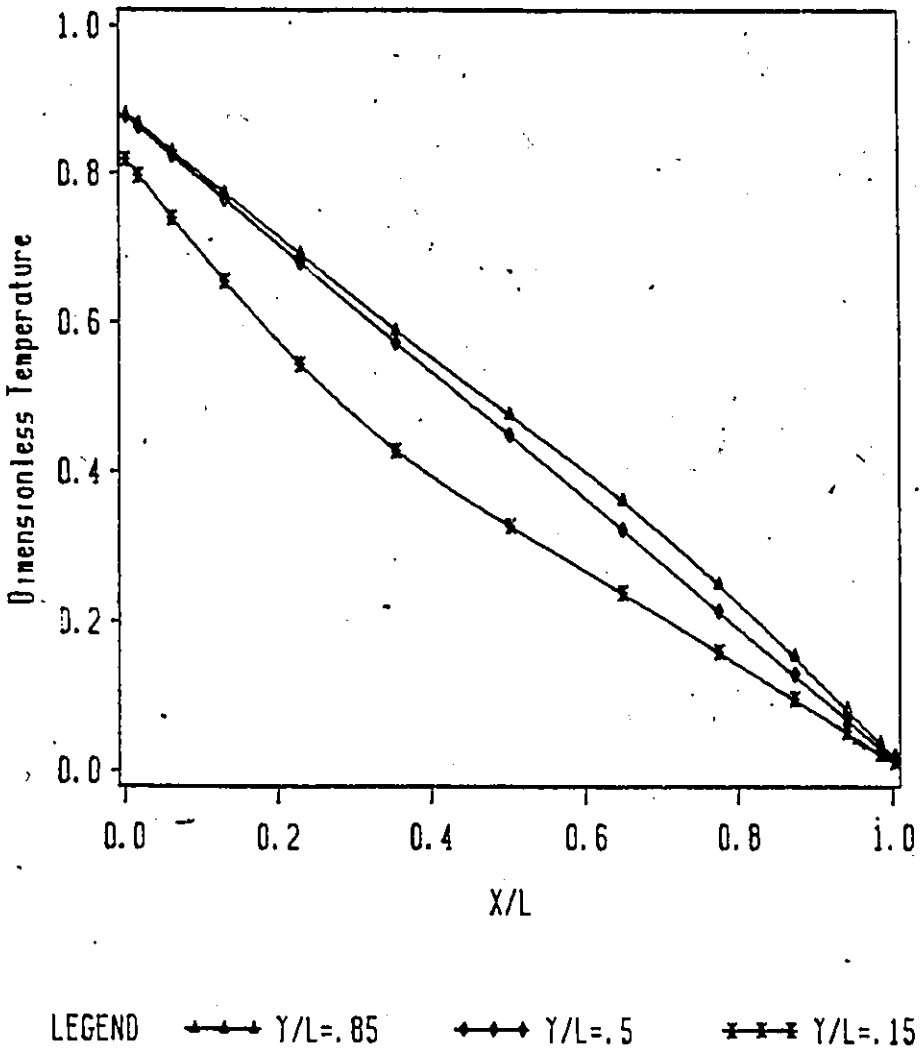

Figure 5.30: Temperature profiles for A=20, Gr=1.0E4, Hi=.007, Ho=.001, Si=0, So=0, Case B

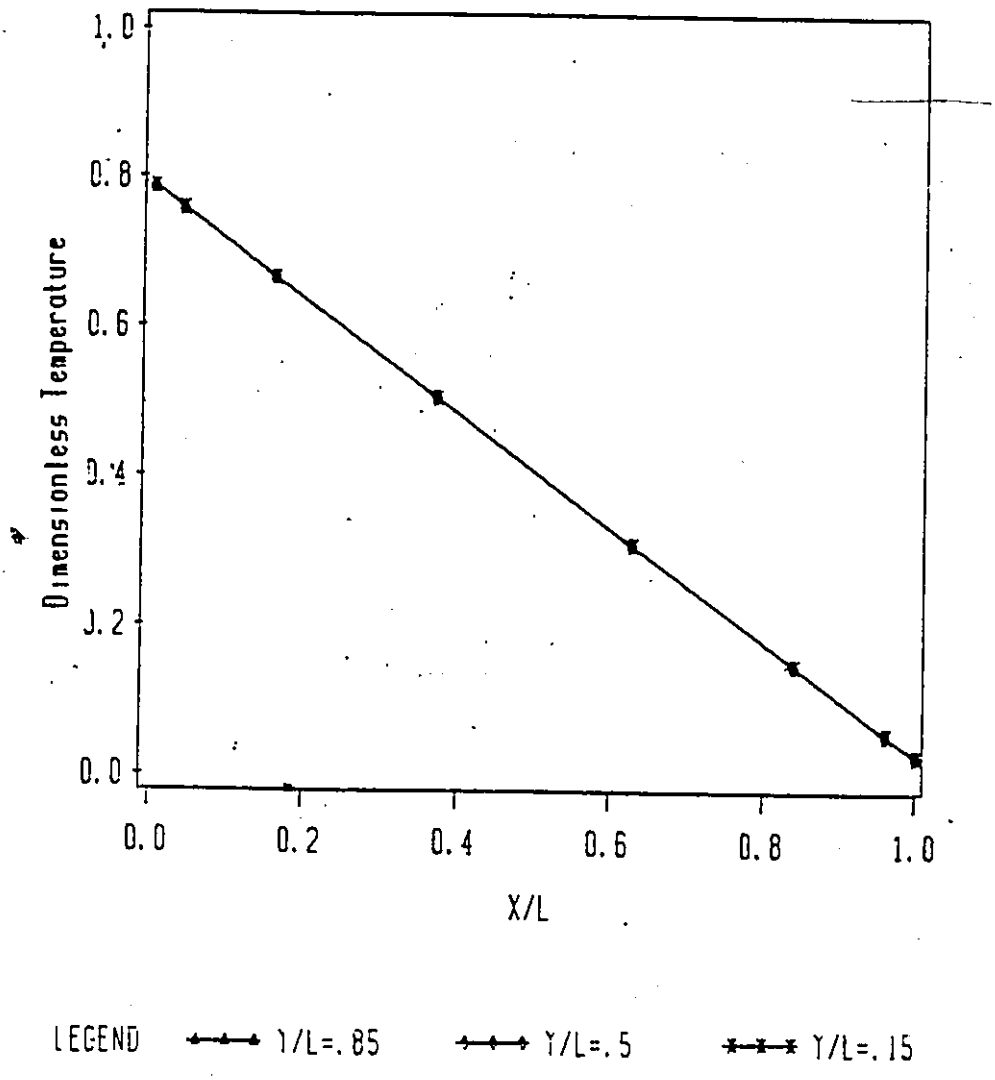

Figure 5.31: Temperature profiles for A=40, Gr=1.0E3, Hi=.007, Ho=.001, Si=0, So=0. Case B

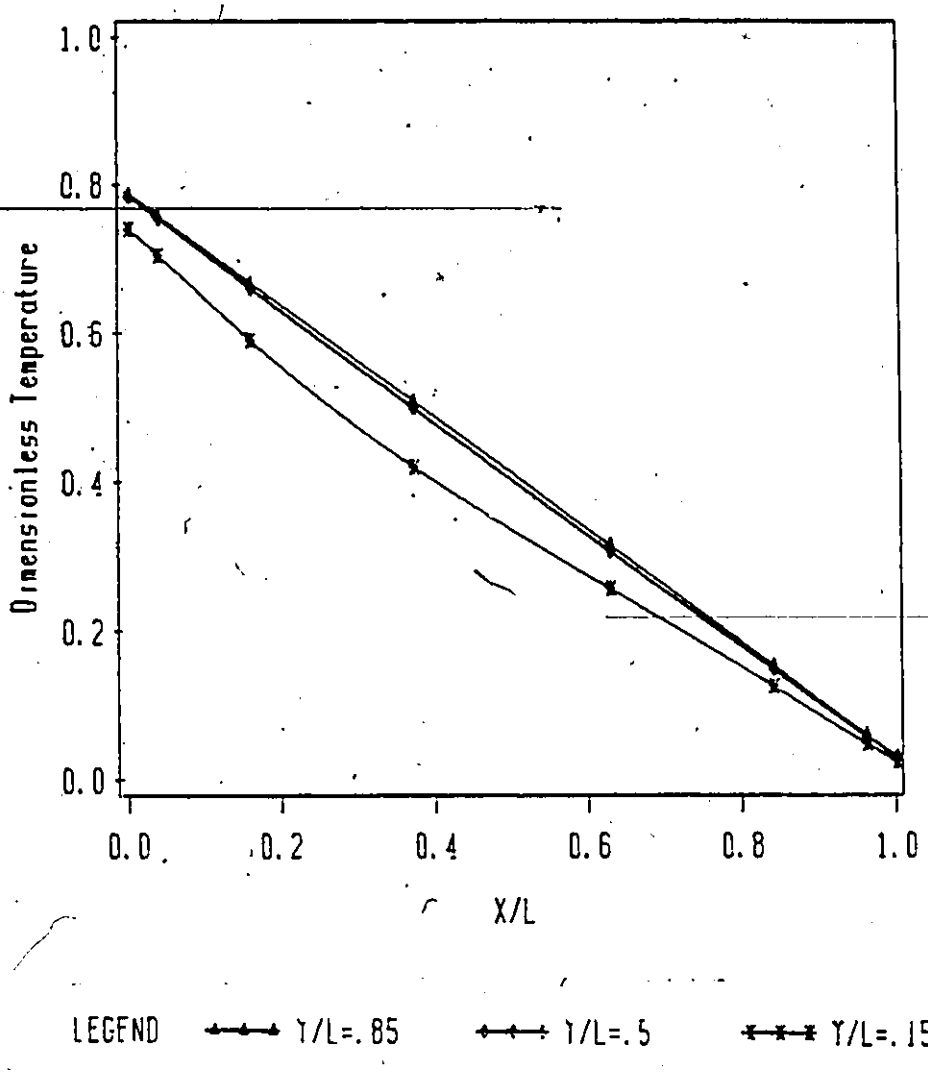

Figure 5.32: Temperature profiles for A=40, Gr=1.0E4, Hi=.007, Hi=.001. Si=0, So=0. Case B

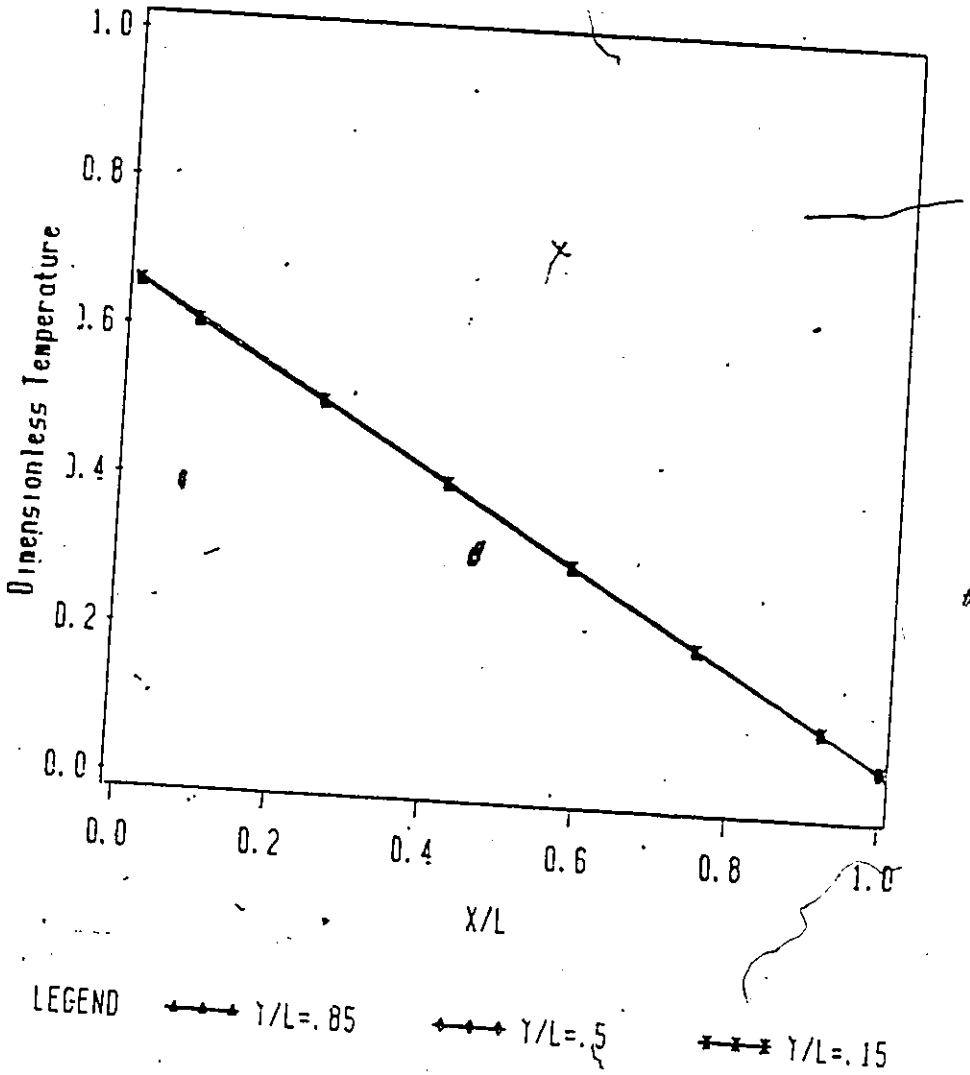

Figure 5.33: Temperature profiles for A=80, Gr=1.0E3, Hi=.007, Ho=.001. Si=0, So=0. Case B

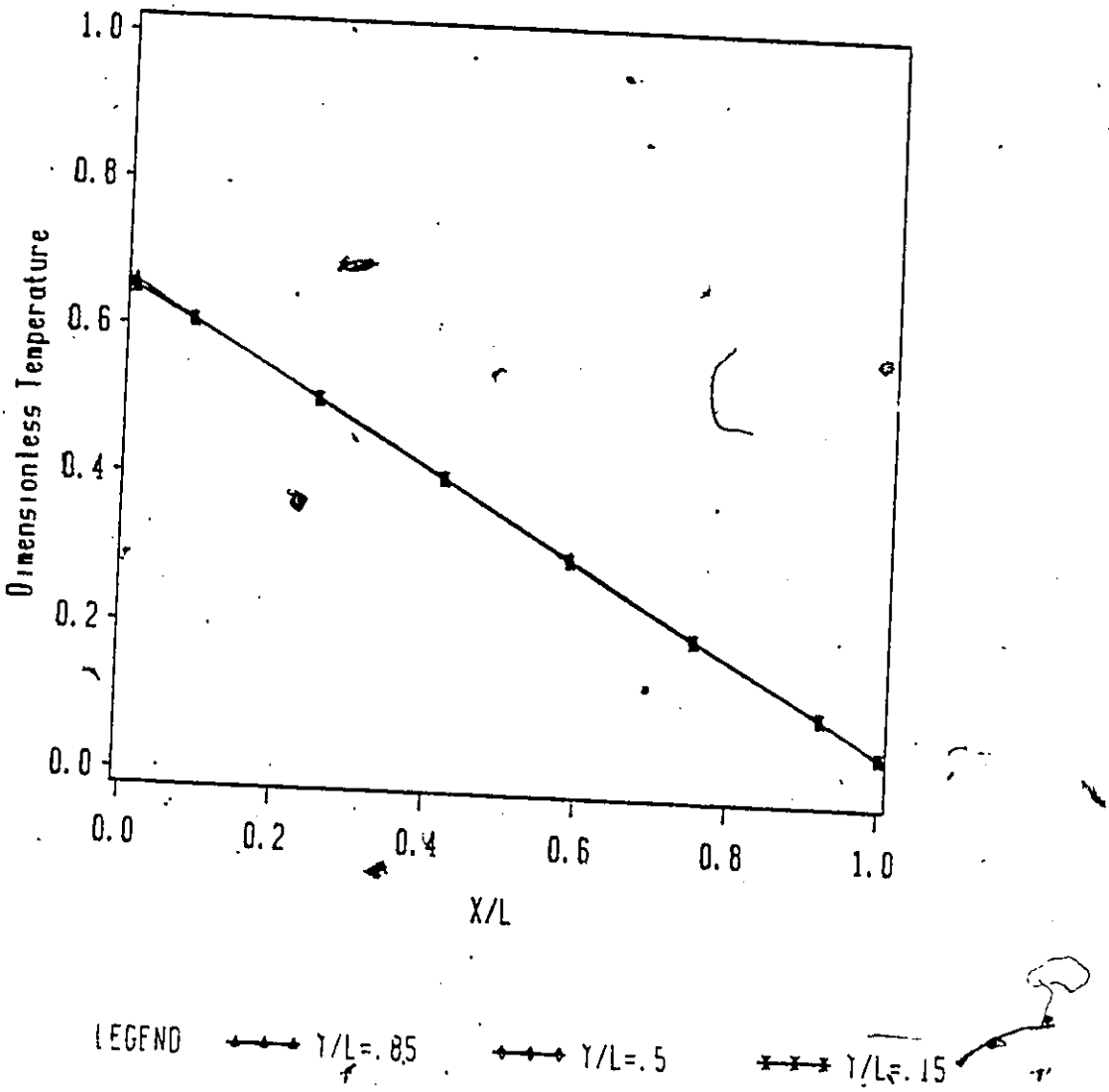

Figure 5.34: Temperature profiles for A=80. Gr=1.0E4. Hi=.007. Ho=.001. Si=0. So=0. Case B

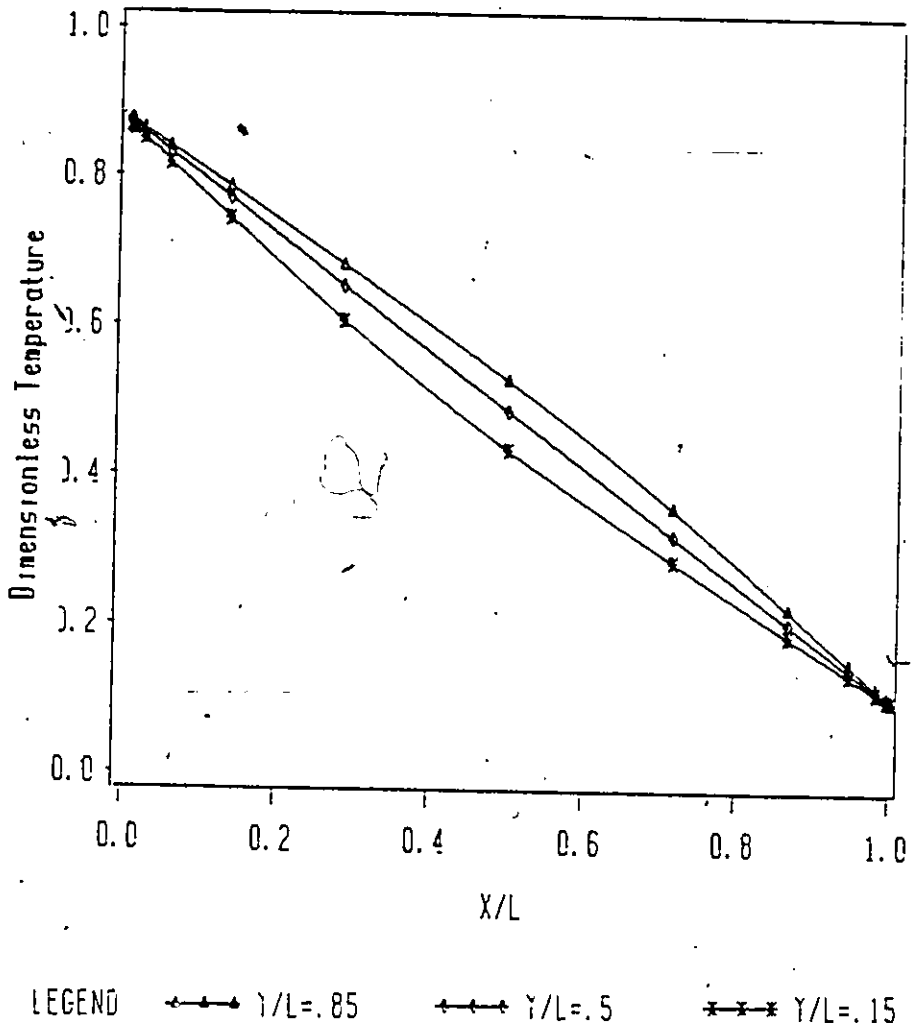

Figure 5.35: Temperature profiles for A=5, Gr=1.0E3, Si=.75, So=.13. N=1.333, Hi=.007, Ho=.001. Case C

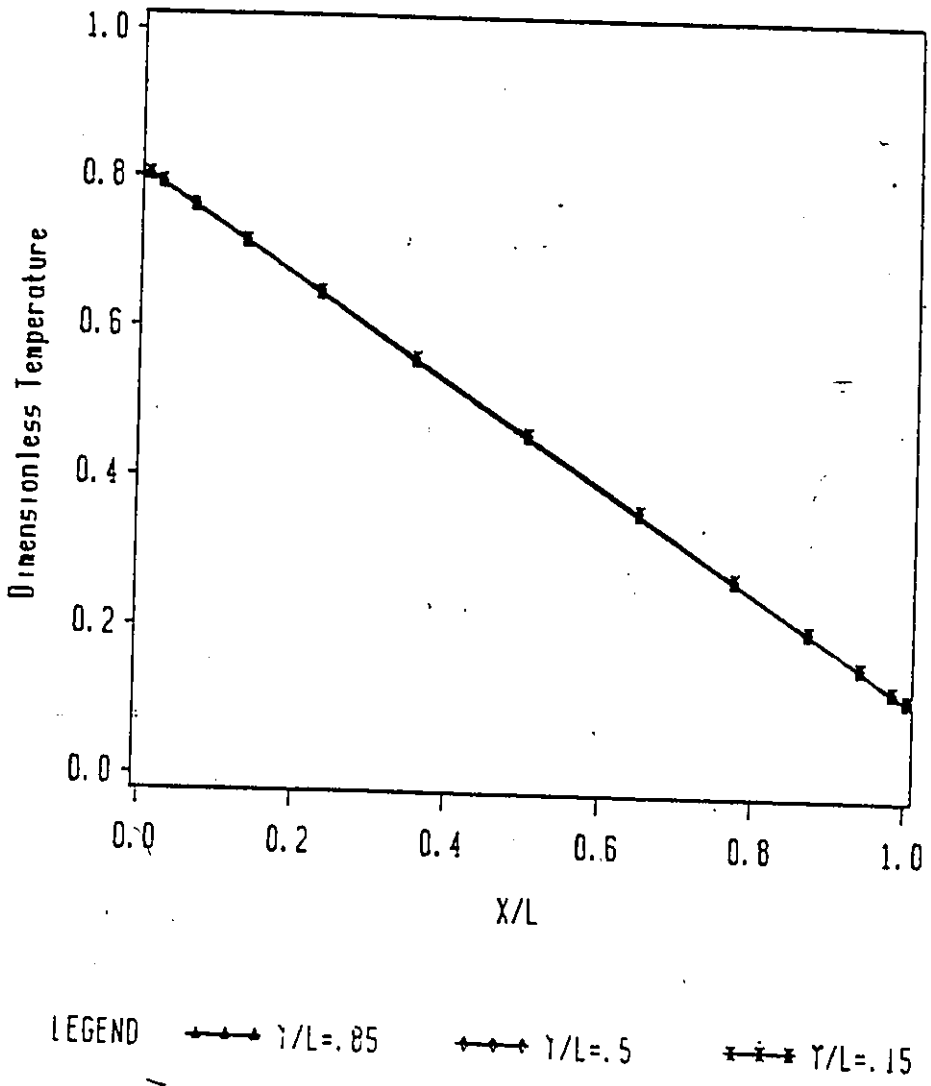

Figure 5.35: Temperature profiles for A=20, Gr=1.0E3, Si=.75, So=.13. N=1.333, Hi=.007, Ho=.001. Case C

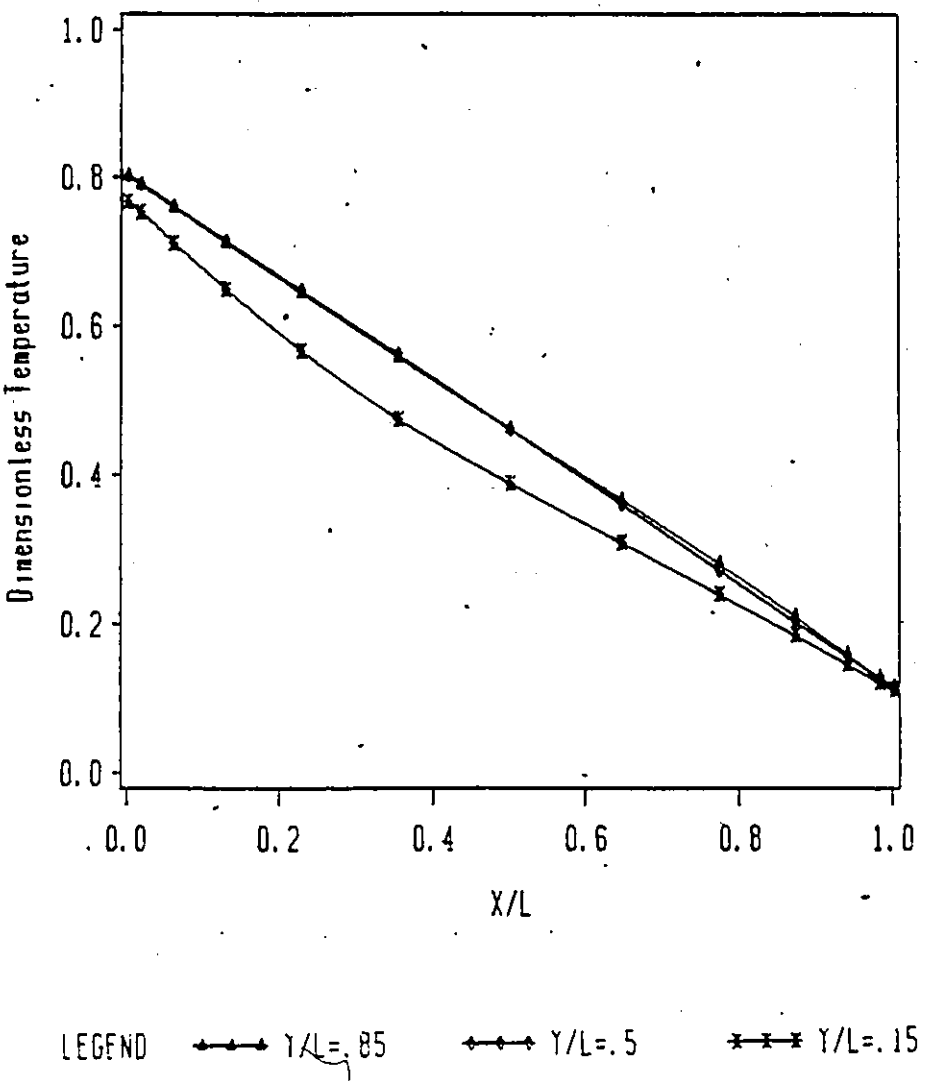

Figure 5.37: Temperature profiles for A=20, Gr=1.0E4, Si=.75, So=.13. N=1.333, Hi=.007, Ho=.001. Case C

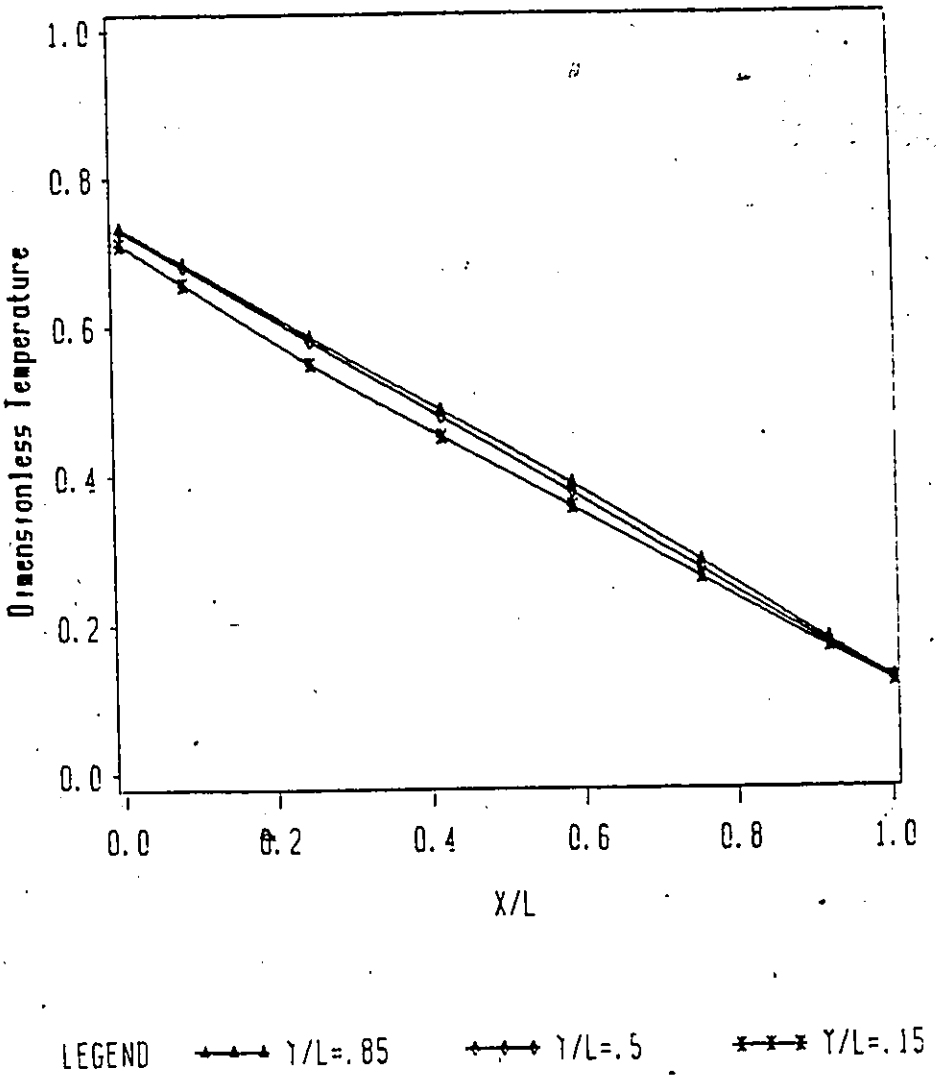

Figure 5.38: Temperature profiles for A=40, Gr=1.0E4, Si=.75, So=.13. N=1.333, Hi=.007, Ho=.001. Case C

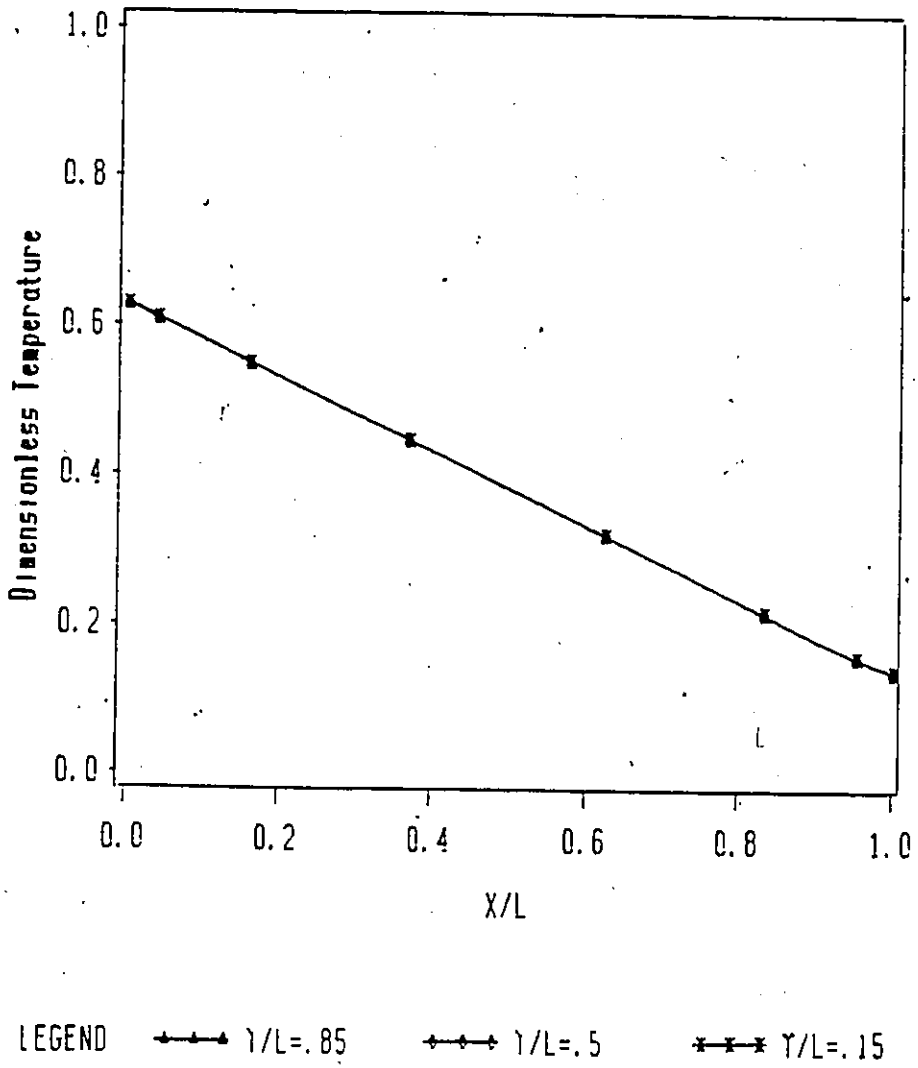

Figure 5.39: Temperature profiles for A=80, Gr=1.0E3, Si=.75, So=.13. N=1.333, Hi=.007, Ho=.001. Case C

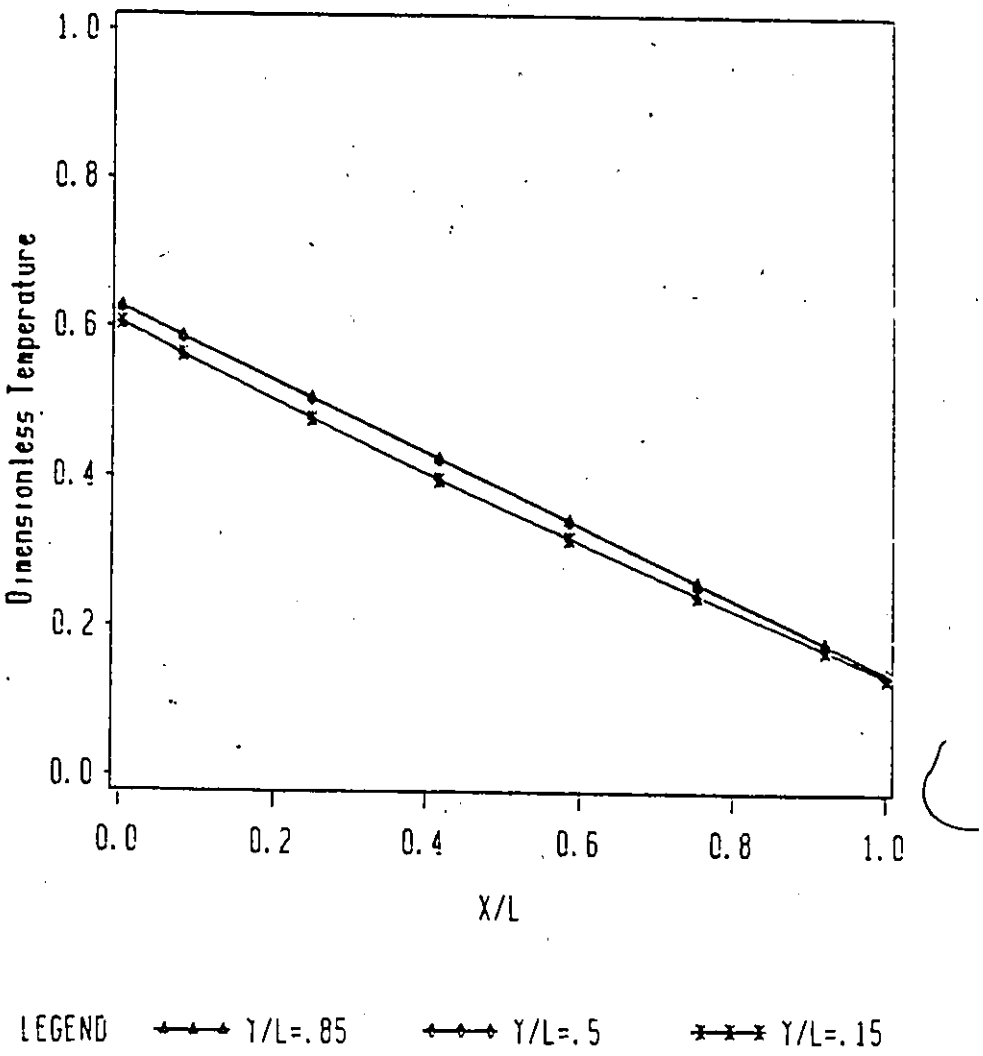

Figure 5.40: Temperature profiles for A=80, Gr=1.0E4, Si=.75, So=.13. N=1.333, Hi=.007, Ho=.001. Case C

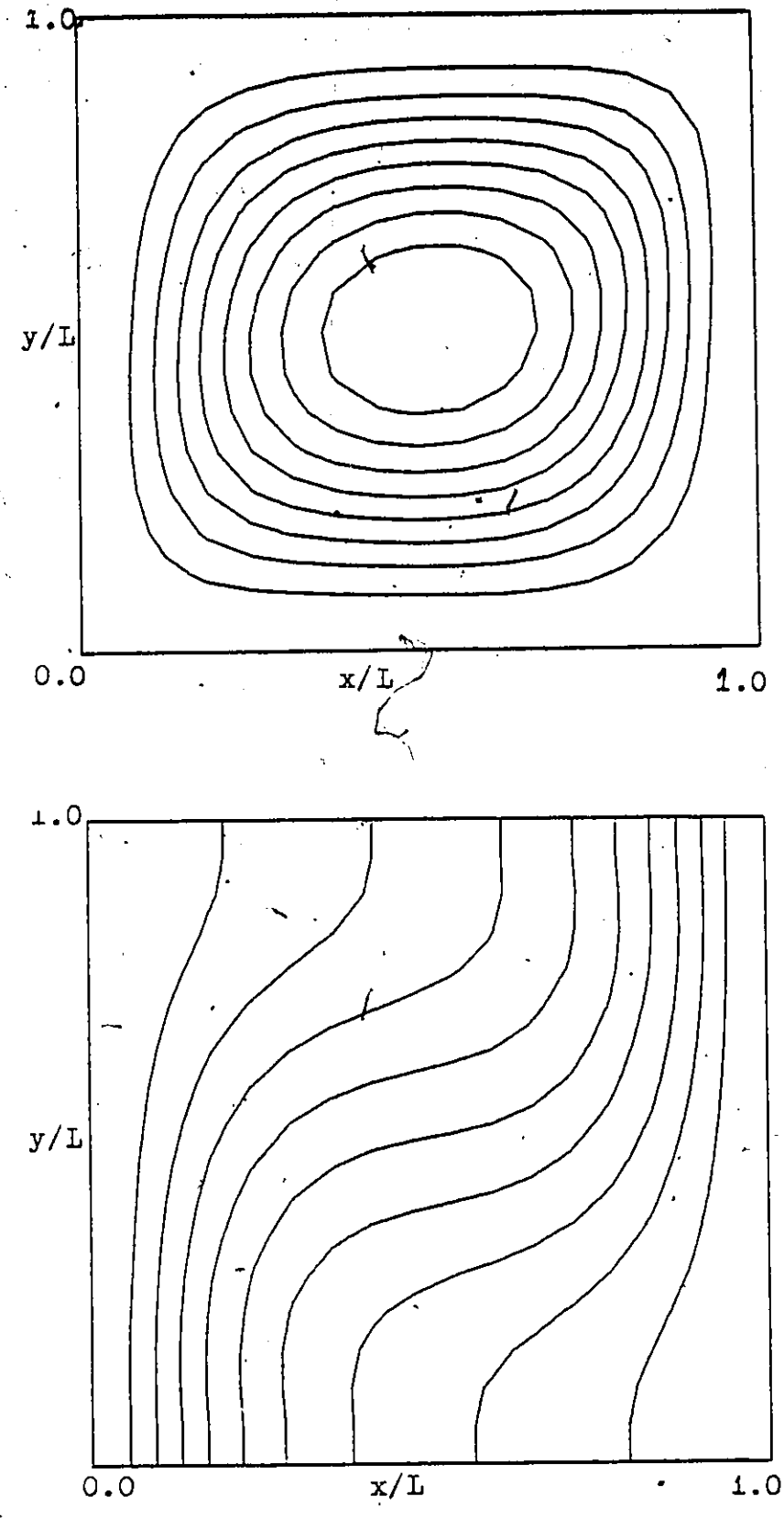

Figure 5.41: Streamlines and Isotherms for A=1, Gr=1.E4, Hi=.007, Ho=.001. Si=0, So=0. Case B

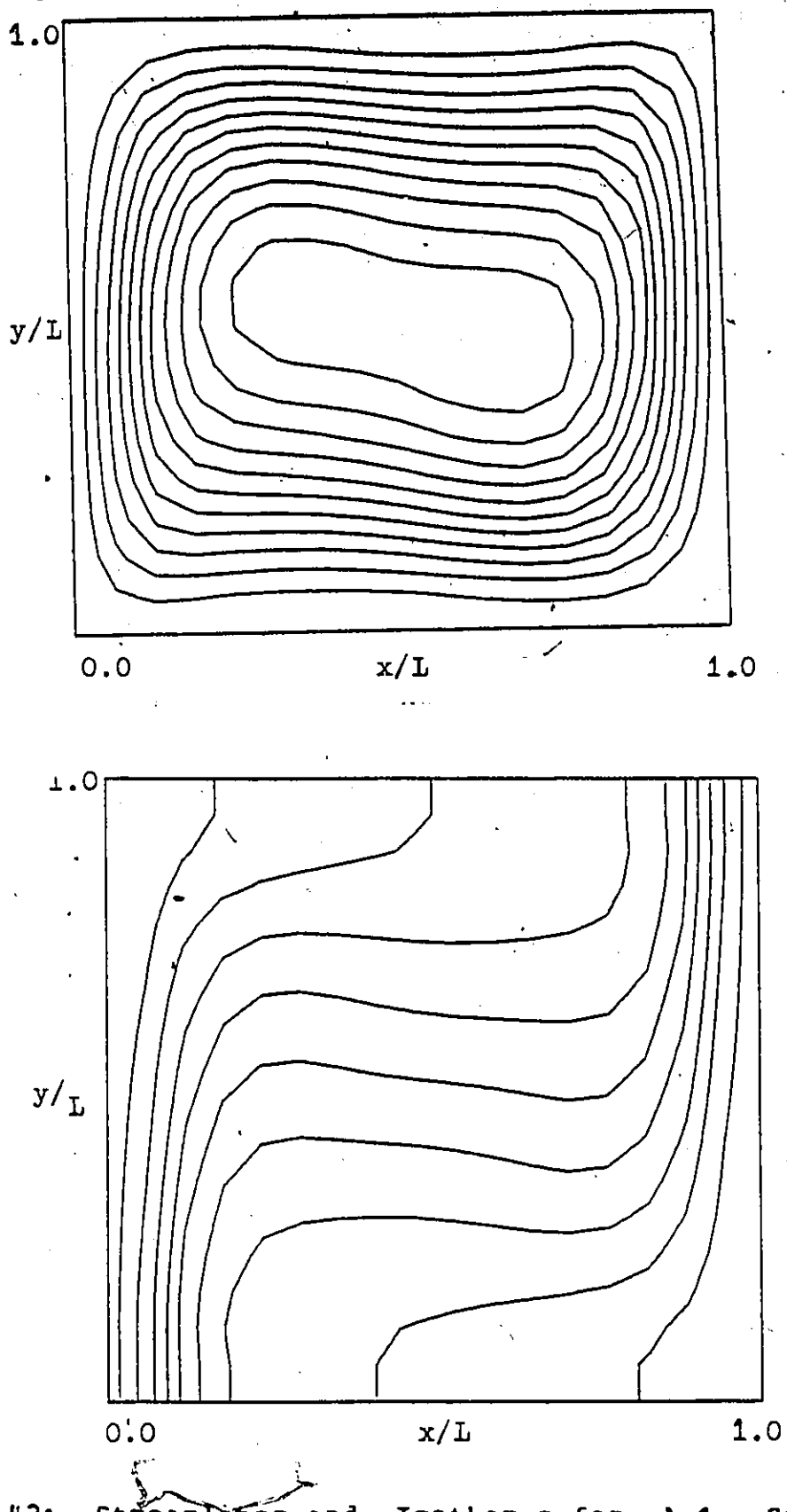

Figure 5.42: Streamlines and Isotherms for A=1, Gr=1.E5, Hi=.007, Ho=.001. Si=0, So=0. Case B

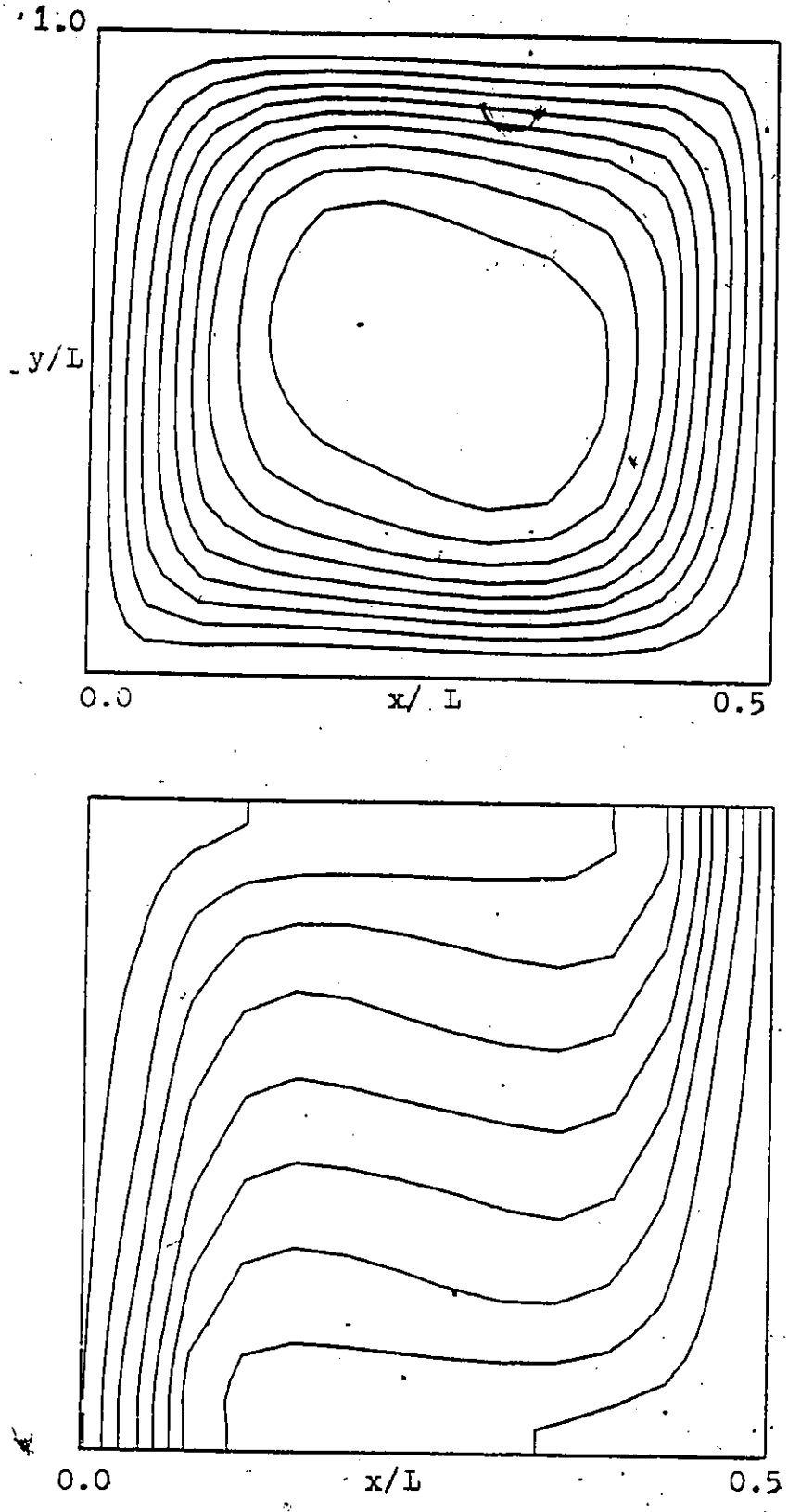

Figure 5.43: Streamlines and Isotherms for A=2, Gr=1.E5, Hi=.007, Ho=.001. Si=0, So=0. Case B

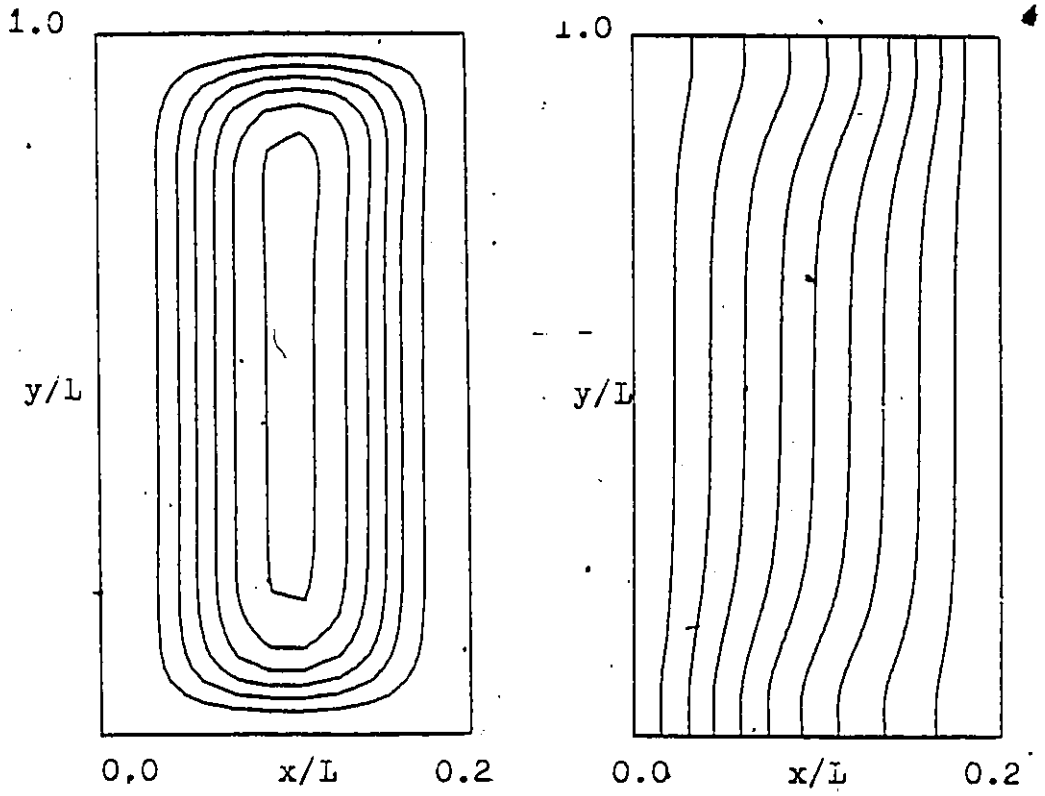

Figure 5.44: Streamlines and Isotherms for A=5. Gr=1.E3. Hi=.007. Ho=.001. Si=0. So=0. Case B

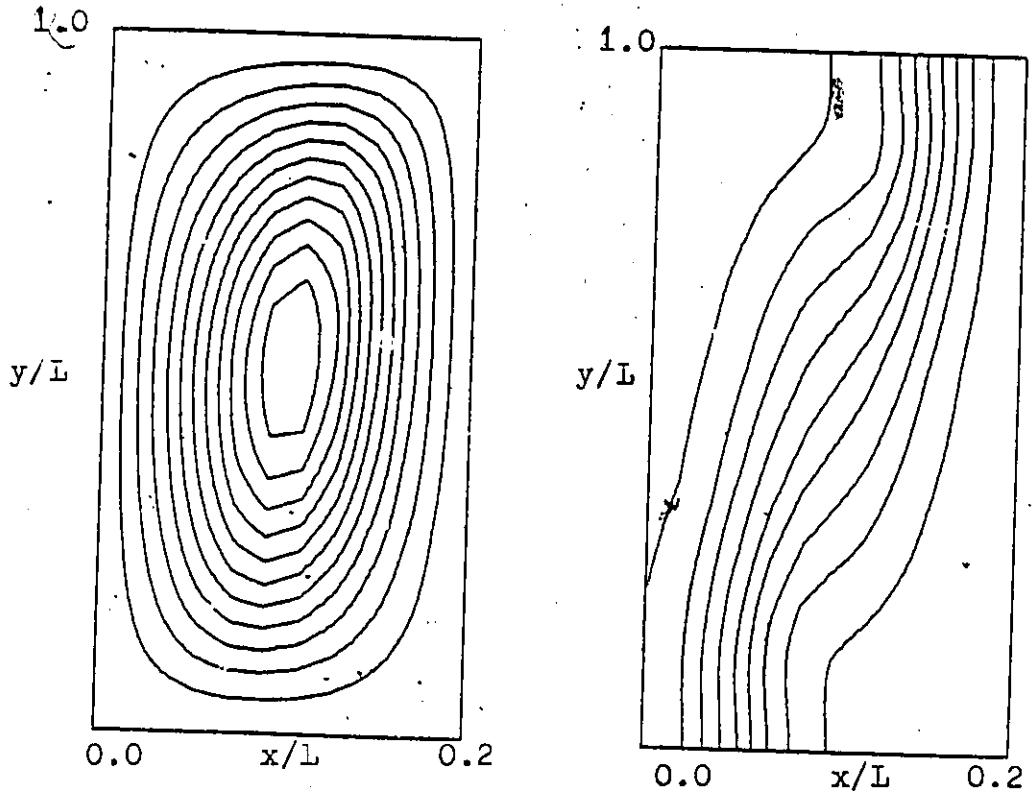

Figure 5.45: Streamlines and Isotherms for A=5, Gr=1.E4, Hi=.007, Ho=.001. Si=0, So=0. Case B

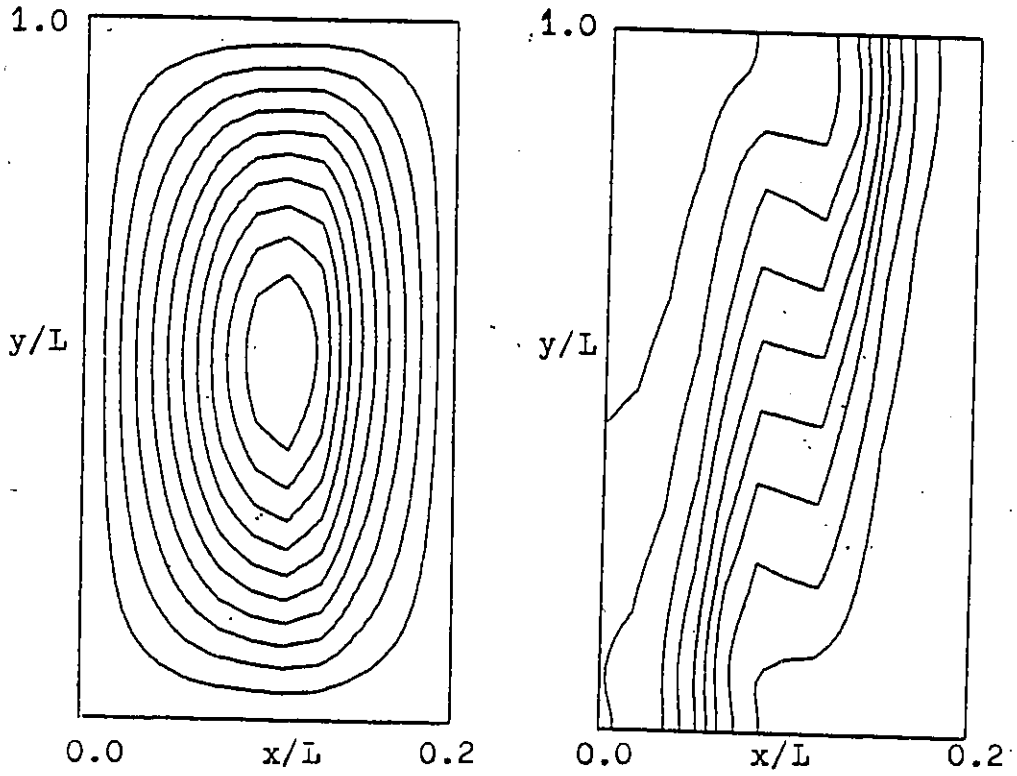

Figure 5.46: Streamlines and Isotherms for A=5, Gr=1.E5, Hi=.007, Ho=.001. Si=0, So=0. Case B

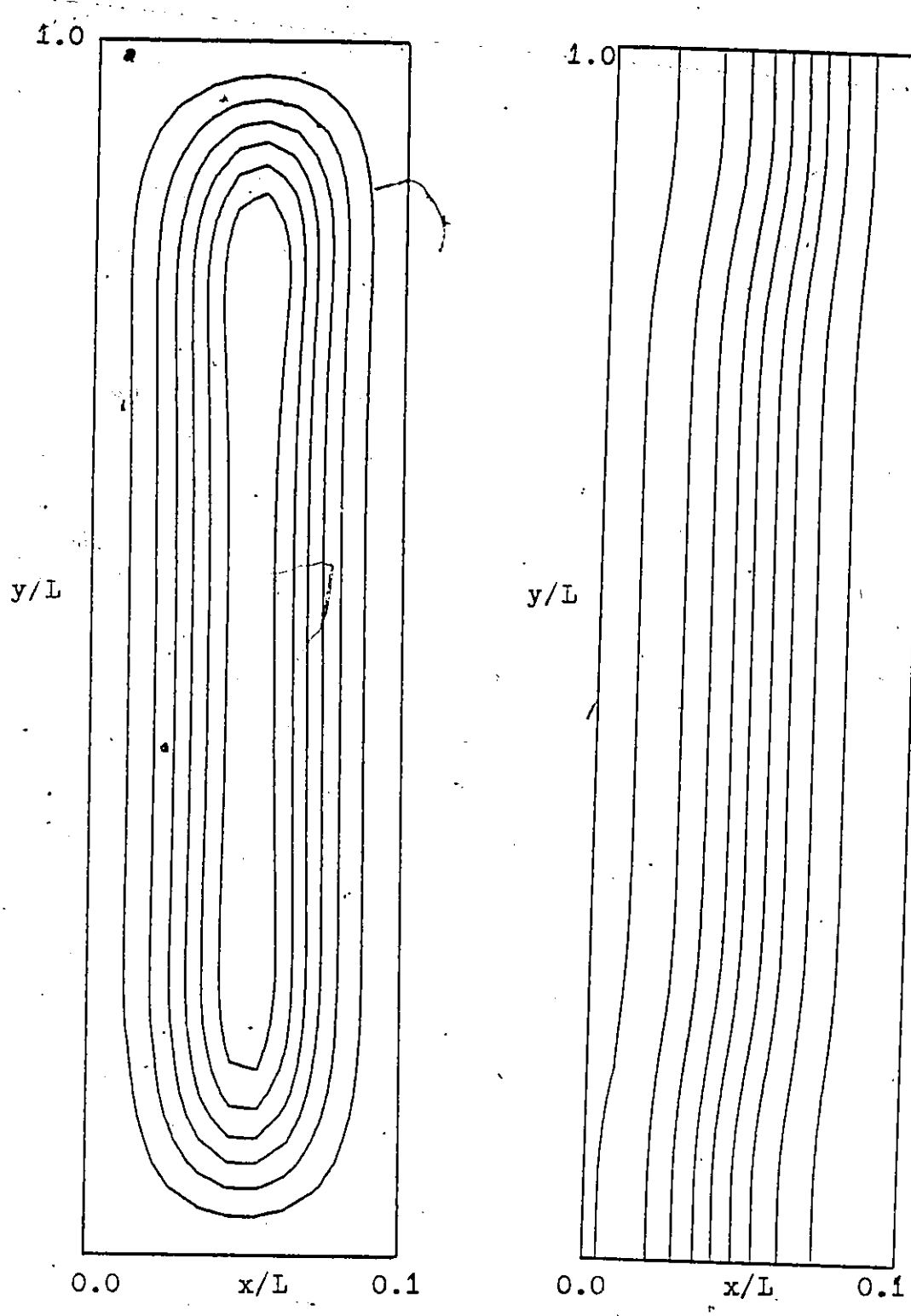

Figure 5.47: Streamlines and Isotherms for A=10, Gr=1.E3, Hi=.007, Ho=.001. Si=0, So=0. Case B

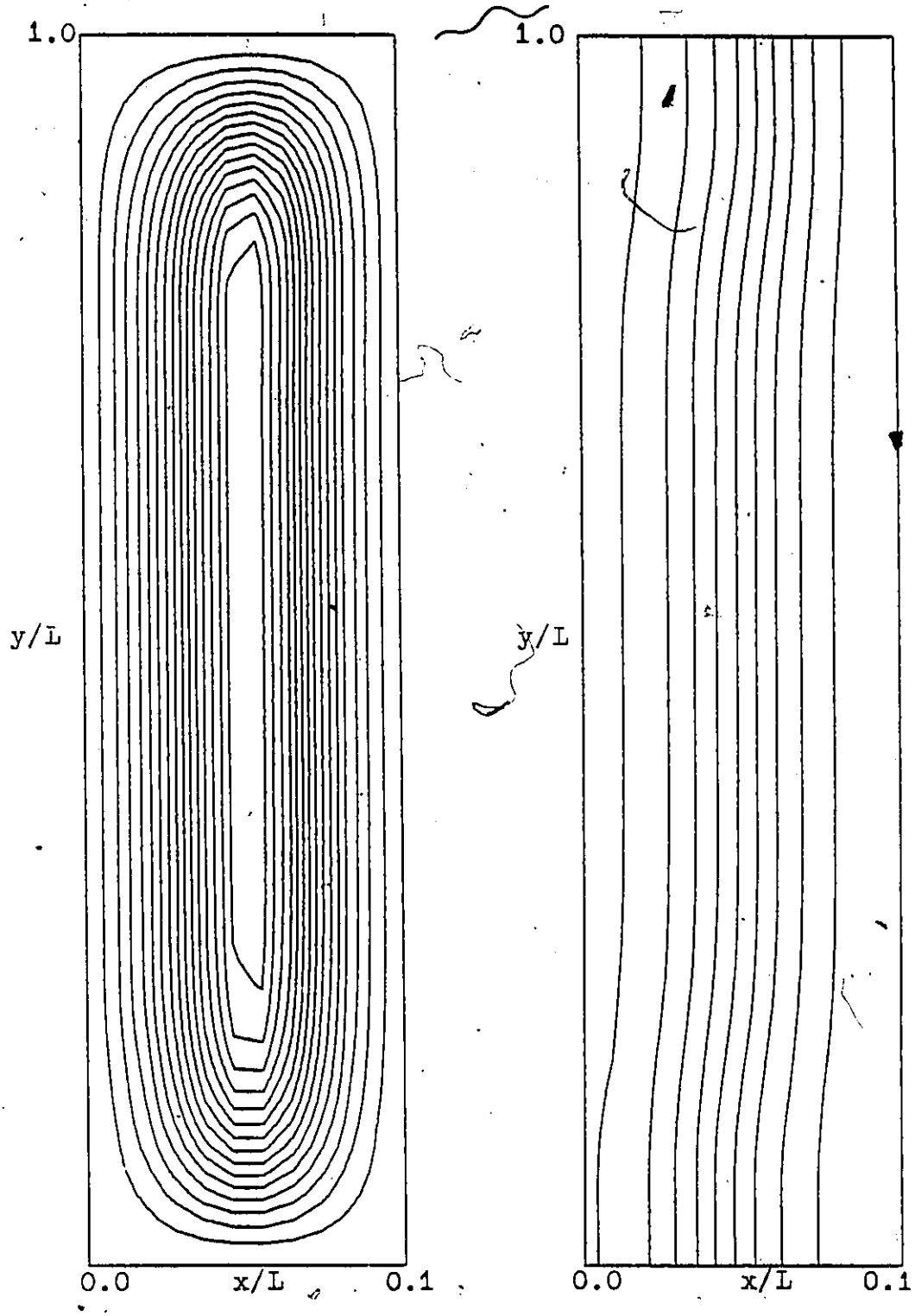

Figure 5.48: Streamlines and Isotherms for A=10, Gr=1.E4, Hi=.007, Ho=.001. Si=0, So=0. Case B

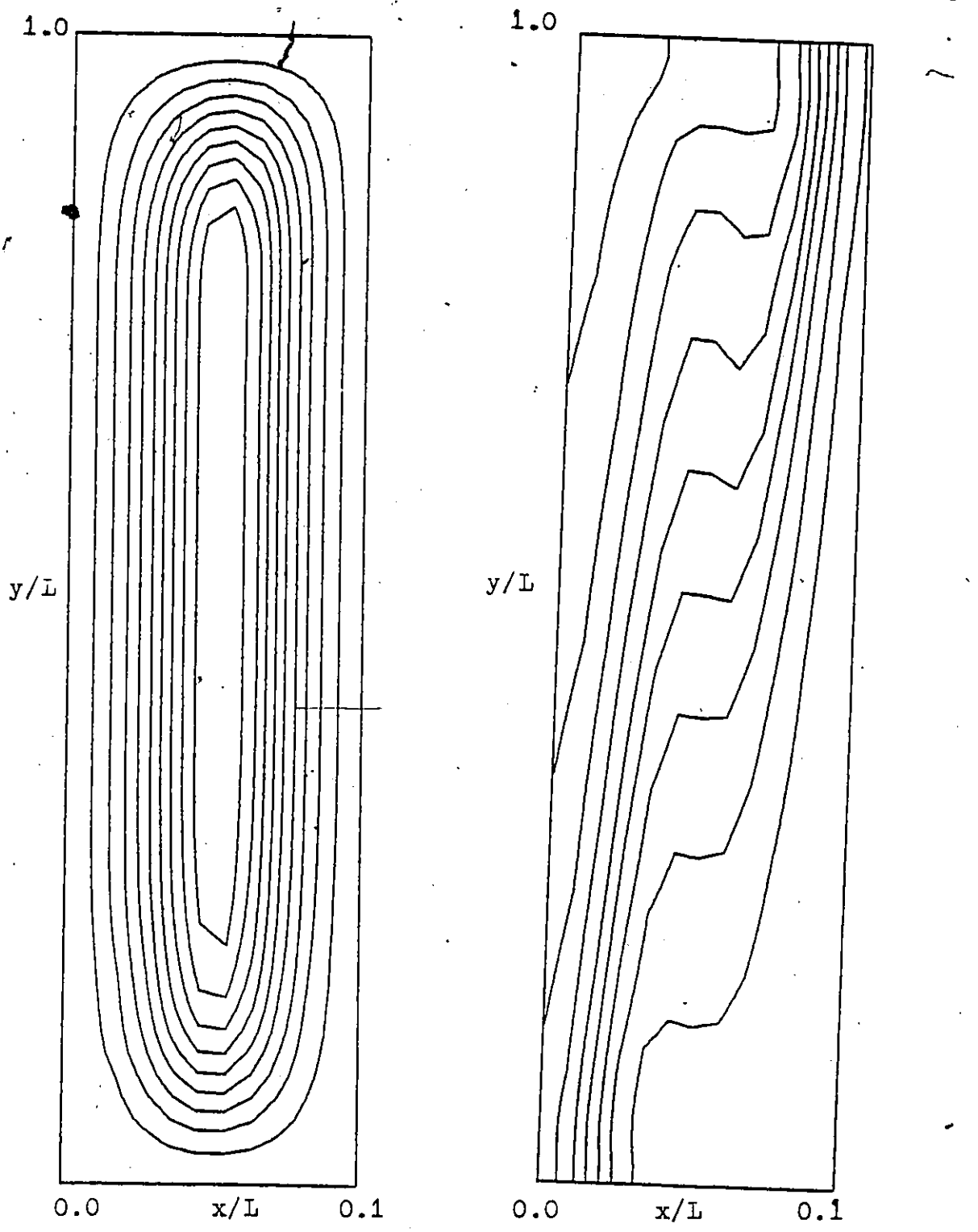

Figure 5.49: Streamlines and Isotherms for A=10, Gr=1.E5, Hi=.007, Ho=.001. Si=0, So=0. Case B

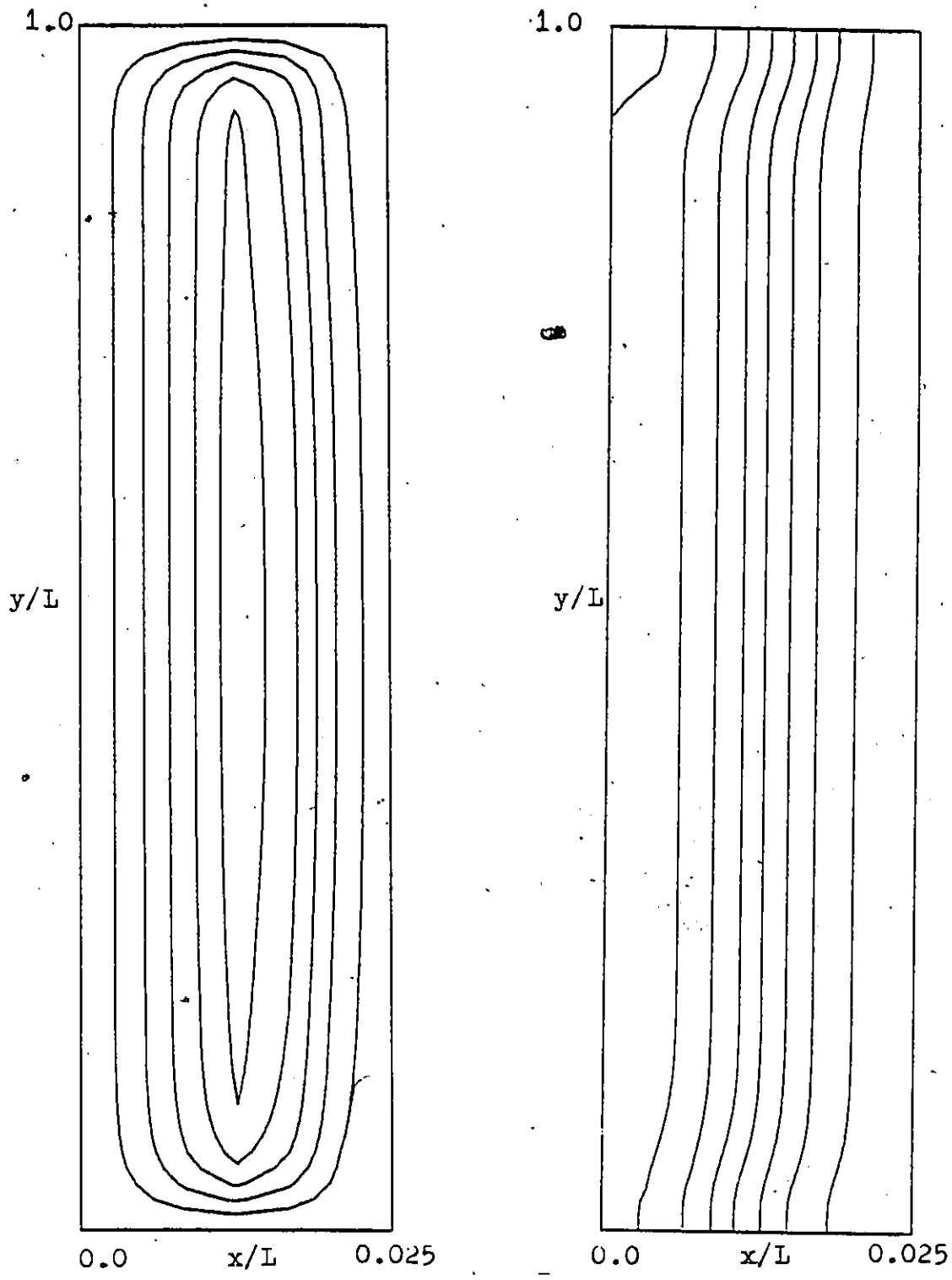

Figure 5.50: Streamlines and Isotherms for A=40, Gr=1.E3, Hi=.007, Ho=.001, Si=0, So=0, Case B

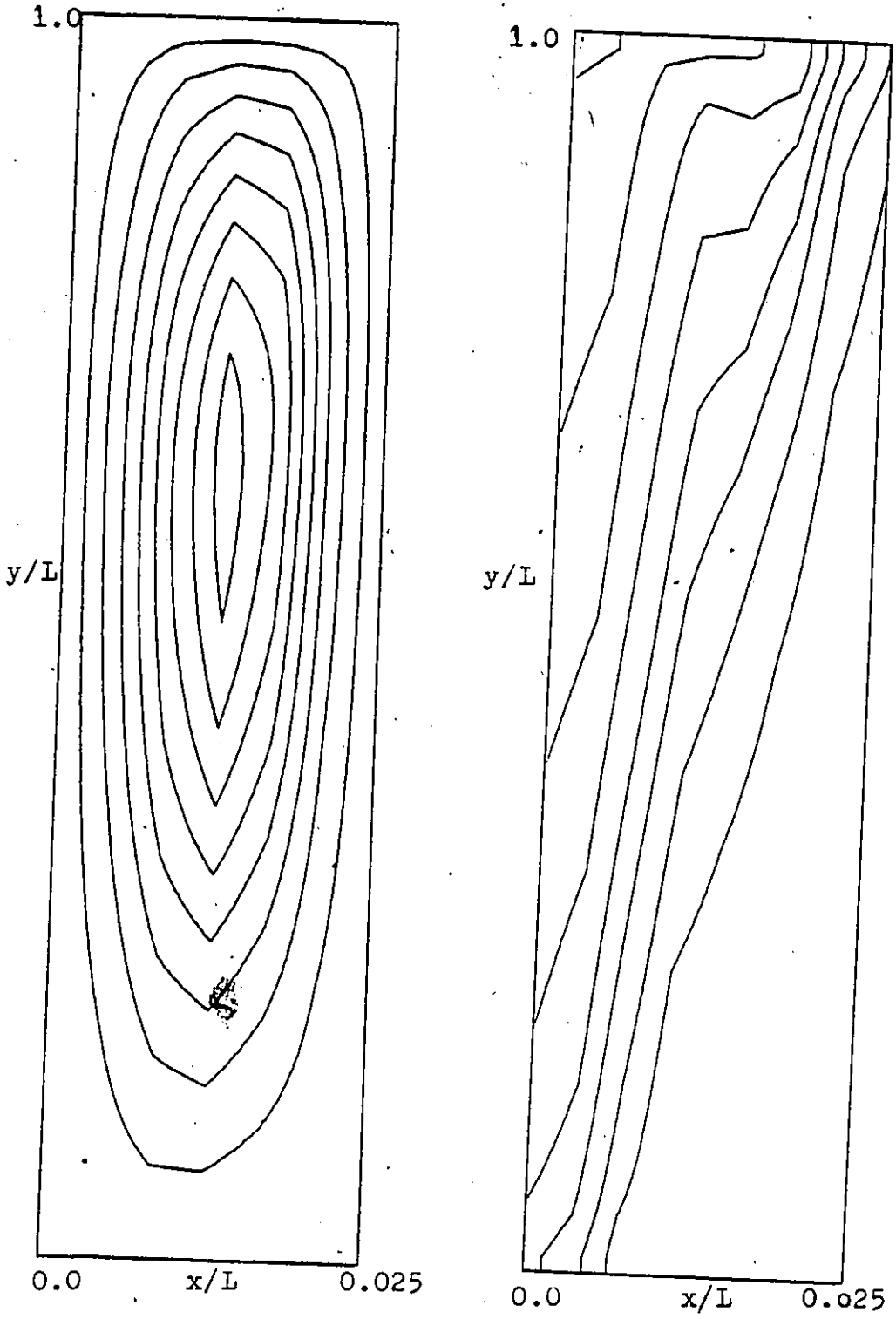

Figure 5.51: Streamlines and Isotherms for A=40, Gr=1.E5, Hi=.007, Ho=.001. Si=0, So=0. Case B

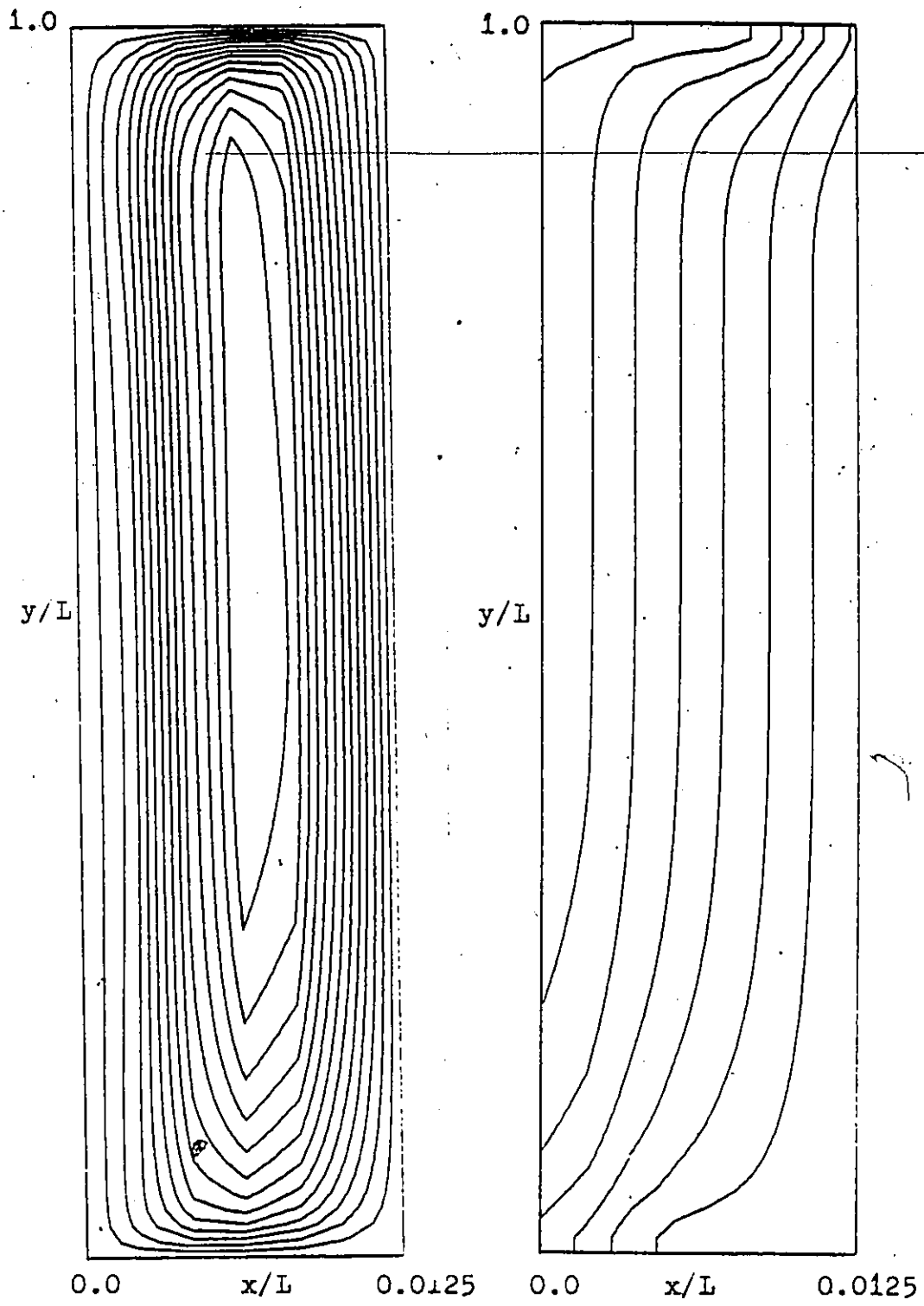

Figure 5.52: Streamlines and Isotherms for A=80, Gr=1.E4, Hi=.007, Ho=.001. Si=0, So=0. Case B

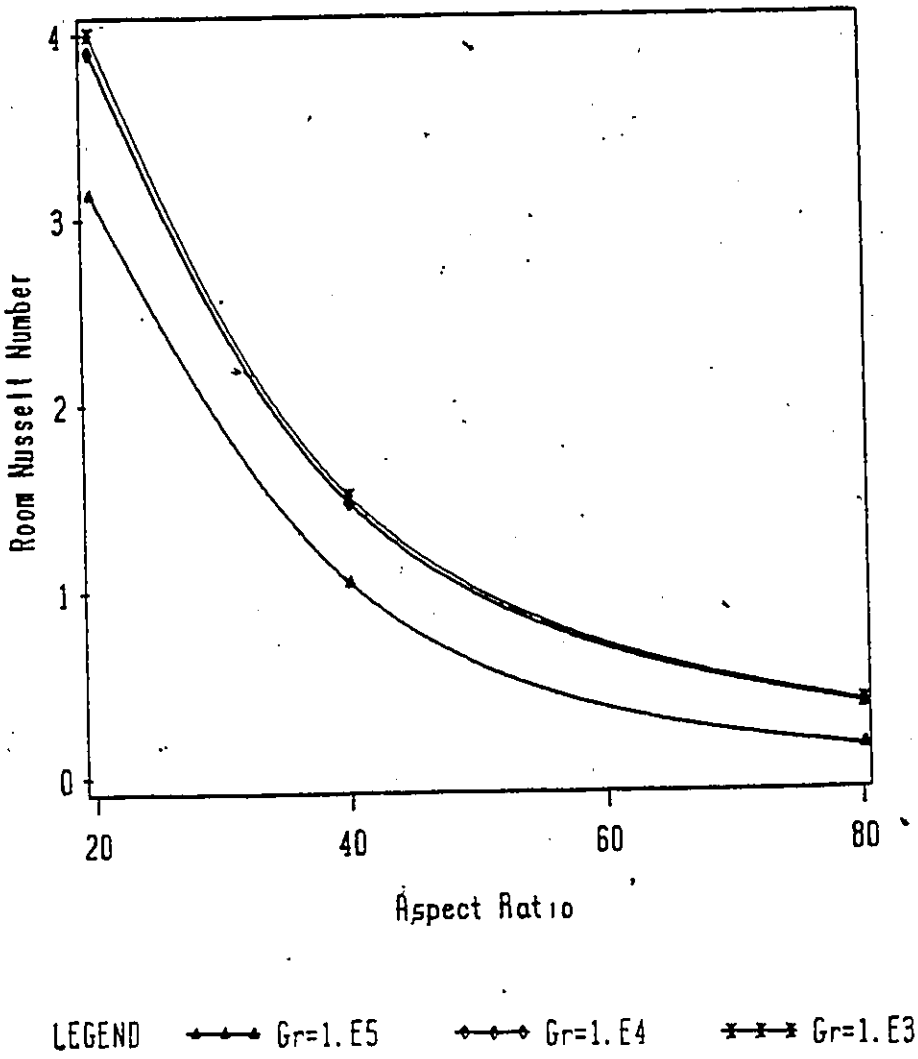

Figure 5.53: Room Nusselt number dependence on aspect ratio, obtained from equation 5.2. Case C.

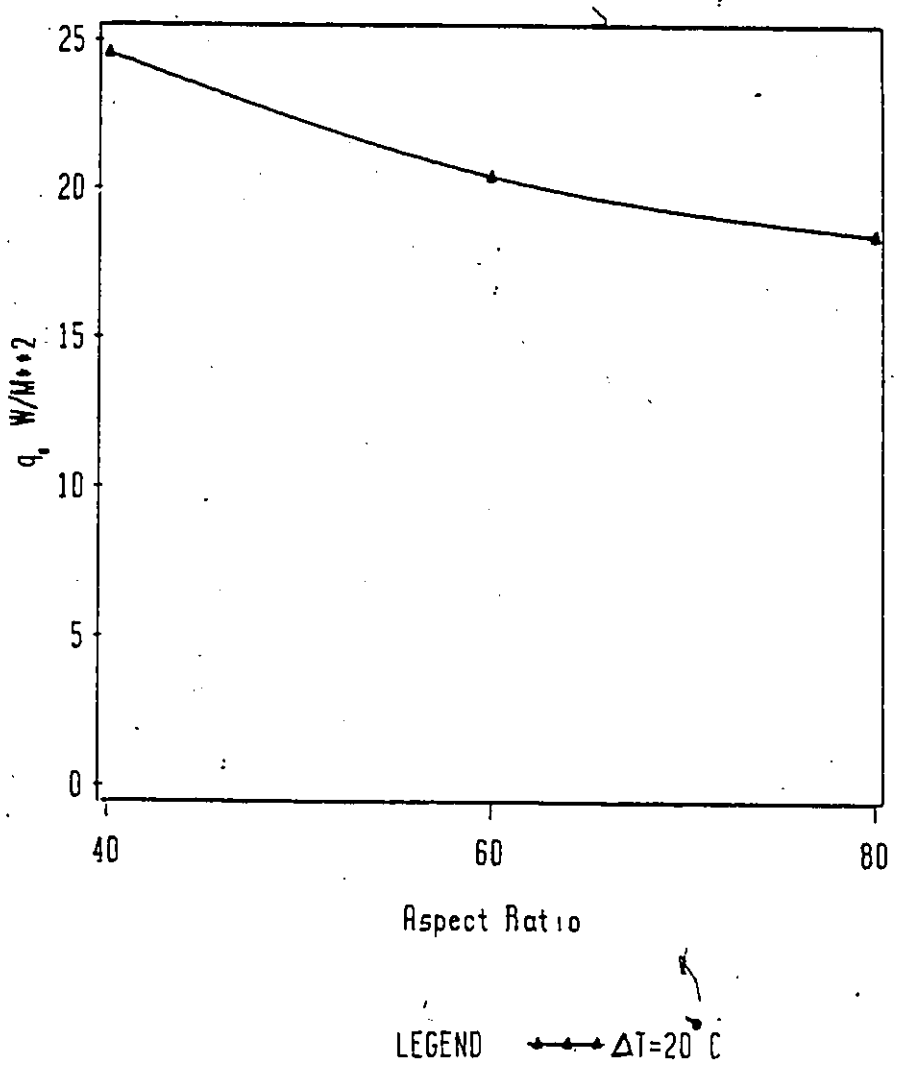

Figure 5.54: Heat flux gain to room, for a window of height 1.0 m. Gap between glass panes varying from .0125 to .025 m. Case C.

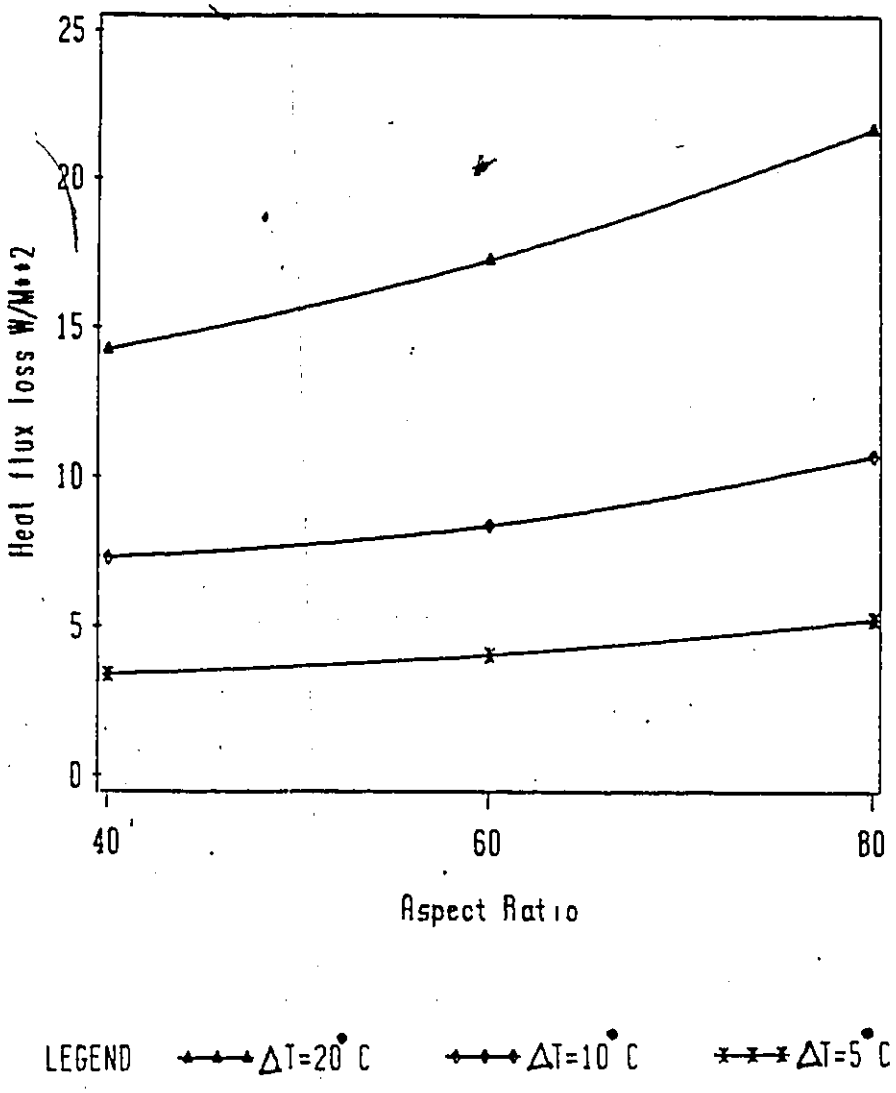

Figure 5.55: Heat flux loss from room for a window of height L=1.0 M. Gap between glass panes varying from .0125 to .025m. Case B. Temperature difference between ambients 20, 10 and 5 Deg.C.

Case A: Temperature difference between glass faces 20° C, Present study

Case B: Temperature difference between the ambients 20° C, Present study

Case S: Flux computed based on thermal resistance concept

$$q = \frac{\text{temperature difference between ambients (20 C)}}{Rt}$$

$$Rt = 1/hi + D/k + 1/ho$$

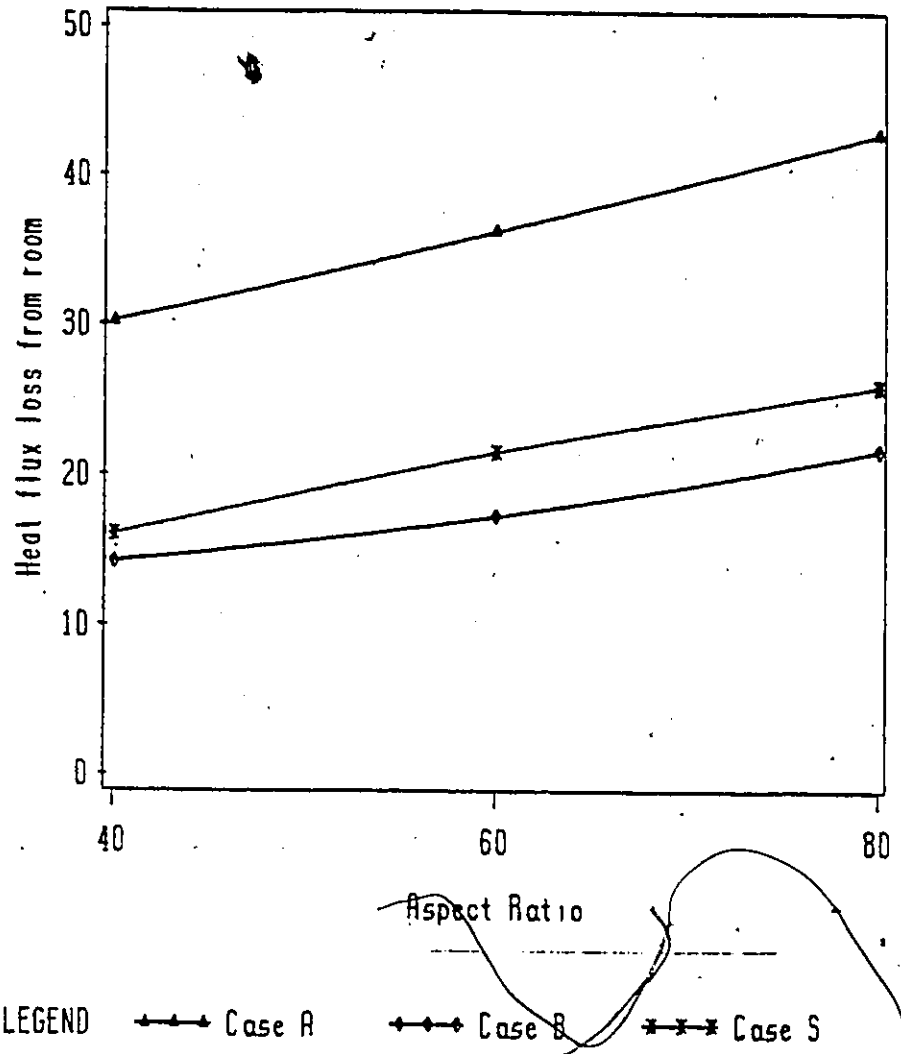

Figure 5.56: Heat flux loss from room for a window of height L=1.0 M. Gap between glass panes varying from .0125 to .025m. Comparision between Cases A, B and S.

Chapter VI

CONCLUSIONS AND RECOMMENDATIONS

The problem of heat and fluid flow through a vertical rectangular cavity up to an aspect ratio of 80 has been analyzed numerically. Its application to a double glazed window has been studied, and the problem formulated to take the environmental variables into account. It has been found that the number of groups on which the heat flux depends is too large to make a complete parametric study possible. Some likely cases have been studied. The complete Navier Stokes equations and the energy equation have been solved using finite domain technique. Some of the conclusions that can be drawn are listed below.

6.1 Conclusions

The governing equations have been correctly formulated and the associated computer code is verified to be correct. The present formulation, when tested, showed overall good agreement with previously published results.

The main thrust of the present study was to model the high aspect ratio (40-80) cavities, as a double glazed win-

dow. The three main factors affecting the heat transfer through the double glazed window are the temperature difference between the two ambients. the wind speed and the solar radiation. To simplify the problem only the heating effect created in the window faces as a result of the radiation absorbed in the glass surfaces was considered. Any radiation exchange between the surfaces was neglected as also the the solar radiation transmitted to the room. A dimensional analysis was carried out and 8 dimensionless parameters Hi. Ho. Ri. Ro. N. Gr. Pr and A were found to influence the heat flux. As the number of parameters is large a complete parametric study is not possible

As a consequence results were obtained for three selected Cases A. B and C. In Case A. the effect of the environmental conditions was not considered. The vertical faces were isothermal. but at different temperatures. This case corresponded to the work of investigators in the past. The results of the present study for this particular case were used to compare with the previous results. This served to validate the code against the numerical and experimental work of other investigators.

In Case B the effect of the wind was considered i.e. convective boundary conditions were applied to the faces. The parameters Hi and Ho were respectively .007 and .001. This

corresponded to a strong wind on the outside and still air on the inside. Heat flux loss in this case was lower than in Case A, as might be expected. Results of Case B were compared with the results from the simplified model designated as Case S. The heat flux values of Case S were 15 to 25% higher than those of the present study.

In Case C the combined effect of the wind and the heat generated in the faces was considered. The solar radiation contributing to the heating effect was approximately 10% of the incident solar radiation of 762 W/M**2, which is the intensity on the earth's surface at 40 Deg. North latitude in the month of July. As a result of this heating there was a net heat gain to the room.

Results were plotted for an average Nusselt number versus the aspect ratio for Grashof number ranging from 10^3 to 10^5. This Nusselt number is a measure of the heat flux from the i-surface to the fluid in the cavity. The quantity of interest to the designer of windows is q, i.e. the flux from the room to the i-face, as given by equations 5.2 and 5.3. A procedure has been outlined for computing this heat flux, using the results of the present study.

In order to cover a wide range of environmental conditions, results are required for a wider range of parametric values.

The fluid flow and heat transfer inside the cavity was also studied. For Grashof numbers less than 1000 the temperature field closely satisfies the Laplace equation. For higher Grashof numbers larger temperature gradients grow near the walls. In the interior region a uniform temperature gradient is established. Three flow regimes have been identified, conduction, transition and boundary layer regime. The horizontal temperature gradient is used as a criterion for determining the flow regimes. In high aspect ratio cavities conduction is the dominant mode of heat transfer. Convection effects occur near the ends.

6.2 Recommendations

The following suggestions are provided as possible ways to improve as well as extend the scope of the present study.

One of the simplifying assumptions made in the present formulation disregarded the radiation interaction occurring between the faces of the cavity. In order to include this effect, the energy balance equations at the faces can be modified, by using the Stefan Boltzmann law and considering the emissivities of the surfaces (Carpenter and Briggs 1976).

The thickness of the glass faces in the present study have been considered very small such that the temperature

drop in the glass is negligible. In order to compute this drop in temperature the calculation domain shall have to be extended to include the solid glass and the fluid in the cavity. This can be accomplished by representing the solid regions outside the fluid domain as regions of very high viscosity. By this means the flow velocity in the solid regions shall be reduced to zero. The problem would now be a conjugate heat transfer problem involving conduction in the solid and convection in the fluid.

The Boussinesq approximation has been made in the present study, which implies that the properties of the fluid do not vary with temperature, except the effect on density which produces the buoyancy effect. As the temperature difference increases this assumption is not strictly valid. The problem could therefore be solved using variable properties of the fluid contained in the cavity.

The adiabatic boundary condition was assumed for the top and bottom end walls in the present study. With air as the fluid in the cavity this is impossible to achieve in practice. The use of a linear temperature profile boundary condition at the ends would provide more realistic results, especially for cavities of low aspect ratio.

In the present study results have been obtained for two sets of parameters. In order to extend the work, results may

be obtained for a range of parameters. The data generated would be of use to designers of windows.

Finally, attempts can be made to reduce the computatioal effort, by considering other solution procedures. Major effort is expended in resolving the problem of the velocity-pressure coupling. For this problem, in addition to the velocity-pressure coupling, there is an additional coupling due to the buoyancy effect. Other variations of the SIMPLE technique can be attempted such as the PUMPIN (Pressure Update by Multiple Path Integration) Mazhar (1981) where the pressure field is updated by integrating the momentum equations along all the paths.

REFERENCES

1. ASHRAE handbook 1985 Fundamentals

2. Batchelor, G.K., (1954) Heat Transfer by Free Convection Across a Closed Cavity Between Vertical Boundaries at Different Temperatures. Quarterly of Applied Mathematics, vol.12, pp 209-233

3. Carpenter, J.R., Briggs and Sernas, V. Combined Radiation and Developing Laminar Free Convection Between Vertical Flat Plates with Asymmetric Heating. Journal of Heat Transfer, pp 95-100, 1976

4. De Graaf, J.G.A. and Van der Held, E.F.M. The Relation Between the Heat Transfer and the Convection Phenomenon in Enclosed Plane Air Layers. Journal of Applied Science Research, vol.3, pp393-409, 1953

5. Eckert, E.R.G. and Carlson, W.O. Natural Convection in an Air Layer Enclosed Between Two Vertical Plates of Different Temperatures. International Journal of Heat and Mass Transfer, vol.2, pp106-120, 1961

6. Elder, J.W. Laminar Free Convection in a Vertical Slot. Journal of Fluid Mechanics, vol. 23, pp77-98, 1965 Emery, A.P. and Chu, N.C. Heat Transfer Through

Vertical Layers. ASME Journal of Heat Transfer, vol. 87, pp110-116, 1965

7. ElSherbiny, S.M., Raithby, G.D. and Hollands, K.G.T. Heat Transfer by Natural Convection Across Vertical and Inclined Air Layers. Journal of Heat Transfer, vol. 104, pp515-520, 1982

8. ElSherbiny, S.M., Hollands, K.G.T. and Raithby, G.D. Effect of Thermal Boundary Conditions on Natural Convection in Vertical and Inclined Air Layers. 20th National Heat Transfer Conference, Milwaukee, Wisconsin August 1981

9. Incropera, F.P. and Dewitt, D.P. Fundamentals of Heat Transfer. John Wiley and Sons, Toronto, 1981

10. Jones, I.P. A Numerical Study of Natural Convection in an Air-Filled Cavity: Comparison With Experiment. Numerical Heat Transfer, vol.2, pp. 193-213, 1979

11. Jacob, M. Free Convection Through Enclosed Plane Gas Layers. Trans. ASME vol. 68, pp189-194, 1946

12. MacGregor, R.K. and Emery, A.F. Free Convection Through Vertical Plane Layers- Moderate and High Prandtl Number Fluids. Journal of Heat Transfer, pp.391-403, Aug.1969

13. Mazhar, Z. An Evaluation of the Segregated Solution Procedures for the Solution of Incompressible Fluid

Flow Problems. Ph.D Thesis, University of Waterloo, Waterloo, 1981

14. Mull, W. and Reiher, H. Gesundh-Ing. Beihefte. Reihei 1, no. 28

15. Mynett, J.A. and Duxbury, D. Temperature Distributions Within Enclosed Plane Air Cells Associated with Heat Transfer by Natural Convection. Proc. Fifth International Heat Transfer Conference, Paper N.C. 3.8 pp. 119-123, 1974

16. Patankar, S.V. Numerical Heat Transfer and Fluid Flow. Hemisphere, Washington, D.C., 1980

17. Raithby, G.D. and Schneider, G.E. Numerical Solution of Problems in Incompressible Fluid Flow: Treatment of the Velocity-Pressure Coupling. Numerical Heat Transfer, vol.2, pp 417-440, 1979

18. Raithby, G.D. and Wong, H.H. Heat Transfer by Natural Convection Across Vertical Air Layers. Numerical Heat Transfer, vol. 4, pp. 447-457, 1981

19. Van Doormaal, J.P., and Raithby, G.D. Enhancements of the SIMPLE Method for Predicting Incompressible Fluid Flows. Numerical Heat Transfer, vol.7, pp.147-163, 1984

20. Yin, S.H., Wung, T.Y. and Chen, K. Natural Convection in an Air Layer Enclosed Within Rectangular Cavities. Int. Journal Heat Mass Transfer, vol.21, pp.307-315, 1978

SELECTED BIBLIOGRAPHY

1. Anderson, R., and Bejan, A. Heat Transfer Through Single and Double Vertical Walls in Natural Convection: Theory and Experiment. International Journal of Heat and Mass Transfer Vol. 24 pp 1611-1620, 1981

2. Anderson, R., and Bejan, A. Natural Convection on Both Sides of a Vertical Wall Separating Fluids at Different Temperatures. Trans. of the ASME, Vol. 102, Nov. 1980

3. Campo, E.M., Sen, M. and Ramos, E. Natural Convection in a Semielliptic Cavity. Numerical Heat Transfer, vol.12, pp.101-119, 1987

4. Coulter, J.P. and Guceri, S.I. Laminar and Turbulent Natural Convection Within Irregularly Shaped Enclosures. Numerical Heat Transfer, vol.12, pp. 211-227, 1987

5. Cebeci, T., Hirsch, R.S. etal. Studies of Numerical Methods for The Plane Navier-Stokes Equations. Computer Methods in Applied Mechanics and Engineering 27, pp.13-44 1981

6. De Vahl Davies, G. Natural Convection of Air in a Square Cavity: A Bench Mark Numerical Solution. Int.

Journal for Numerical Methods in Fluids, vol.3, 249-264, 1983

7. De Vahl Davies, G. and Jones, I.P. Natural Convection in a Square Cavity: A Comparison Exercise. Int. Journal for Numerical Methods in Fluids, vol.3, 227-248 1983

8. De Vahl Davis Laminar Natural Convection in an Enclosed Rectangular Cavity. Int. Journal of Heat Mass Transfer, vol.11, pp.1675-1693, 1968

9. Douglas, J. and Gunn, J.E. A General Formulation of Alternating Direction Methods -Part I Parabolic and Hyperbolic Problems. Numeriche Mathematik, vol.6, pp428-453, 1964

10. Ghia, U., Ghia, K.N. and Shin, C.T. High-Re Solutions for Incompressible Flow Using the Navier- Stokes Equations and a Multigrid Method. Journal of Computational Physics, vol.48, no.3, Dec. 1982

11. Harlow, F.H. and Welch, J.E. Numerical Calculation of Time-Dependent Viscous Incompressible Flow of Fluid with Free Surface. The Physics of Fluids, vol.8, no.12, Dec. 1965

12. Huang, D.Y. and Hsieh, S.S. Analysis of Natural Convection in a Cylindrical Enclosure. Numerical Heat Transfer, vol.12, pp.121-135, 1987

13. Humphrey, J.A.C., Avedisian, C.T., Tourneau, B.W. and Chen, M.M. Significant Questions in Buoyancy Affected Enclosure or Cavity Flows. The winter annual meeting of ASME, Anaheim, California, 1986.

14. Korpela, S.A., Lee, Y. and Drummond, J.E. Heat Transfer Through a Double Pane Window. Journal of Heat Transfer, Aug. 1982, Vol.104, pp 539-544

15. Martynenko, O.G. Laminar Free Convection From a Vertical Plate. Int. Journal of Heat Mass Transfer, vol.27, no.6, pp.869-881 1984

16. Lock, G.S.H., and Ko, R.S. Coupling Through a Wall Between Two Free Convective Systems. Int. Journal of Heat and Mass Transfer, vol.16, pp.2087-2096 1973
Numerical Heat Transfer, vol.2, pp.193-213, 1979

17. Kierkus, W.T. An Analysis of Laminar Free Convection Flow and Heat Transfer about an Inclined Isothermal Plate. Int. Journal of Heat Mass Transfer, vol.11, pp.241-253, 1968

18. Patankar, S.V. and Spalding, D.B. Heat and Mass Transfer in Boundary Layers.

19. Sparrow, E.M. and Prakash, C. Interaction Between Internal Natural Convection in an Enclosure and an External Natural Convection Boundary-Layer Flow. Int. Journal of Heat Mass Transfer, vol.24, no.5, pp.895-907, 1981

20. Trevisan, O.V. and Bejan, A. Combined Heat and Mass Transfer by Natural Convection in a Vertical Enclosure. Journal of Heat Transfer, vol.109, pp. 104-112, 1987

21. Viskanta, R. and Abrams, M. Thermal Interaction of Two Streams in Boundary Layer Flow Separated by a Plate. Int. Journal of Heat Mass Transfer, vol.14, pp.1311-1321

22. Viskanta, R. and Lankford, D.W. Coupling of Heat Transfer Between Two Natural Convection Systems Separated by a Vertical Wall. Int. Journal of Heat and Mass Transfer, vol.24, no.5, pp. 1171-1177, 1981

Appendix A

GRID SENSTIVITY ANALYSIS

A grid senstivity analysis has been carried out for an aspect ratio of 78.7 and a Grashof number of 5.43E3. which corresponds to one of the cases of the experimental study carried out by Yin (1978). Grid sizes of 6X60. 8X80 and 12X90 have been used. The values of tempemperature have been plotted in Figure A.1. It is shown that the results are grid independent.

Figures A.2 and A.3 show a plot of the temperature distribution across the cavity at Y/L=.15. .5 and .85. for an aspect ratio of 1. and a Grashof number of 1.0E5. The results are found to be grid independent.

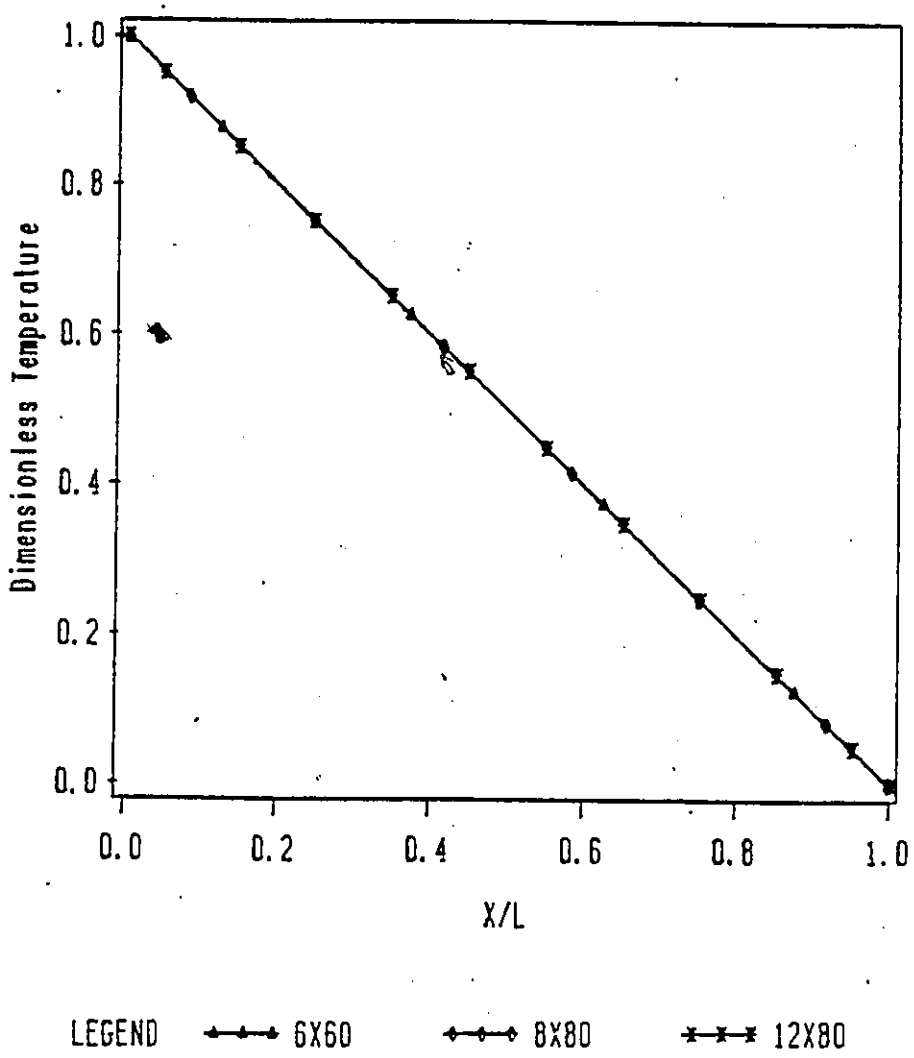

Figure A.1: Grid senstivity analysis. Temperature profiles plotted, at Y/L=.5 for gridsizes 6X60. 8X80 and 12X80. Parameters used A=78.7. Gr=5.43E3.

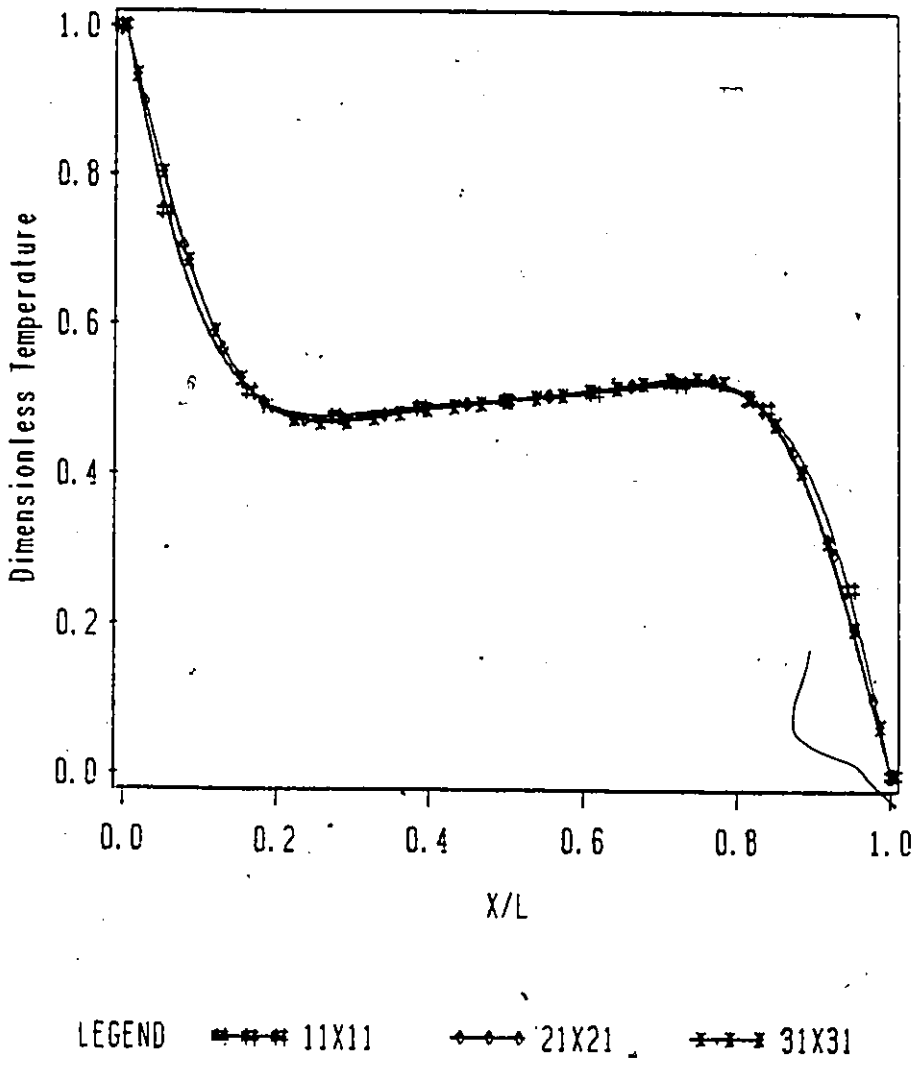

Figure A.2: Grid senstivity analysis. Temperature profiles plotted, at Y/L=.5 for grid sizes 11X11, 21X21 and 31X31. Parameters used A=1, Gr=1.E5

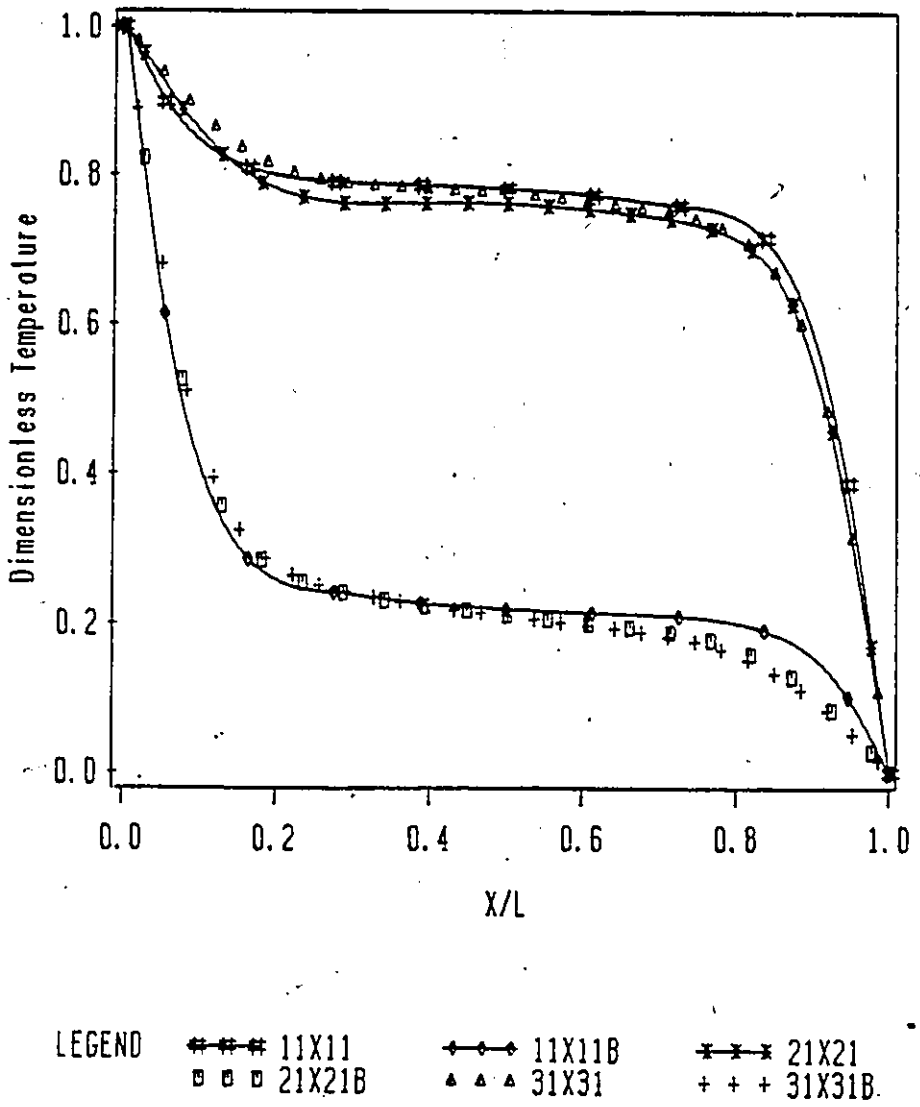

Figure A.3: Grid senstivity analysis. Temperature profiles plotted, at Y/L=.85 and Y/L=.15 for grid sizes 11X11, 21X21 and 31X31. parameters used A=1, Gr=1.E5

Appendix B

NUMERICAL_CODE_WINDSAV

A listing of the numerical code that has been used in solving the double glazed window problem is included in tis appendix.

The code solves the Navier Stokes equations and the energy equation in Cartesian coordinates. Primitive variables in a staggered grid are used. The code is designed to use variable grid spacing. laminar flow and two dimensional problems.

The code is based on Patankars(1980) SIMPLE algorithm.

```
C     NUMERICAL CODE USED TO STUDY HEAT TRANSFER ACROSS A CLOSED
C     CAVITY. AND ITS APPLICATION TO A DOUBLE GLAZED WINDOW
C
C     WINDSAV
C     PROGRAM WILL SOLVE FOR RECTANGULAR CAVITY
C     WILL USE SIMPLER ALGORITHM, ADI, POWER LAW SCHEME
C
      COMMON /XPARA/ KIT,EU,EV,ET,AR,BETAX,BETAY,ALPHA,THETA,ITEST
     1/PROP/GRR,GRW,GRL,PR,GAM,TIN,TOUT,TCAIR,HCON,QCON
     1/WIND2/HOK,HIK,SHI,SHO,ZETA
     1/XGEOM/JMAX,KMAX,J1,J2,J3,K1,K2,K3,XMIN,XMAX,YMIN,YMAX
     1/XGEOM1/JUMAX,KUMAX
     1/XVAR1/U(70,95),V(70,95),UH(70,95),VH(70,95),P(70,95)
     1/XVAR2/PC(70,95),T(70,95),TO(70,95),PS(70,95),PSI(70,95)
     1/XCOFF1/AUP(70,70),AUN(70,70),AUS(70,70),AUE(70,70)
     1/XCOFF2/AUW(70,95),SU(70,95)
     1/XCOFF3/AVP(70,95),AVN(70,95),AVS(70,95),AVE(70,95)
     1/XCOFF4/AVW(70,70),SV(70,70),SP(70,70)
     1/XCOFF5/APN(70,95),APS(70,95),APE(70,95),APW(70,95)
     1/XNUMB/RHS(100),AA(100),BB(100),CC(100),DD(100)
     1/XMET/DX(95),DXX(95),DY(95),DYY(95),X(95),Y(95),XND(95),YZ(95)
     1/XCHK/RESU,RESV,REST,RESM
      ITEST=0
      JMAX=41
      KMAX=41
      J1=JMAX-1
      J2=JMAX-2
      J3=JMAX-3
      K1=KMAX-1
      K2=KMAX-2
      K3=KMAX-3
      KM=KMAX/2
      XMIN=0.0
      YMAX=1.0
      YMIN=0.0
C  VALUES OF PARAMETERS
      AR=1.
      XMAX=YMAX/AR
      GRW=1.0E5
      HIK=.0
      HOK=.0
      SHI=.0
      SHO=.0
      ZETA=1.333
      PR=0.71
      RESU=.0
      RESV=.0
      RESM=.0
      DO 50 J=1,JMAX
      DO 60 K=1,KMAX
      T(J,K)=1.0
      TO(J,K)=.0
      P(J,K)=0.0
      PC(J,K)=0.0
      PS(J,K)=0.
      U(J,K)=0.0
      V(J,K)=0.0
      UH(J,K)=.0
      VH(J,K)=.0
      AUP(J,K)=1.E20
      AUN(J,K)=1.E20
      AUS(J,K)=1.E20
      AUE(J,K)=1.E20
      AUW(J,K)=1.E20
      AVP(J,K)=1.E20
      AVN(J,K)=1.E20
      AVS(J,K)=1.E20
      AVE(J,K)=1.E20
      AVW(J,K)=1.E20
   60 CONTINUE
   50 CONTINUE
      GAM=1.
      GRL=1000.
      ALPHA=0.9
      THETA=1.8
      BETAX=5.1
      BETAY=5.1
      EU=4.
      EV=4.
      ET=1.
```

```
      CALL XGRID
      DO 11 JM=1,600
25    KIT=KIT+1
13    CALL XBOUND
      CALL XCOFF
      CALL XPRESS
      CALL XUMOM
      CALL XVMOM
      CALL XPCORR
      CALL XVCORR
      CALL XTEMP
      IF(KIT.GE.500) GOTO 120
11    CONTINUE
120    CALL XPUT
      CALL SLINE
      STOP
      END
      SUBROUTINE XBOUND
      COMMON /XPARA/ KIT,EU,EV,ET,AR,BETAX,BETAY,ALPHA,THETA,ITEST
     1/WIND2/HOK,HIK,SHI,SHO,ZETA
     1/PROP/GRR,GRW,GRL,PR,GAM,TIN,TOUT,TCAIR,HCON,QCON
     1/XGEOM/JMAX,KMAX,J1,J2,J3,K1,K2,K3,XMIN,XMAX,YMIN,YMAX
     1/XVAR1/U(70,95),V(70,95),UH(70,95),VH(70,95),P(70,95)
     1/XVAR2/PC(70,95),T(70,95),TO(70,95),PS(70,95),PSI(70,95)
     1/XCOFF1/AUP(70,95),AUN(70,95),AUS(70,95),AUE(70,95)
     1/XCOFF2/AUW(70,95),SU(70,95)
     1/XCOFF3/AVP(70,95),AVN(70,95),AVS(70,95),AVE(70,95)
     1/XCOFF4/AVW(70,95),SV(70,95),SP(70,95)
     1/XCOFF5/APN(70,95),APS(70,95),APE(70,95),APW(70,95)
     1/XNUMB/RHS(100),AA(100),BB(100),CC(100),DD(100)
     1/XMET/DX(95),DXX(95),DY(95),DYY(95),X(95),Y(95),XZ(95),YZ(95)
     1/XCHK/RESU,RESV,REST,RESM
      K=1
      DO 10 J=1,JMAX
      V(J,K)=0.
      VH(J,K)=V(J,K)
10    CONTINUE
      K=K1
      DO 20 J=1,JMAX
      V(J,K)=0.
      VH(J,K)=V(J,K)
20    CONTINUE
      J=1
      DO 30 K=1,K1
      V(J,K)=-V(J+1,K)
      VH(J,K)=V(J,K)
30    CONTINUE
      J=JMAX
      DO 40 K=1,K1
      V(J,K)=-V(J-1,K)
      VH(J,K)=V(J,K)
40    CONTINUE
      J=1
      DO 50 K=1,KMAX
      U(J,K)=0.0
      UH(J,K)=U(J,K)
50    CONTINUE
      J=J1
      DO 60  K=1,KMAX
      U(J,K)=.0
      UH(J,K)=U(J,K)
60    CONTINUE
      K=1
      DO 80 J=1,J1
      U(J,K)=-U(J,K+1)
      UH(J,K)=U(J,K)
80    CONTINUE
      K=KMAX
      DO 70 J=1,J1
      U(J,K)=-U(J,K-1)
      UH(J,K)=U(J,K)
70    CONTINUE
      KM=KMAX/2
      IPASS=0
      IF(IPASS.EQ.1) GOTO 121
      J=1
      CIN=1.+HIK/DX(J)
      DO 90 K=2,K1
      T(J,K)=((HIK*T(J+1,K)/DX(J))+(1.+SHI)/(1.+ZETA*SHO+SHI))/CIN
      ITEST=0
```

```
      IF(ITEST.EQ.0) GOTO 90
      PRINT 800,J,K,T(J,K),DLR,SOI,CIN
  800 FORMAT(' INTEMP=',I3,I3,4F10.6)
   90 CONTINUE
      J=JMAX
      COUT=1.+HOK/DX(J-1)
      DO 91 K=1,KMAX
      T(J,K)=(HOK*T(J-1,K)/DX(J-1)+ZETA*SHO/(1.+ZETA*SHO+SHI))/COUT
      ITEST=0
      IF(ITEST.EQ.0) GOTO 91
      PRINT 810,J,K,T(J,K),DLR,SOO,COUT
  810 FORMAT(' OUTTEMP=',I3,I3,4F10.6)
   91 CONTINUE
  131 K=1
      DO 100 J=1,J1
      T(J,K)=T(J,K+1)
  100 CONTINUE
      K=KMAX
      DO 110 J=1,J1
      T(J,K)=T(J,K-1)
  110 CONTINUE
      RETURN
      END
      SUBROUTINE XGRID
      COMMON /XPARA/ KIT,EU,EV,ET,AR,BETAX,BETAY,ALPHA,THETA,ITEST
     1/PROP/GRR,GRW,GRL,PR,GAM,TIN,TOUT,TCAIR,HCON,QCON
     1/XGEOM/JMAX,KMAX,J1,J2,J3,K1,K2,K3,XMIN,XMAX,YMIN,YMAX
     1/XMET/DX(95),DXX(95),DY(95),DYY(95),X(95),Y(95),XND(95),YZ(95)
     1/XCHK/RESU,RESV,REST,RESM
      DIMENSION XTE(95)
      XMAX=YMAX/AR
      PRINT 500,XMAX,XMIN,YMAX,YMIN
  500 FORMAT(' CORD=',4F6.4)
      ALX=.5
      ZIE=1./J2
      ETA=1./K2
      A1=1.-ALX
      A2=1.+2.*ALX
      B1=(BETAX+1.)/(BETAX-1.)
      B2=BETAX+2.*ALX
      B3=BETAX-2.*ALX
      X(1)=XMIN
      X(J1)=XMAX
      Y(1)=YMIN
      Y(K1)=YMAX
      XND(1)=0.
      XND(JMAX)=1.
      XTE(1)=0.
      XTE(JMAX)=1.
      DO 110 J=2,J1
      E1=(ZIE*(J-1)-ALX)/A1
      B11=B1**E1
      X(J)=XMAX*(B2*B11-B3)/(A2*(1.+B11))
      DXX(J-1)=X(J)-X(J-1)
  110 CONTINUE
      DX(1)=DXX(1)*.5
      DX(J1)=DXX(J2)*.5
      DO 210 J=2,J2
      DX(J)=(DXX(J)+DXX(J-1))*.5
  210 CONTINUE
      DO 212 J=2,J1
      XND(J)=XND(J-1)+DX(J-1)
      XTE(J)=XND(J)/XMAX
  212 CONTINUE
      ALY=.5
      A1=1.-ALY
      A2=1.+2.*ALY
      B1=(BETAY+1.)/(BETAY-1.)
      B2=BETAY+2.*ALY
      B3=BETAY-2.*ALY
      DO 100 K=2,K1
      E1=(ETA*(K-1)-ALY)/A1
      B11=B1**E1
      Y(K)=YMAX*(B2*B11-B3)/(A2*(1.+B11))
      DYY(K-1)=Y(K)-Y(K-1)
  100 CONTINUE
      DO 310 K=2,K2
      DY(K)=(DYY(K)+DYY(K-1))*.5
  310 CONTINUE
      DY(1)=DYY(1)*.5
```

```
      DY(K1)=DYY(K2)*.5
      DO 77 J=1,JMAX
      PRINT 977,J,X(J),DX(J),DXX(J),XTE(J)
   77 CONTINUE
      DO 78 K=1,KMAX
      PRINT 978,K,Y(K),DY(K),DYY(K)
   78 CONTINUE
  977 FORMAT(' XCORD=',I3,6F8.4)
  978 FORMAT(' YCORD=',I3,6F8.4)
      RETURN
      END
C  ---------------------------
C  COMPUTE VELOCITY COPFFICIENTS AUN AUS AUE AUW
C   AVN AVS AVE AVW
C   ---------------------------------
      SUBROUTINE XCOFF
      COMMON /XPARA/ KIT,EU,EV,ET,AR,BETAX,BETAY,ALPHA,THETA,ITEST
     1/PROP/GRR,GRW,GRL,PR,GAM,TIN,TOUT,TCAIR,HCON,QCON
     1/XGEOM/JMAX,KMAX,J1,J2,J3,K1,K2,K3,XMIN,XMAX,YMIN,YMAX
     1/XVAR1/U(70,95),V(70,95),UH(70,95),VH(70,95),P(70,95)
     1/XVAR2/PC(70,95),T(70,95),TO(70,95),PS(70,95),PSI(70,95)
     1/XCOFF1/AUP(70,95),AUN(70,95),AUS(70,95),AUE(70,95)
     1/XCOFF2/AUW(70,95),SU(70,95)
     1/XCOFF3/AVP(70,95),AVN(70,95),AVS(70,95),AVE(70,95)
     1/XCOFF4/AVW(70,95),SV(70,95),SP(70,95)
     1/XCOFF5/APN(70,95),APS(70,95),APE(70,95),APW(70,95)
     1/XNUMB/RHS(100),AA(100),BB(100),CC(100),DD(100)
     1/XMET/DX(95),DXX(95),DY(95),DYY(95),X(95),Y(95),XND(95),YZ(95)
     1/XCHK/RESU,RESV,REST,RESM
      DO 100 J=2,J2
      DO 120 K=2,K1
      F=((V(J+1,K)+V(J,K))*.5)*DX(J)
      D=1.*GAM*DX(J)/DY(K)
      IF(K.EQ.K1) D=.5*D
      PE=F/D
      CALL PECLET (PE,Z)
      AUN(J,K)=D*Z+AMAX1(-F,0.)
      F=((V(J+1,K-1)+V(J,K-1))*.5)*DX(J)
      D=1.*GAM*DX(J)/DY(K-1)
      IF(K.EQ.2) D=.5*D
      PE=F/D
      CALL PECLET (PE,Z)
      AUS(J,K)=D*Z+AMAX1(F,0.)
      F=((U(J+1,K)+U(J,K))*.5)*DYY(K-1)
      D=1.*GAM*DYY(K-1)/DXX(J)
      PE=F/D
      CALL PECLET (PE,Z)
      AUE(J,K)=D*Z+AMAX1(-F,0.)
      F=((U(J-1,K)+U(J,K))*.5)*DYY(K-1)
      D=1.*GAM*DYY(K-1)/DXX(J-1)
      PE=F/D
      CALL PECLET (PE,Z)
      AUW(J,K)=D*Z+AMAX1(F,0.)
      AUPO=GAM*DX(J)*DYY(K-1)
      AUP(J,K)=AUE(J,K)+AUW(J,K)+AUN(J,K)+AUS(J,K)
      UH(J,K)=(AUE(J,K)*U(J+1,K)+AUW(J,K)*U(J-1,K)+AUN(J,K)*
     1U(J,K+1)+AUS(J,K)*U(J,K-1))/AUP(J,K)
    9 ITEST=0
      IF(ITEST.EQ.0) GOTO 120
      PRINT 722,J,K,AUN(J,K),AUS(J,K),AUE(J,K),AUW(J,K),AUP(J,K)
  120 CONTINUE
  100 CONTINUE
  500 FORMAT (I3,I3,5F10.4,2X,I3)
  722 FORMAT(' UCOEF=',I3,I3,5P12.6)
      DO 200 J=2,J1
      DO 200 K=2,K2
      F=((V(J,K+1)+V(J,K))*.5)*DXX(J-1)
      D=1.*GAM*DXX(J-1)/DYY(K)
      PE=F/D
      CALL PECLET (PE,Z)
      AVN(J,K)=D*Z+AMAX1(-F,0.)
      F=((V(J,K-1)+V(J,K))*.5)*DXX(J-1)
      D=1.*GAM*DXX(J-1)/DYY(K-1)
      PE=F/D
      CALL PECLET (PE,Z)
      AVS(J,K)=D*Z+AMAX1(F,0.)
      F=((U(J,K)+U(J,K+1))*.5)*DY(K)
      D=1.*GAM*DY(K)/DX(J)
      IF(J.EQ.J1) D=.5*D
      PE=F/D
```

```
      CALL PECLET (PE,Z)
      AVE(J,K)=D*Z+AMAX1(-F,0.)
      F=((U(J-1,K)+U(J-1,K+1))*.5)*DY(K)
      D=1.*GAM*DY(K)/DX(J-1)
      IF(J.EQ.2)  D=.5*D
      PE=F/D
      CALL PECLET (PE,Z)
      AVW(J,K)=D*Z+AMAX1(F,0.)
      AVPO=GAM*DXX(J-1)*DY(K)
      AVP(J,K)=AVN(J,K)+AVS(J,K)+AVE(J,K)+AVW(J,K)
      SV(J,K)=GRL*(T(J,K+1)+T(J,K))*DXX(J-1)*DY(K)*.5
      VH(J,K)=(AVS(J,K)*V(J,K-1)+AVN(J,K)*V(J,K+1)+AVE(J,K)*
     1V(J+1,K)+AVW(J,K)*V(J-1,K)+
     1 SV(J,K))/AVP(J,K)
      ITEST=0
      IF(ITEST.EQ.0) GOTO 200
      PRINT 666,J,K,AVN(J,K),AVS(J,K),AVE(J,K),AVW(J,K),AVP(J,K)
  666 FORMAT(' VCOEF=',I3,I3,5F10.6)
  200 CONTINUE
  777 FORMAT (I3,I3,6F9.4,2X,I3)
  555 FORMAT (I3,I3,F10.4,2X,I3)
      RETURN
      END
C  ------------------------
CC COMPUTE PRESSURE FIELD
C  ------------------------
      SUBROUTINE XPRESS
      DIMENSION RP(180),SB(70,95)
      COMMON /XPARA/ KIT,EU,EV,ET,AR,BETA,ALPHA,THETA,ITEST
     1/PROP/GRR,GRW,GRL,PR,GAM,TIN,TOUT,TCAIR,HCON,QCON
     1/XGEOM/JMAX,KMAX,J1,J2,J3,K1,K2,K3,XMIN,XMAX,YMIN,YMAX
     1/XVAR1/U(70,95),V(70,95),UH(70,95),VH(70,95),P(70,95)
     1/XVAR2/PC(70,95),T(70,95),TO(70,95),PS(70,95),PSI(70,95)
     1/XCOFF1/AUP(70,95),AUN(70,95),AUS(70,95),AUE(70,95)
     1/XCOFF2/AUW(70,95),SU(70,95)
     1/XCOFF3/AVP(70,95),AVN(70,95),AVS(70,95),AVE(70,95)
     1/XCOFF4/AVW(70,95),SV(70,95),SP(70,95)
     1/XCOFF5/APN(70,95),APS(70,95),APE(70,95),APW(70,95)
     1/XNUMB/RHS(100),AA(100),BB(100),CC(100),DD(100)
     1/XMET/DX(95),DXX(95),DY(95),DYY(95),X(95),Y(95),XND(95),YZ(95)
     1/XCHK/RESU,RESV,REST,RESM
      RP(1)=0.
      RP=4.
      KT=1
    2 DO 55 J=2,J1
      DO 55 K=2,K1
      SP(J,K)=(UH(J-1,K)-UH(J,K))*DYY(K-1)+
     1 (VH(J,K-1)-VH(J,K))*DXX(J-1)
   55 CONTINUE
C  COMPUTE COEFFICIENTS APN APS APE APW
C  SOLVE BY ADI AND TDMA
      DO 100 J=2,J1
      DO 110 K=2,K1
      IF(J.EQ.2) GOTO 5
      APW(J,K)=DYY(K-1)*DYY(K-1)/(AUP(J-1,K))
    5 IF(J.EQ.J1) GOTO 8
      APE(J,K)=DYY(K-1)*DYY(K-1)/(AUP(J,K))
    8 IF(K.EQ.K1) GOTO 9
      APN(J,K)=DXX(J-1)*DXX(J-1)/(AVP(J,K))
    9 IF(K.EQ.2)  GOTO 11
      APS(J,K)=DXX(J-1)*DXX(J-1)/(AVP(J,K-1))
   11 IF(J.EQ.2) APW(J,K)=0.
      IF(K.EQ.2) APS(J,K)=0.
      IF(J.EQ.J1) APE(J,K)=0.
      IF(K.EQ.K1) APN(J,K)=0.
      AA(K)=-APS(J,K)
      CC(K)=-APN(J,K)
      SB(J,K)=APN(J,K)+APS(J,K)+APE(J,K)+APW(J,K)
      BB(K)=SB(J,K)-APE(J,K)*(THETA-1.)
      RHS(K)=APW(J,K)*P(J-1,K)+APE(J,K)*(P(J+1,K)-(
     1  THETA-1.)*P(J,K))+SP(J,K)
      ITEST=0
      IF(ITEST.EQ.0) GOTO 110
      PRINT 6110,J,K,APN(J,K),APS(J,K),APE(J,K),APW(J,K)
 6110 FORMAT(' PRESCO',I4,I4,4F10.6)
  110 CONTINUE
      K=1
      AA(K)=.0
      BB(K)=1.
      CC(K)=-1.0
```

```
      RHS(K)=.0
      K=KMAX
      AA(K)=-1.
      BB(K)=1.
      CC(K)=.0
      RHS(K)=.0
      CALL TRIDAG (AA,BB,CC,DD,RHS,1,KMAX)
      DO 91 K=1,KMAX
      P(J,K)=P(J,K)+(RHS(K)-P(J,K))
   91 CONTINUE
  100 CONTINUE
      DO 300 K=2,K1
      DO 310 J=2,J1
      AA(J)=-APW(J,K)
      CC(J)=-APE(J,K)
      SB(J,K)=APN(J,K)+APS(J,K)+APE(J,K)+APW(J,K)
      BB(J)=SB(J,K)-APN(J,K)*(THETA-1.)
      RHS(J)=APS(J,K)*P(J,K-1)+APN(J,K)*(P(J,K+1)-(
     1  THETA-1.)*P(J,K))+SP(J,K)
      ITEST=0
      IF(ITEST.EQ.0) GOTO 310
      PRINT 722,J,K,APN(J,K),APS(J,K),APE(J,K),APW(J,K)
  310 CONTINUE
      J=1
      AA(J)=.0
      BB(J)=1.
      CC(J)=-1.0
      RHS(J)=.0
      J=JMAX
      AA(J)=-1.
      BB(J)=1.
      CC(J)=.0
      RHS(J)=.0
      CALL TRIDAG (AA,BB,CC,DD,RHS,1,JMAX)
      DO 85 J=1,JMAX
      P(J,K)=P(J,K)+(RHS(J)-P(J,K))
   85 CONTINUE
  300 CONTINUE
  400 DO 90 J=2,J2
      DO 95 K=2,K1
      UH(J,K)=UH(J,K)+DYY(K-1)*(P(J,K)+P(J+1,K))/AUP(J,K)
   95 CONTINUE
   90 CONTINUE
      DO 97 J=2,J1
      DO 99 K=2,K2
      VH(J,K)=VH(J,K)+DXX(J-1)*(P(J,K)-P(J,K+1))/AVP(J,K)
   99 CONTINUE
   97 CONTINUE
      RES=0.0
      KT=KT+1
      DO 77 J=2,J1
      DO 66 K=2,K1
      RE=(APE(J,K)*P(J+1,K)+APW(J,K)*P(J-1,K)+APN(J,K)
     1*P(J,K+1)+APS(J,K)*P(J,K-1)+SP(J,K)-SB(J,K)*P(J,K))**2
      RES=RES+RE
      ITEST=0
      IF(ITEST.EQ.0) GOTO 66
      PRINT 777,J,K,RE,RES,P(J,K),SP(J,K),KT
   66 CONTINUE
   77 CONTINUE
      RP(KT)=(RES)**0.5
      ITEST=0
      IF(ITEST.EQ.0) GOTO 702
      PRINT 677,RP(KT),KT,KIT
  677 FORMAT(' RP=',F10.6,2I5)
  702 IF(RP(KT).GT.ALPHA*RP(2)) GOTO 2
  777 FORMAT(I3,I3,4F12.6,2X,I4)
  606 ITEST=0
      IF(ITEST.EQ.0) GOTO 500
      DO 222 J=2,J1
      DO 222 K=2,K1
      PRINT 333,J,K,APN(J,K),APS(J,K),APE(J,K),APW(J,K),SB(J,K)
  222 CONTINUE
  333 FORMAT(' PRCOF',I3,I3,5F10.6)
  722 FORMAT(I3,I3,4F12.6)
  500 RETURN
      END
      SUBROUTINE XUMOM
      COMMON /XPAPA/ KIT,EU,EV,ET,AR,BETAX,BETAY,ALPHA,THETA,ITEST
     1/PROP/GRR,GRW,GRL,PR,GAM,TIN,TOUT,TCAIR,HCON,QCON
```

```
      1/XGEOM/JMAX,KMAX,J1,J2,J3,K1,K2,K3,XMIN,XMAX,YMIN,YMAX
      1/XVAR1/U(70,95),V(70,95),US(70,95),VS(70,95),P(70,95)
      1/XVAR2/PC(70,95),T(70,95),TO(70,95),PS(70,95),PSI(70,95)
      1/XCOFF1/AUP(70,95),AUN(70,95),AUS(70,95),AUE(70,95)
      1/XCOFF2/AUW(70,95),SU(70,95)
      1/XCOFF3/AVP(70,95),AVN(70,95),AVS(70,95),AVE(70,95)
      1/XCOFF4/AVW(70,95),SV(70,95),SP(70,95)
      1/XCOFF5/APN(70,95),APS(70,95),APE(70,95),APW(70,95)
      1/XNUMB/RHS(100),AA(100),BB(100),CC(100),DD(100)
      1/XMET/DX(95),DXX(95),DY(95),DYY(95),X(95),Y(95),XND(95),YZ(95)
      1/XCHK/RESU,RESV,REST,RESM
       DO 50 J=1,J1
       DO 50 K=2,KMAX
       US(J,K)=U(J,K)
       PS(J,K)=P(J,K)
   50  CONTINUE
       DO 10 J=2,J2
       DO 20 K=2,K1
       IF((J.EQ.1).OR.(J.EQ.J1)) GOTO 5
       AA(K)=-AUS(J,K)
       CC(K)=-AUN(J,K)
       BB(K)=(1.+1./EU)*AUP(J,K)
       RHS(K)=AUE(J,K)*US(J+1,K)+AUW(J,K)*US(J-1,K)
      1+(PS(J,K)-PS(J+1,K))*DYY(K-1)+AUP(J,K)*U(J,K)/EU
    5  IF((J.EQ.1).OR.(J.EQ.J1))  RHS(K)=0.
       IF((J.EQ.1).OR.(J.EQ.J1))  BB(K)=1.
       IF((J.EQ.1).OR.(J.EQ.J1))   AA(K)=0.
       IF((J.EQ.1).OR.(J.EQ.J1))   CC(K)=0.
   20  CONTINUE
       K=1
       AA(K)=.0
       BB(K)=1.
       CC(K)=1.
       RHS(K)=.0
       K=KMAX
       AA(K)=1.
       BB(K)=1.
       CC(K)=0.
       RHS(K)=.0
       CALL TRIDAG (AA,BB,CC,DD,RHS,1,KMAX)
       DO 21 K=1,KMAX
       US(J,K)=US(J,K)+(RHS(K)-US(J,K))
   21  CONTINUE
   10  CONTINUE
  600  FORMAT (I3,I3,F10.4,2X,I3)
       RETURN
       END
       SUBROUTINE XVMOM
       COMMON /XPARA/ KIT,EU,EV,ET,AR,BETAX,BETAY,ALPHA,THETA,ITEST
      1/PROP/GRP,GRW,GRL,PR,GAM,TIN,TOUT,TCAIP,HCON,QCON
      1/XGEOM/JMAX,KMAX,J1,J2,J3,K1,K2,K3,XMIN,XMAX,YMIN,YMAX
      1/XVAR1/U(70,95),V(70,95),US(70,95),VS(70,95),P(70,95)
      1/XVAR2/PC(70,95),T(70,95),TO(70,95),PS(70,95),PSI(70,95)
      1/XCOFF1/AUP(70,95),AUN(70,95),AUS(70,95),AUE(70,95)
      1/XCOFF2/AUW(70,95),SU(70,95)
      1/XCOFF3/AVP(70,95),AVN(70,95),AVS(70,95),AVE(70,95)
      1/XCOFF4/AVW(70,95),SV(70,95),SP(70,95)
      1/XCOFF5/APN(70,95),APS(70,95),APE(70,95),APW(70,95)
      1/XNUMB/RHS(100),AA(100),BB(100),CC(100),DD(100)
      1/XMET/DX(95),DXX(95),DY(95),DYY(95),X(95),Y(95),XND(95),YZ(95)
      1/XCHK/RESU,RESV,REST,RESM
       DO 50 J=1,JMAX
       DO 50 K=2,K1
       VS(J,K)=V(J,K)
       PS(J,K)=P(J,K)
   50  CONTINUE
       DO 10  J=2,J1
       DO 20  K=2,K2
       AA(K)=-AVS(J,K)
       CC(K)=-AVN(J,K)
       BB(K)=(1.+1./EV)*AVP(J,K)
       RHS(K)=AVE(J,K)*VS(J+1,K)+AVW(J,K)*VS(J-1,K)+
      1(PS(J,K)-PS(J,K+1))*DXX(J-1)+SV(J,K)+AVP(J,K)*V(J,K)/EV
   20  CONTINUE
       K=1
       CC(K)=.0
       BB(K)=1.0
       RHS(K)=0.0
       AA(K)=0.0
       K=K1
```

```
      AA(K)=.0
      BB(K)=1.
      CC(K)=.0
      RHS(K)=.0
      CALL TRIDAG (AA,BB,CC,DD,RHS,1,K1)
      DO 21 K=2,K2
      VS(J,K)=VS(J,K)+(RHS(K)-VS(J,K))
   21 CONTINUE
   10 CONTINUE
      RETURN
      END
C ------------------------------
C    CORRECT THE PRESSURE FIELD
C ------------------------------
      SUBROUTINE XPCORR
      DIMENSION RP(180),SP(70,95)
      COMMON /XPARA/ KIT,EU,EV,ET,AR,BETAX,BETAY,ALPHA,THETA,ITEST
     1/PROP/GRR,GRW,GRL,PR,GAM,TIN,TOUT,TCAIR,HCON,OCON
     1/XGEOM/JMAX,KMAX,J1,J2,J3,K1,K2,K3,XMIN,XMAX,YMIN,YMAX
     1/XVAR1/U(70,95),V(70,95),US(70,95),VS(70,95),P(70,95)
     1/XVAR2/PC(70,95),T(70,95),TO(70,95),PS(70,95),PSI(70,95)
     1/XCOFF1/AUP(70,95),AUN(70,95),AUS(70,95),AUE(70,95)
     1/XCOFF2/AUW(70,95),SU(70,95)
     1/XCOFF3/AVP(70,95),AVN(70,95),AVS(70,95),AVE(70,95)
     1/XCOFF4/AVW(70,95),SV(70,95),SP(70,95)
     1/XCOFF5/APN(70,95),APS(70,95),APE(70,95),APW(70,95)
     1/XNUMB/RHS(100),AA(100),BB(100),CC(100),DD(100)
     1/XMET/DX(95),DXX(95),DY(95),DYY(95),X(95),Y(95),XND(95),YZ(95)
     1/XCHK/RESU,RESV,REST,RESM
      RP(1)=0.0
      KT=1
      DO 22 J=1,JMAX
      DO 22 K=1,KMAX
      PC(J,K)=.0
   22 CONTINUE
    2 DO 55 J=2,J1
      DO 55 K=2,K1
      SP(J,K)=(US(J-1,K)-US(J,K))*DYY(K-1)+
     1 (VS(J,K-1)-VS(J,K))*DXX(J-1)
      ITEST=0
      IF(ITEST.EQ.0) GOTO 55
      PRINT 888,J,K,U(J,K),US(J,K),V(J,K),VS(J,K)
   55 CONTINUE
      DO 100 J=2,J1
      DO 110 K=2,K1
      AA(K)=-APS(J,K)
      CC(K)=-APN(J,K)
      SB(J,K)=APN(J,K)+APS(J,K)+APE(J,K)+APW(J,K)
      BB(K)=SB(J,K)-APE(J,K)*(THETA-1.)
      RHS(K)=APW(J,K)*PC(J-1,K)+APE(J,K)*(PC(J+1,K)-(
     1  THETA-1.)*PC(J,K))+SP(J,K)
      ITEST=0
      IF(ITEST.EQ.0) GOTO 110
      PRINT 722,J,K,APN(J,K),APS(J,K),APE(J,K),APW(J,K)
  110 CONTINUE
      K=1
      AA(K)=.0
      BB(K)=1.
      CC(K)=-1.0
      RHS(K)=.0
      K=KMAX
      AA(K)=-1.
      BB(K)=1.
      CC(K)=.0
      RHS(K)=.0
      CALL TRIDAG (AA,BB,CC,DD,RHS,1,KMAX)
      DO 91 K=1,KMAX
      PC(J,K)=PC(J,K)+(RHS(K)-PC(J,K))
   91 CONTINUE
  100 CONTINUE
      DO 300 K=2,K1
      DO 310 J=2,J1
      AA(J)=-APW(J,K)
      CC(J)=-APE(J,K)
      SB(J,K)=APN(J,K)+APS(J,K)+APE(J,K)+APW(J,K)
      BB(J)=SB(J,K)-APN(J,K)*(THETA-1.)
      RHS(J)=APS(J,K)*PC(J,K-1)+APN(J,K)*(PC(J,K+1)-(
     1  THETA-1.)*PC(J,K))+SP(J,K)
      ITEST=0
      IF(ITEST.EQ.0) GOTO 310
```

```
      PRINT 722,J,K,APN(J,K),APS(J,K),APE(J,K),APW(J,K)
  310 CONTINUE
      J=1
      AA(J)=.0
      BB(J)=1.
      CC(J)=-1.0
      RHS(J)=.0
      J=JMAX
      AA(J)=-1.
      BB(J)=1.
      CC(J)=.0
      RHS(J)=.0
      CALL TRIDAG (AA,BB,CC,DD,RHS,1,JMAX)
      DO 85 J=1,JMAX
      PC(J,K)=PC(J,K)+(RHS(J)-PC(J,K))
   85 CONTINUE
  300 CONTINUE
      DO 90 J=2,J2
      DO 95 K=2,K1
      US(J,K)=US(J,K)+DYY(K-1)*(PC(J,K)-PC(J+1,K))/AUP(J,K)
   95 CONTINUE
   90 CONTINUE
      DO 97 J=2,J1
      DO 99 K=2,K2
      VS(J,K)=VS(J,K)+DXX(J-1)*(PC(J,K)-PC(J,K+1))/AVP(J,K)
   99 CONTINUE
   97 CONTINUE
      RES=0.0
      KT=KT+1
      DO 77 J=2,J1
      DO 66 K=2,K1
      RE=(APE(J,K)*PC(J+1,K)+APW(J,K)*PC(J-1,K)+APN(J,K)
     1*PC(J,K+1)+APS(J,K)*PC(J,K-1)+SP(J,K)-SB(J,K)*PC(J,K))**2
      RES=RES+RE
      ITEST=0
      IF(ITEST.EQ.0) GOTO 66
      PRINT 777,J,K,RE,RES,PC(J,K),SP(J,K),KT
   66 CONTINUE
   77 CONTINUE
      RP(KT)=(RES)**0.5
      ITEST=0
      IF(ITEST.EQ.0) GOTO 604
      PRINT 677,RP(KT),KT,KIT
  677 FORMAT(' RPC=',F12.4,2I5)
  604 IF(RP(KT).GT.ALPHA*RP(2)) GOTO 2
  722 FORMAT(I3,I3,4F12.5)
  777 FORMAT(I3,I3,4F12.6,2X,I4)
  888 FORMAT(I3,I3,4F12.5)
  111 RETURN
      END
C  ----------------------
C  CORRECT THE VELOCITY FIELD
C ----------------------------
      SUBROUTINE XVCORR
      COMMON /XPARA/ KIT,EU,EV,ET,AR,BETAX,BETAY,ALPHA,THETA,ITEST
     1/PROP/GRR,GRW,GRL,PR,GAM,TIN,TOUT,TCAIR,HCON,OCON
     1/XGEOM/JMAX,KMAX,J1,J2,J3,K1,K2,K3,XMIN,XMAX,YMIN,YMAX
     1/XVAR1/U(70,95),V(70,95),US(70,95),VS(70,95),P(70,95)
     1/XVAR2/PC(70,95),T(70,95),TO(70,95),PS(70,95),PSI(70,95)
     1/XCOFF1/AUP(70,95),AUN(70,95),AUS(70,95),AUE(70,95)
     1/XCOFF2/AUW(70,95),SU(70,95)
     1/XCOFF3/AVP(70,95),AVN(70,95),AVS(70,95),AVE(70,95)
     1/XCOFF4/AVW(70,95),SV(70,95),SP(70,95)
     1/XCOFF5/APN(70,95),APS(70,95),APE(70,95),APW(70,95)
     1/XNUMB/RHS(100),AA(100),BB(100),CC(100),DD(100)
     1/XMET/DX(95),DXX(95),DY(95),DYY(95),X(95),Y(95),XND(95),YZ(95)
     1/XCHK/RESU,RESV,REST,RESM
      DO 90 J=2,J2
      DO 95 K=2,K1
      U(J,K)=US(J,K)+DYY(K-1)*(PC(J,K)-PC(J+1,K))/AUP(J,K)
   95 CONTINUE
   90 CONTINUE
      DO 97 J=2,J1
      DO 99 K=2,K2
      V(J,K)=VS(J,K)+DXX(J-1)*(PC(J,K)-PC(J,K+1))/AVP(J,K)
   99 CONTINUE
   97 CONTINUE
      RETURN
      END
C  ----------------------------
```

```
C  COMPUTE THE TEMPERATURE FIELD
C  ------------------------------
      SUBROUTINE XTEMP
      DIMENSION PP(180)
      COMMON /XPARA/ KIT,EU,EV,PT,AR,BETAX,BETAY,ALPHA,THETA,ITEST
     1/PROP/GRR,GRW,GRL,PR,GAM,TIN,TOUT,TCAIR,HCON,QCON
     1/WIND/DELT,SOO,SOI,DTR,DLR,HTI,HTO
     1/WIND2/HOK,HIK,SHI,SHO,ZETA
     1/XGEOM/JMAX,KMAX,J1,J2,J3,K1,K2,K3,XMIN,XMAX,YMIN,YMAX
     1/XVAR1/U(70,95),V(70,95),US(70,95),VS(70,95),P(70,95)
     1/XVAR2/PC(70,95),T(70,95),TO(70,95),PS(70,95),PSI(70,95)
     1/XCOFF1/ATP(70,95),ATN(70,95),ATS(70,95),ATE(70,95)
     1/XCOFF2/ATW(70,95),ST(70,95)
     1/XCOFF3/AVP(70,95),AVN(70,95),AVS(70,95),AVE(70,95)
     1/XCOFF4/AVW(70,95),SV(70,95),SP(70,95)
     1/XCOFF5/APN(70,95),APS(70,95),APE(70,95),APW(70,95)
     1/XNUMB/RHS(100),AA(100),BB(100),CC(100),DD(100)
     1/XMET/DX(95),DXX(95),DY(95),DYY(95),X(95),Y(95),XND(95),YZ(95)
     1/XCHK/RESU,RESV,REST,RESM
      KT=1
      GAM=1./PR
      DO 5 J=1,JMAX
      DO 5 K=1,KMAX
      ST(J,K)=.0
    5 CONTINUE
      J=JMAX
      SOLO=0.
      SOLIN=0.
      DO 7 K=1,KMAX
      ST(J,K)=0.
    7 CONTINUE
      J=1
      DO 8 K=1,KMAX
      ST(J,K)=0.
    8 CONTINUE
    2 DO 10  J=2,J1
      DO 20  K=2,K1
      F=U(J-1,K)*DYY(K-1)
      D=1.*GAM*DYY(K-1)/DX(J-1)
      PE=F/D
      CALL PECLET (PE,Z)
      ATW(J,K)=D*Z+AMAX1(F,0.)
      F=U(J,K)*DYY(K-1)
      D=1.*GAM*DYY(K-1)/DX(J)
      PE=F/D
      CALL PECLET (PE,Z)
      ATE(J,K)=D*Z+AMAX1(-F,0.)
      F=V(J,K)*DXX(J-1)
      D=1.*GAM*DXX(J-1)/DY(K)
      PE=F/D
      CALL PECLET (PE,Z)
      ATN(J,K)=D*Z+AMAX1(-F,0.)
      F=V(J,K-1)*DXX(J-1)
      D=1.*GAM*DXX(J-1)/DY(K-1)
      PE=F/D
      CALL PECLET (PE,Z)
      AA(K)=-ATS(J,K)
      CC(K)=-ATN(J,K)
      ATPO=GAM*DXX(J-1)*DYY(K-1)
      ATP(J,K)=ATN(J,K)+ATS(J,K)+ATE(J,K)+ATW(J,K)
      BB(K)=ATP(J,K)*(1.+1./ET)
      RHS(K)=ATE(J,K)*T(J+1,K)+ATW(J,K)*T(J-1,K)+ATP(J,K)*T(J,K)/ET
     1   +ST(J-1,K)*DYY(K-1)*DXX(J-1)+ST(J+1,K)*DYY(K-1)*DXX(J-1)
   20 CONTINUE
      K=1
      CC(K)=1.0
      BB(K)=-1.0
      AA(K)=0.0
      RHS(K)=0.0
      K=KMAX
      AA(K)=1.00
      BB(K)=-1.0
      CC(K)=0.00
      RHS(K)=0.0
      CALL TRIDAG (AA,BB,CC,DD,RHS,1,KMAX)
      DO 21 K=1,KMAX
      T(J,K)=T(J,K)+(RHS(K)-T(J,K))
      TO(J,K)=T(J,K)
   21 CONTINUE
   10 CONTINUE
```

```
      RES=0.0
      KT=KT+1
      DO 77 J=2,J1
      DO 66 K=2,K1
      RE=(ATE(J,K)*T(J+1,K)+ATW(J,K)*T(J-1,K)+ATN(J,K)
     1*T(J,K+1)+ATS(J,K)*T(J,K-1)-ATP(J,K)*T(J,K))**2
      RES=RES+RE
   66 CONTINUE
   77 CONTINUE
      RP(KT)=(RES)**0.5
      IF(RP(KT).GT.ALPHA*RP(2)) GOTO 2
  666 FORMAT (I3,I3,5F10.4,2X,I3)
  600 RETURN
      END
      SUBROUTINE PECLET (P,A)
      A=(1.0-(0.1*ABS(P)))**5
      IF(A.LT.0.0)  A=0.0
      RETURN
      END
      SUBROUTINE TRIDAG (A,B,C,D,F,NL,NU)
      DIMENSION A(100),B(100),C(100),D(100),F(100)
      D(NL)=C(NL)/B(NL)
      F(NL)=F(NL)/B(NL)
      NLP1=NL+1
      DO 11 N=NLP1,NU
      Z=1./(B(N)-A(N)*D(N-1))
      D(N)=C(N)*Z
   11 F(N)=(F(N)-A(N)*F(N-1))*Z
      NUPNL=NU+NL
      DO 41  NN=NLP1,NU
      N=NUPNL-NN
   41 F(N)=F(N)-D(N)*F(N+1)
      RETURN
      END
      SUBROUTINE SLINE
      COMMON /XPARA/ KIT,EU,EV,ET,AR,BETAX,BETAY,ALPHA,THETA,ITEST
     1/XGEOM/JMAX,KMAX,J1,J2,J3,K1,K2,K3,XMIN,XMAX,YMIN,YMAX
     1/XVAR1/U(70,95),V(70,95),US(70,95),VS(70,95),P(70,95)
     1/XVAR2/PC(70,95),T(70,95),TO(70,95),PS(70,95),PSI(70,95)
     1/XNUMB/RHS(100),AA(100),BB(100),CC(100),DD(100)
     1/XMET/DX(95),DXX(95),DY(95),DYY(95),X(95),Y(95),XZ(95),YZ(95)
      DIMENSION OMG(70,95),RES(70,95),XT(95),YT(95)
      XT(1)=X(1)
      YT(1)=Y(1)
      DO 6 J=2,JMAX
      XT(J)=XT(J-1)+DX(J-1)
    6 CONTINUE
      DO 8 K=2,KMAX
      YT(K)=YT(K-1)+DY(K-1)
    8 CONTINUE
      DO 10 J=1,JMAX
      DO 10 K=1,KMAX
      PSI(J,K)=.0
      OMG(J,K)=0.
   10 RES(J,K)=.0
      DO 12 J=2,J2
      DO 12 K=2,K2
      OMG(J,K)=(V(J+1,K)-V(J,K))/DX(J)-(U(J,K+1)-U(J,K))/DY(K)
   12 CONTINUE
      KS=1
    2 DO 14 J=2,J2
      DO 16 K=2,K2
      AA(K)=1./DYY(K-1)**2
      BB(K)=-2./DXX(J-1)**2-2./DYY(K-1)**2
      CC(K)=1./DYY(K-1)**2
      RHS(K)=-PSI(J-1,K)/DXX(J-1)**2-PSI(J+1,K)/DXX(J-1)**2-OMG(J,K)
      ITEST=0
      IF(ITEST.EQ.0) GOTO 16
      PRINT 800,K,AA(K),BB(K),CC(K),RHS(K),KS
  800 FORMAT(' STREAM=',I3,3F13.3,F14.3,I5)
  811 FORMAT(' VORT=',I4,I4,F15.3)
   16 CONTINUE
      K=1
      AA(K)=.0
      BB(K)=1.
      CC(K)=0.
      RHS(K)=.0
      K=K1
      AA(K)=0.
      BB(K)=1.
```

```
      CC(K)=.0
      RHS(K)=.0
      CALL TRIDAG(AA,BB,CC,DD,RHS,1,K1)
      DO 18 K=2,K2
      PSI(J,K)=PSI(J,K)+.8*(RHS(K)-PSI(J,K))
   18 CONTINUE
      DO 20 K=2,K2
      RES(J,K)=ABS(.8*(RHS(K)-PSI(J,K)))
   20 CONTINUE
   14 CONTINUE
      IF(GRW.LE.1.E5) EPI=1.
      IF(GRW.LE.1.E4) EPI=.1
      IF(GRW.LE.1.E3) EPI=.01
      KS=KS+1
      DO 22 J=2,J2
      DO 22 K=2,K2
      IF(RES(J,K).GT.EPI) GOTO 2
      PSI(J,K)=ABS(PSI(J,K))
   22 CONTINUE
  822 FORMAT(' RESIDU=',I4,I4,F10.3,I4)
      PRINT 970
  970 FORMAT(1H0,30X,'STREAMFUNC FIELD')
      WRITE(6,88)((PSI(J,KMAX+1-K),J=1,J1),K=1,K1,2)
   88 FORMAT(7(F6.2,1X)/)
      PRINT 974
      WRITE(6,78)((T(J,K1+1-K),J=1,JMAX),K=1,KMAX,2)
  974 FORMAT(1H1,30X,'THE GLTEMPERATURE FIELD')
   78 FORMAT(8(F6.2,1X)/)
      DO 26 J=1,J1
      DO 26 K=1,K1
      WRITE(3,989) X(J),Y(K),PSI(J,K)
   26 CONTINUE
      DO 36 J=1,JMAX
      DO 36 K=1,KMAX
      WRITE(4,989) XT(J),YT(K),T(J,K)
   36 CONTINUE
  988 FORMAT(3F10.4,I4,' SAST=')
  989 FORMAT(3F10.4)
  999 FORMAT(3F10.4,I4,' SAS=')
      RETURN
      END
      SUBROUTINE XPUT
      COMMON /XPARA/ KIT,EU,EV,ET,AR,BETAX,BETAY,ALPHA,THETA,ITEST
     1/PROP/GRR,GRW,GRL,PP,GAM,TIN,TOUT,TCAIR,HCON,OCON
     1/XGEOM/JMAX,KMAX,J1,J2,J3,K1,K2,K3,XMIN,XMAX,YMIN,YMAX
     1/XVAR1/U(70,95),V(70,95),US(70,95),VS(70,95),P(70,95)
     1/XVAR2/PC(70,95),T(70,95),TO(70,95),PS(70,95),PSI(70,95)
     1/XCOFF1/AUP(70,95),AUN(70,95),AUS(70,95),AUE(70,95)
     1/XCOFF2/AUW(70,95),SU(70,95)
     1/XCOFF3/AVP(70,95),AVN(70,95),AVS(70,95),AVE(70,95)
     1/XCOFF4/AVW(70,95),SV(70,95),SP(70,95)
     1/XCOFF5/APN(70,95),APS(70,95),APE(70,95),APW(70,95)
     1/XNUMB/RHS(100),AA(100),BB(100),CC(100),DD(100)
     1/XMET/DX(95),DXX(95),DY(95),DYY(95),X(95),Y(95),XZ(95),YZ(95)
     1/XCHK/RESU,RESV,REST,RESM
      DIMENSION U1(1800),V1(1800),OMG(70,70),RES(70,70)
      DIMENSION HEAT(70,95),HT(1800),FLUX(70,95)
      DO 66 J=2,J1
      DO 66 K=2,K2
      REV=(AVE(J,K)*V(J+1,K)+AVW(J,K)*V(J-1,K)+AVN(J,K)
     1*V(J,K+1)+AVS(J,K)*V(J,K-1)-AVP(J,K)*V(J,K))**2
      RESV=RESV+REV
   66 CONTINUE
      RESV=RESV**.5
      DO 77 J=2,J1
      DO 77 K=2,K2
      REU=(AUE(J,K)*U(J+1,K)+AUW(J,K)*U(J-1,K)+AUN(J,K)
     1*U(J,K+1)+AUS(J,K)*U(J,K-1)-AUP(J,K)*U(J,K))**2
      RESU=RESU+REU
   77 CONTINUE
      RESU=RESU**.5
      DO 88 J=2,J1
      DO 88 K=2,K1
      RESM=RESM+SP(J,K)**2
   88 CONTINUE
      RESM=(RESM/(J2*K2))**.5
      HTAVG=.0
      OVFLUX=.0
      RFLUX=.0
      DO 86 J=2,JMAX
```

```
      DO 86 K=2,KMAX
      FLUX(J,K)=ABS(T(J-1,K)-T(J,K))*DY(K-1)/DX(J-1)
   86 CONTINUE
      J=JMAX
      DO 79 K=2,KMAX
      OVFLUX=OVFLUX+FLUX(J,K)
   79 CONTINUE
      J=2
      DO 69 K=2,KMAX
      RFLUX=RFLUX+FLUX(J,K)
   69 CONTINUE
      RFLUX=RFLUX*XMAX
      KM=KMAX/2
      OVFLUX=OVFLUX*XMAX
      WRITE(6,78)((T(J,K1+1-K),J=1,JMAX),K=1,KMAX,2)
   78 FORMAT(8(F5.2,1X)/)
      PRINT 972
      PRINT 964
      PRINT 920,RESU,RESV,RESM
      PRINT 930,RFLUX,OVFLUX,GRW,GRL,KIT
      DO 87 J=1,JMAX
      DO 87 K=1,KMAX
      PRINT 960,J,K,U(J,K),V(J,K),T(J,K),P(J,K),KIT
   87 CONTINUE
  980 FORMAT(4F10.3,I4,' ISO=')
  960 FORMAT(I3,I3,' GLA=',2F12.4,F10.5,F14.2,I6)
  972 FORMAT(1H0,30X,'THE HEAT TRANSFER FIELD')
  188 FORMAT(9(F5.2,1X)/)
  964 FORMAT(1H0,30X,'THE HEAT FLUX FIELD')
  148 FORMAT(8(F5.2,1X)/)
  920 FORMAT(' RESU=',F10.6,' RESV=',F10.6,' RESM=',F10.6)
  930 FORMAT (' RFLUX=',F7.4,' OVFLUX=',F7.4,
     1        ' GRW=',E10.4,' GRL=',E10.4,I5)
  950 FORMAT (' HCON=',F8.4,' QCON=',F8.4,' TCAIR=',F8.4,I4)
  910 FORMAT (I3,I3,3F10.6,2X,I4)
  900 FORMAT (I3,I3,4F10.4,F10.6,2X,I4)
      RETURN
      END
```

VITA AUCTORIS

1950	Born in New Delhi, India on March 21
1965	Completed high school at the Rashtriya Indian Military College, Dehradun, India.
1972	Received the Degree of Bachelor of Technology (Honors) from the Indian Institute of Technology, Kharagpur, India.
1973-1981	Worked as a Design Engineer for Bharat Heavy Electricals, New Delhi, and Keltron Controls, Trivandrum, India.
1985	Received the Degree of Master of Applied Science in Mechanical Engineering from the University of Windsor, Windsor, Canada.
1988	Currently a candidate for the Degree of Doctor of Philosophy in Mechanical Engineering at the University of Windsor, Windsor, Canada.